

**Behaviour of a Reduced-Scale Fully Grouted Reinforced
Concrete Block Masonry Building**

By

Jordan Marc Vandervelde

B. Eng. Mgmt.

A Thesis

Submitted to the School of Graduate Studies

In Partial Fulfillment of the Requirements

For the Degree of

Master of Applied Science

McMaster University

©Jordan Vandervelde November, 2010

Jordan Vandervelde

McMaster University – Civil Engineering

M.A.Sc. Thesis

MASTER OF APPLIED SCIENCE (2010)

McMaster University

(CIVIL ENGINEERING)

Hamilton, Ontario

Title: Behaviour of Reduced-Scale Fully Grouted Concrete Block Masonry Building

Author: Jordan Vandervelde, B Eng. & Mgmt. (McMaster University)

Advisors: Dr. R. Drysdale and Dr. W. El-Dakhakhni

Number of Pages: xv; 214.

Abstract

Much of the experimental research on shear wall elements in reinforced masonry has been performed on shear walls in isolation. These elements have typically been removed from their structural system and artificial idealized loading is placed on them. Testing is limited to these types of experiments because of limitations of laboratory equipment or the potential cost constraints of attempting tests on full building systems. Full-scale testing as well as some reduced scale testing has been performed at McMaster University over recent years. However, in order to examine larger walls as well as full building structures, the focus of research has turned more towards reduced-scale testing. First, half-scale tests were completed, and now, as part of a new test program, testing utilizes one-third scale concrete blocks.

This thesis focuses on the ductile response of a one-third scale reinforced, fully grouted, concrete block shear wall building. As the name implies, the lateral load resisting system consists solely of reinforced masonry shear walls. Documentation is presented of the building response in terms of stiffness, torsion and post-yielding lateral loading. Further examination is presented related to the diaphragm action and associated inter-wall coupling behaviour. The load-displacement characteristics of the structure are then broken down into the response of the individual shear wall elements within the structure. These response characteristics are then related back to previous studies of the same wall configurations tested in isolation.

The primary objective of the thesis is to provide a foundation to build a relationship between the behaviour of reinforced masonry shear walls tested in isolation and their behaviour in a building or system setting. This, along with future research in this area will provide comparisons between current design practice and observed performance for the purpose of potentially amending design practices related to seismic provisions as found in the National Building Code of Canada (2010) as well as the masonry design standard CSA S304.1 (2004).

The results of this study show a positive response for the use of one-third scale testing as well as testing of full systems. Although relatively brittle reinforcing steel limited the ability of the structure to achieve the expected ductility level the test results did show excellent promise for the hypothesis presented. This experimental program showed the potential of reinforced masonry shear walls to resist seismic loading while acting as part of a structural system.

Acknowledgements

I wish to thank God for his unwavering support and strength during this time in my life. I'd also like to thank Dr. Drysdale and Dr. El-Dakhakhni for the continued patience, insight and encouragement during the course of this research. They have taught me true fundamentals of engineering and structural understanding to levels not achievable by reading books. Many thanks go to the technicians at the ADL, Kent Wheeler and David Perret. Their knowledge and help throughout the course of the laboratory testing was and still is greatly appreciated. I'd also like to express appreciation to Paul Hereema, Kevin Hughes, Bennett Banting and Joe Wierzbicki for their help when extra hands were required.

I'd also like to thank the Ontario Masonry Contractors Association, the Canadian Masonry Design Centre for providing expert help during construction, as well as the mason himself; Tim Maxson. Appreciation also goes to the Canadian Concrete Masonry Producers Association for providing the block making equipment as well as Niagara Block Inc. for allowing us use of their facility and expertise. Finally, thanks go to Lec Steel for providing the reinforcing steel for this experimental program.

Table of Contents

Abstract.....	iii
Acknowledgements.....	v
Table of Contents.....	vi
List of Figures	xi
List of Tables	xv
1 Introduction	1
1.1 Background	1
1.2 Problem Statement.....	3
1.3 Research Significance and Objectives.....	6
1.4 Scope.....	7
1.5 Literature Review.....	8
1.5.1 Introduction	8
1.5.2 Masonry Codes and Standards	8
1.5.3 Seismic Reduction Factor.....	9
1.5.4 Masonry Codes	11
1.5.5 Reinforced Masonry Shear Wall Behaviour	14
1.5.6 Plastic Hinging.....	16
1.5.7 Testing of Building Systems	19
1.5.8 Testing of Diaphragm Influence.....	24
1.5.9 Torsional System Behaviour.....	26
1.5.10 Effects of Scaling	30
1.6 Conclusion.....	32
2 Experimental Program	33
2.1 Introduction	33
2.2 Design and Construction of the Test Building.....	34
2.2.1 Introduction	34

2.2.2	Selection of Wall Dimensions	35
2.2.3	Building Layout and Dimensions	37
2.3	Construction.....	39
2.3.1	Foundation	39
2.3.2	Construction of Block Walls	42
2.3.3	Grouting of the Block Walls	43
2.4	Design Details.....	44
2.4.1	General Wall properties.....	45
2.4.2	The C-Wall (Wall 8)	45
2.4.3	The Double Wall (Walls 1 and 2).....	47
2.4.4	Centre Wall (Wall 5).....	48
2.4.5	Out- of-Plane Walls (Walls 3, 4, 6, and 7)	49
2.4.6	Overview of Structure	50
2.5	Details of Design	52
2.5.1	Design for Flexure	52
2.5.2	Design for Shear	53
2.5.3	Floor Slab Design.....	53
2.5.4	Special Provisions for Floor Slabs.....	55
2.6	Material Properties	58
2.6.1	Steel Properties.....	58
2.6.2	Foundation Slab Concrete Properties	60
2.6.3	Slab Concrete	61
2.6.4	Mortar Properties	62
2.6.5	Grout Properties	63
2.6.6	Block Properties	64
2.6.7	Prism Properties.....	65
2.7	Building Test Setup	68
2.7.1	General Configuration of Test Setup	69

2.8	Measurements and Instrumentation.....	76
2.8.1	External Instrumentation.....	76
2.8.2	Internal Instrumentation.....	77
2.9	General Test Procedure.....	80
2.10	Conclusion.....	81
3	Test Results.....	82
3.1	Introduction.....	82
3.2	Preliminary Cyclic Loading.....	83
3.2.1	20% of Yield Load Cycle.....	84
3.2.2	40% of Yield Load Cycle.....	85
3.3	Pushover Test of Shear Wall Structure.....	86
3.3.1	General Observations.....	88
3.3.1.1	Definition of First Yield.....	89
3.3.1.2	0.07% Drift.....	90
3.3.1.3	0.17% Drift.....	90
3.3.1.4	0.26% Drift.....	91
3.3.1.5	0.38% Drift.....	96
3.3.1.6	0.51% Drift.....	99
3.3.1.7	0.65% Drift.....	103
3.3.1.8	0.80% Drift.....	106
3.3.1.9	0.96% Drift.....	110
3.3.1.10	1.13% Drift.....	113
3.3.1.11	1.26% Drift.....	118
3.3.1.12	1.55% to 2.03% Drift.....	122
3.4	Conclusion.....	128
4	Analysis of Test Results.....	130
4.1	Introduction.....	130
4.2	General Building Response.....	130

4.2.1	Initial Prediction of Structural Response	130
4.2.2	Coupling Behaviour	133
4.3	General Experimental Observations	137
4.3.1	Displacement Response	138
4.3.2	Torsional Response	138
4.3.3	In-Plane Wall Displacements	143
4.3.4	Establishment of Experimental First Yield	146
4.4	Seismic Reduction Factor	147
4.4.1	Structural Stiffness	148
4.4.1.1	Observed Elastic Stiffness	148
4.4.2	Equal Area Method to Quantify Ductility	151
4.5	Theoretical Analysis of Individual Walls.....	155
4.5.1	General.....	155
4.5.2	Predicted Lateral Capacity, Curvature and Deflection.....	156
4.5.3	Equivalent Plastic Hinge Length	157
4.5.3.1	CSA S304.1	158
4.5.3.2	Literature and Comparisons.....	158
4.6	Individual Wall Responses	161
4.6.1	North Portion of the Double Wall (Wall 1)	162
4.6.2	South Portion of the Coupled Wall (Wall 2).....	167
4.6.3	North Out-of-Plane Walls (Walls 3 and 6).....	170
4.6.4	The Centre Wall (Wall 5)	172
4.6.5	South Out-of-Plane Walls (Walls 4 and 7).....	175
4.6.6	The C-Wall (Wall 8)	178
4.7	Conclusions	181
4.7.1	Predicted and Experimental Building Capacity and Deflections.....	181
4.7.2	Building Response	182
4.7.2.1	Torsion	182

4.7.2.2	In-Plane Behaviour	182
4.7.2.3	Ductility	183
4.7.3	Individual Wall Behaviour	184
5	Conclusions and Recommendations	185
5.1	Conclusions	185
5.1.1	Use of Third Scale for Testing Structures	185
5.1.2	Ductility of Reinforcing Bars	185
5.1.3	Building Ductility	186
5.1.4	Ductility of Individual Walls	186
5.1.5	Deformations in Walls	187
5.1.6	Torsion	189
5.2	The Effects of the Reduction in Stiffness	189
5.2.1	Structural Period	190
5.2.2	Normalized Period	191
5.2.3	Post-Yield Stiffness	191
5.2.4	Structural Stiffness and Period	192
5.3	Recommendations	193
5.3.1	Test Setup Modifications	193
5.3.2	Building Layout	194
5.3.3	Reinforcing Steel	194
5.4	Overall Conclusions	194
	References	196
	Appendix A: Flexural Design	202
	Appendix B: Mortar Cube Data	203
	Appendix C: Test Frame Shop Drawings	204
	Appendix D: Displacement Prediction	213

List of Figures

Figure 1.1: Seismic Reduction Factors Based on Equal Energy (Shedid, 2006)	5
Figure 2.1: Blocks Used for Construction	35
Figure 2.2: Typical Rectangular Wall	36
Figure 2.3: C-Wall (Wall 8) block layout	37
Figure 2.4: Final Layout of Experimental Building	38
Figure 2.5: Reinforcing Bar Locations in the Foundation Slab	40
Figure 2.6: Photograph of Reinforcement Prior to Placing the Slab Concrete	41
Figure 2.7: Partially Completed Wall Construction	43
Figure 2.8: Plan Side and End Views of C-Wall (Wall 8)	46
Figure 2.9: Plan and Elevation of Double Wall (Walls 1 and 2)	48
Figure 2.10: Plan and Elevation of Centre Wall (Wall 5)	49
Figure 2.11: Elevation of Out-of-Plane Walls (Walls 3, 4, 6, and 7)	50
Figure 2.12: 3D Model of Specimen	51
Figure 2.13: Floor Slab Reinforcing	54
Figure 2.14: Slab Cross Section	55
Figure 2.15: Formation of Hinges Using Grooves in the Concrete Slab	56
Figure 2.16: Close Up of Groove and Slot at the Hinge Location	57
Figure 2.17: Stress Strain Relationship for D7 Reinforcing Bars	59
Figure 2.18: Stress-Strain Relationship for the W1.7 Wire Reinforcing	60
Figure 2.19: Void in Prism from Fourth Stage of Grouting	67
Figure 2.20: Stress-Strain Relationship for Prisms from Construction Phase 1	69
Figure 2.21: Elevation View of Test Frame	70
Figure 2.22: Plan View of the Test Frame	70
Figure 2.23: Detailed Test Setup	74
Figure 2.24: Loading Mechanism Plan	75
Figure 2.25: LVDT Position for the Out-of-Plane Walls	77
Figure 2.26: LVDT Position for the In-Plane Walls	77
Figure 2.27: Typical Strain Gauge on a Vertical Reinforcing Bar	78
Figure 2.28: Typical Strain Gauge Positions	79
Figure 2.29: String Pot Locations in Plan	80
Figure 3.1: Wall and Slot Layout	83
Figure 3.2: Load-Displacement Plot for 20% of Yield Loading Cycle	85
Figure 3.3: Load-Displacement Plot for 40% of Yield Loading Cycle	86
Figure 3.4: Pushover Curve for the Shear Wall Structure	87

Figure 3.5: Flexural Cracking in Centre Wall (Wall 5) at 0.17% Drift	91
Figure 3.6: Cracking on North West Out-of-Plane Wall (Wall 6)	92
Figure 3.7: Cracking on North East Out-of-Plane Wall (Wall 3)	93
Figure 3.8: Cracking on North Portion of the Double Wall (Wall 1)	93
Figure 3.9: Cracking on South Portion of the Double Wall (Wall 2)	94
Figure 3.10: Cracking on Centre Wall (Wall 5)	94
Figure 3.11: Cracking on C-Wall (Wall 8)	95
Figure 3.12: Cracking of the First Story Slab between Portions of the Double Wall (Walls 1 and 2)	95
Figure 3.13: Cracking on North West Out-of-Plane Wall (Wall 6)	97
Figure 3.14: Cracking on North Portion of the Double Wall (Wall 1)	97
Figure 3.15: Cracking on South Portion of the Double Wall (Wall 2)	98
Figure 3.16: Cracking on Centre Wall (Wall 5)	98
Figure 3.17: Cracking on C-Wall (Wall 8)	99
Figure 3.18: Cracking on North East and West Out-of-Plane Walls (Walls 3 and 6).....	100
Figure 3.19: Cracking on North Portion of the Double Wall (Wall 1)	101
Figure 3.20: Cracking on South Portion of the Double Wall (Wall 2)	101
Figure 3.21: Cracking on Centre Wall (Wall 5)	102
Figure 3.22: Cracking on C-Wall (Wall 8)	102
Figure 3.23: Cracking on North East Out-of-Plane Wall (Wall 3)	104
Figure 3.24: Cracking on North Portion of the Double Wall (Wall 1)	104
Figure 3.25: Cracking on South Portion of the Double Wall (Wall 2)	105
Figure 3.26: Cracking on Centre Wall (Wall 5)	105
Figure 3.27: Cracking on C-Wall (Wall 8)	106
Figure 3.28: Cracking on North West Out-of-Plane Wall (Wall 6)	107
Figure 3.29: Cracking on North East Out-of-Plane Wall (Wall 3)	107
Figure 3.30: Cracking on North Portion of the Double Wall (Wall 1)	108
Figure 3.31: Cracking on South Portion of the Double Wall (Wall 2)	108
Figure 3.32: Cracking in Second Story of the Double Wall (Walls 1 and 2) and First Floor Slab.....	109
Figure 3.33: Cracking on Centre Wall (Wall 5)	109
Figure 3.34: Cracking on C-Wall (Wall 8)	110
Figure 3.35: Cracking on North East and North West Out-of-Plane (Walls 3 and 6).....	111
Figure 3.36: Cracking on North Portion of the Double Wall (Wall 1)	111
Figure 3.37: Cracking on South Portion of the Double Wall (Walls 2)	112
Figure 3.38: Cracking on C-Wall (Wall 8)	112
Figure 3.39: Cracking on Second Story of C-Wall (Wall 8)	113

Figure 3.40: Cracking on North West Out-of-Plane Wall (Wall 6)	114
Figure 3.41: Cracking on North East Out-of-Plane Wall (Wall 3)	114
Figure 3.42: Cracking on North Portion of the Double Wall (Wall 1)	115
Figure 3.43: Cracking on South Portion of the Double Wall (Wall 2)	115
Figure 3.44: Cracking in Slab Between Double Wall (Walls 1 and 2) at First Story.....	116
Figure 3.45: Cracking in Centre Wall (Wall 5)	116
Figure 3.46: Cracking on C-Wall (Wall 8)	117
Figure 3.47: Cracking on Second Story of C-Wall (Wall 8)	117
Figure 3.48: Cracking on North West Out-of-Plane Wall (Wall 6)	119
Figure 3.49: Cracking on North East Out-of-Plane Wall (Wall 3)	119
Figure 3.50: Cracking on North Portion of the Double Wall (Wall 1) at the Second Level	120
Figure 3.51: Cracking on South Portion of the Double Wall (Wall 2)	120
Figure 3.52: Cracking in Centre Wall (Wall 5)	121
Figure 3.53: Cracking on First Story of C-Wall (Wall 8)	121
Figure 3.54: Cracking on Second Story of C-Wall (Wall 8)	122
Figure 3.55: Cracking in North Portion of the Double Wall (Wall 1).....	124
Figure 3.56: Cracking in South Portion of the Double Wall (Wall 2).....	124
Figure 3.57: Cracking in Second Story of the North Portion of the Double Wall (Wall 1)	125
Figure 3.58: Cracking in Second Story of the South Portion of the Double Wall (Wall 2)	125
Figure 3.59: Uplift on North Portion of the Double Wall (Wall 1)	126
Figure 3.60: Cracking in Second Story of C-Wall (Wall 8)	126
Figure 3.61: Slab Failure Between Portions of the Double Wall (Walls 1 and 2) after Bar Rupture	127
Figure 3.62: Slab Failure Between the North Portion of the Double Wall (Walls 1 and 2) and the North East Out-of-Plane Wall (Wall 3).....	127
Figure 4.1: Preliminary Idealized Elastic-Plastic Building Behaviour	131
Figure 4.2: Weak Beam-Strong Pier Mechanism (Drysdale and Hamid, 2005)	133
Figure 4.3: Development of Plastic Moment through Idealized Hinges	135
Figure 4.4: Movement of Slab Corners	140
Figure 4.5: Movement of the Top Floor Slab South Face and Representation of Overall Building Movement.....	142
Figure 4.6: In-Plane Deflection of In-Plane Walls	143
Figure 4.7: Load-displacement Curves for In-Plane Walls (Wierzbicki, 2010)	144
Figure 4.8: Actual Building Response as Plotted versus Predictions	145

Figure 4.9: Load Displacement Cycles of $0.2\Delta y$ and $0.4\Delta y$	149
Figure 4.10: Pre-Yield Building Stiffness	149
Figure 4.11: Building Secant Stiffness Degradation	151
Figure 4.12: Elastic-Plastic Idealization for Reinforced Masonry Shear Walls.....	152
Figure 4.13: Idealized Elasto-Plastic Building Response	153
Figure 4.14: Wall Layout	163
Figure 4.15: Average Curvature Profile: North Portion of the Double Wall (Wall 1)	163
Figure 4.16: Average Curvature vs. Gross Load: North Portion of the Double Wall (Wall 1)	165
Figure 4.17: Predicted Displacement Based on Measured Average Curvature for Wall 1	166
Figure 4.18: Average Curvature Profile: South Portion of the Double Wall (Wall 2).....	168
Figure 4.19: Average Curvature vs. Gross Load: South Portion of the Double Wall (Wall 2)	169
Figure 4.20: Predicted Displacement Based on Measured Average Curvature for Wall 2	169
Figure 4.21: Average Curvature Profile: North East Out-of-Plane Wall (Wall 3)	170
Figure 4.22: Average Curvature Profile: North West Out-of-Plane Wall (Wall 6)	171
Figure 4.23: Average Curvature Profile: Centre Wall (Wall 5)	173
Figure 4.24: Average Curvature vs. Gross Load: Centre Wall (Wall 5).....	174
Figure 4.25: Predicted Displacement Based on Measured Average Curvature for Wall 5	174
Figure 4.26: Average Curvature Profile: South East Out-of-Plane Wall (Wall 4)	176
Figure 4.27: Average Curvature Profile: South West Out-of-Plane Wall (Wall 7)	177
Figure 4.28: Average Curvature Profile: C-Wall (Wall 8)	178
Figure 4.29: Average Curvature vs. Gross Load: C-Wall (Wall 8)	180
Figure 4.30: Predicted Displacement Based on Measured Average Curvature for Wall 8	181

List of Tables

Table 2.1: Geometric and Reinforcing Ratio for Each Wall.....	51
Table 2.2: Flexural Ultimate and Yield Strengths for all Walls.....	53
Table 2.3: Reinforcing Steel Yield Strength.....	60
Table 2.4: Floor Slab Concrete Compressive Strength.....	61
Table 2.5: Grout Strength	63
Table 2.6: Block Compressive Strength.....	64
Table 2.7: Prism Compressive Strengths.....	66
Table 2.8: Prism Stiffness Characteristics	68
Table 4.1: Summary of Building Analysis for Effect of Coupling	136
Table 4.2: Gross Load at Predicted Yield Curvature	146
Table 4.3: Predicted Conditions at Ultimate Capacity of Individual Walls.	157
Table 4.4: Predicted Equivalent Plastic Hinge Lengths Based on Various Equations versus Measured Extent of Plasticity.	160

1 Introduction

1.1 Background

Masonry is an ancient material still widely used in construction today. In times past, all masonry construction was unreinforced, taking advantage of the high compressive strength of the material. It was well-known that unreinforced masonry is not capable of carrying significant bending or shear stresses present in structures undergoing seismic loading. Reinforcing of masonry to improve resistance to seismic loading can be dated as far back as 1755 (Tobriner, 1984). Reinforcements were first made with wood framing located inside the structure and progressed to iron bars contained within the masonry. However, reinforced masonry was not widespread and most new construction was still unreinforced (Tobriner, 1984). Therefore, masonry structures in high seismic regions were very susceptible to collapse under earthquake loading. This was evidenced by the major destruction that occurred during the San Francisco (1906), San Fernando (1971) and many other earthquakes throughout recent history. As a result, masonry was no longer permitted or was severely restricted in its use as a building material in some high seismic areas. Furthermore, with the increasing prevalence of earthquake design in modern structural engineering, the use of masonry was further decreased. A key contributor to this reduced use of masonry as an engineering material is conservative code requirements causing prohibitively expensive designs which cannot compete with more modern materials. Current research is being

established to align current code requirements more closely to the actual behaviour of reinforced masonry as well as identifying new ways to improve seismic response of masonry structures.

Even when new methods of designing and constructing masonry with reinforcing were developed, masonry still had the stigma of an incapable seismic performer attached to it. In recent decades, significant research has been performed in the area of improving the seismic performance of buildings constructed of this material. The main focus of this research has been to achieve the ductility necessary to perform adequately during a seismic event. In order to attain this, modern masonry structures use lateral load resisting elements that are reinforced using bars similar to those found in reinforced concrete and detailed in a manner so as to promote ductility far beyond initial yield of the reinforcement.

The main building elements used to resist lateral loading in structural reinforced masonry buildings are shear walls. In a building setting, multiple shear walls are detailed and reinforced to supply the required lateral stiffness and load bearing capacity. In the event of an earthquake, they are the primary energy absorbing mechanism. Consequently, many experimental programs have been carried out to examine the behaviour of such walls under different axial and lateral loading conditions as well as with different reinforcing details (Paulay et al. 1982, Shing et al. 1989a, Shing et al. 1989b, Shing et al. 1990a, Shing et al. 1990b, Paulay and Priestley 1993, Kikuchi et al. 1999 and Shedid et al. 2008.) These different configurations are required to examine

the different failure mechanisms for shear walls. The two general modes are flexural and shear failure with flexural failure being the more desirable of the two.

Much of the research at this current state of knowledge is related to the performance of shear walls in isolation; that is, a structural element taken out of its normal context. This provides very useful information to researchers but does not present a complete picture of the behaviour of this element within a structural system. As such, current research trends, including this study, are turning towards testing of complete systems.

1.2 Problem Statement

The purpose of this study is to provide preliminary knowledge with regard to the ductility of reinforced masonry elements in a system setting. The testing will be performed on 1/3 scale masonry, units which has been shown by Abboud et al. (1990) at Drexel University among others to be representative of full scale masonry behaviour.

This project is part of a multiphase testing program that includes material, assemblage and component testing. Even the test conducted within this study only attempts to encompass one characteristic of a complete structure. In this case, inter-wall and diaphragm coupling actions were intended to be controlled through special design provisions of the inter-story slab. This plan was to allow this thesis study to focus mainly on the nature of load sharing and combined ductility of combinations of different shear walls.

As part of the ongoing testing program, tests in many different areas are being performed. However, certain tests are directly related to this research. For example, the characteristics of the individual walls found within this study's structure were tested separately by Wierzbicki (2010). These tests provide a clear picture of the behaviour of these elements outside of the context of the building system. With this information in hand, a direct comparison can be made between individual component behaviour and how those components behave within a structural system setting.

Structures undergoing seismic excitation will absorb energy in either an elastic or inelastic manner. To remain in the elastic state, the structure may have to possess a significant level of strength which is not feasible either architecturally or economically. In modern earthquake engineering, an equal displacement approach has been adopted. A perfectly elastic structure will attract a lateral seismic loading of V_e . A ductile structure that behaves plastically after V_p must be detailed in a manner such that the post-yield damage is minimized so as to allow plastic deformation. In other words, both structures achieve the same displacement, yet the more ductile structure requires much less strength. This reduction in required design strength is characterized by R ; a seismic reduction factor. As shown in Figure 1.1, lower design forces can be used through detailing a structure such that it may undergo inelastic deformation.

The limitation of this equal displacement principle is that the lower the lateral load capacity, the more ductility without loss of strength is required. However, the

need for large plastic displacements can lead to problems of excessive permanent drift that may affect the building function.

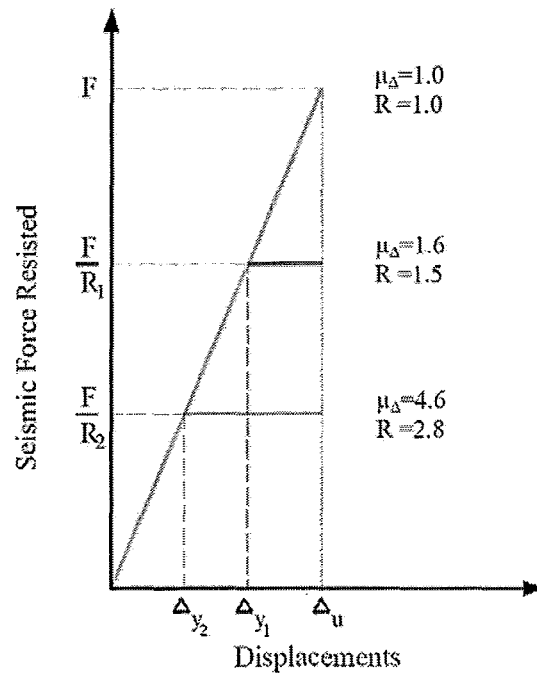


Figure 1.1: Seismic Reduction Factors Based on Equal Energy (Shedid, 2006)

As suggested previously, certain detailing is required to allow for load reduction factors to be used. As shown in Figure 1.1, the required strength for the more ductile structure is significantly less than the elastic strength requirement. This reduction in elastic demand is accounted for with force reduction factors. Therefore, the structure need only be designed for a strength of V_p , which is only V_e/R , where R is the reduction factor, if the appropriate level of ductility can be provided. The National Building Code of Canada (NBCC, 2010), referencing the detailing requirements found in the Canadian masonry design standard, CSA S304.1 (2004), allows a maximum load reduction factor of

2.0 for specially detailed masonry elements. Compared to reinforced concrete, which can have a reduction factor of 4.0 with the appropriate detailing, it becomes obvious that masonry is at a severe competitive disadvantage.

The main reason for this difference is the lack of sufficient proof of masonry's ability to achieve much higher levels of ductility. As mentioned previously, much research is geared towards masonry shear walls. Evidence of shear walls being able to achieve ductility levels of 12 times yield are available (Shedid et al. 2008). Since these principles have been well established, it is time to study these elements in the system setting so as to examine the effects of structural redundancy, torsion, and inter-wall coupling behaviour.

1.3 Research Significance and Objectives

The objective of this study is to bridge the gap between element behaviour and system behaviour in the area of reinforced masonry. Utilizing tests performed on the individual elements found in this experimental structure (Weirsbicki, 2010), a comparison between the two can be made. Data from these studies will inform researchers of the effects of redundancy on the system performance due to combinations of dissimilar walls and inter-wall coupling. It will also show whether the redundancy inherent in a system can provide additional energy dissipation to improve seismic performance on top of the given ductility levels of the individual elements. The end goal of the research program which encompasses, assemblage, element and system testing is to provide information leading to the modification of the seismic reduction

factors found in CSA S304.1 (2004) to more accurately reflect the true behaviour of reinforced masonry structures.

1.4 Scope

This is the first step in a major test program at McMaster University intended to bridge the gap between element and system testing. As such, this particular test attempts to limit the parameters being evaluated.

For this test program, testing of an experimental shear wall building was chosen to achieve the above objectives. The main parameter to be examined is structural redundancy which is inherent to the building system and must be addressed. It was intentionally made more complicated by choosing walls having large differences in strength and stiffness. As will be shown in Section 2.5, special design details were adopted in the building specimen in an attempt to control the effect of inter-wall coupling. Individual wall instrumentation was chosen to be concentrated on the first story of the structure while the global displacement of the structure was monitored at the level of each floor slab. Data collected included vertical and horizontal deflections along with reinforcing bar strains and lateral load. From this, the load-displacement response of the structure can be presented to establish the displacement ductility of the structure. Also, more detailed data will be examined including the extent of plasticity in the wall elements and their curvature profiles.

1.5 Literature Review

1.5.1 Introduction

In recent decades, many different parameters such as aspect ratio, axial load level, and reinforcement levels have been examined with respect to reinforced masonry shear walls. This literature review will focus on identifying the most relevant knowledge of reinforced masonry systems to date. Very few papers and projects actually involve representative reinforced masonry buildings. Therefore, while these few projects will be presented, other relevant research material will also be touched on including current standards and codes, general flexural shear wall behaviour, reinforced masonry structural behaviour, diaphragm behaviour, structural inelastic torsional response as well as the effects of test specimens scaling on the observed system behaviour.

1.5.2 Masonry Codes and Standards

In Canada, the National Building Code of Canada (NBCC, 2010) is the principle guide for the design of structures. It contains instructions on seismic design for all building types including masonry construction through referencing the Canadian Standards Association's Masonry Design for Building, CSA S304.1 (2004). As mentioned previously, if a structure is detailed in such a manner so as to safely undergo plastic deformations without significant loss of strength, a load reduction factor can be applied to the structural element. The NBCC (2010) defines the allowable reduction factors to be used for different construction types.

1.5.3 Seismic Reduction Factor

The study of earthquakes and their effects on structures has become increasingly necessary over the past century due to the severe effects of large loss of life and damage to the structural infrastructure. Many factors affect the response of a structure for different seismic excitations. Miranda and Bertero (1994) gathered together all previous research in the area of seismic reduction factors and presented them in a common manner. They concluded that choice of reductions in required strength stemmed from the maximum tolerable displacement ductility demand, the period of the system and the soil conditions at the site. They also noted that other factors that would affect the reduction factor in a less significant way would be the hysteretic behaviour and damping of the structure as well as the distance to the epicentre of the earthquake. By presenting this compiled information, their goal was to encourage the use of ductility, period and site conditions for strength reductions factors along with estimates of overstrength to be used in seismic design.

The above approach was described and adopted in a similar manner by the Applied Technology Counsel (ATC, 1995). Their design philosophy allows for non-catastrophic inelastic deformation of a structure given a very rare seismic event. This limitation is to account for the fact that it would be uneconomical and impractical to design all structures to remain elastic through any possible seismic event. As such, the reduction from strength required for elastic behaviour, given equal energy absorption, is accounted for via the use of force reduction factors usually described by an R with

subscripts describing the reason for the reduction. These factors are based on structural ductility, over-strength, period of vibration and system redundancy (ACT, 1995).

In Canada, as defined by the NBCC (2010), there are two seismic reduction factors, one based on ductility defined as R_d , and one based on over-strength defined as R_o . These are also dependent on the parameters mentioned above.

These factors have been established over many years of research in this area. Chopra (1995) showed that the force modification factor is heavily dependent on the fundamental period of the structure. If a structure is very stiff, its period of vibration will be very low. Described as the equal acceleration principle, the stiff structure will accelerate with the ground behaving elastically and therefore have no reduction at all ($R = 1.0$). In a masonry system, this would be the case if the initial stiffness continued to exist over the complete seismic event. However, as masonry deforms, it cracks, and this cracked structure will have a reduced stiffness and, therefore, a longer period of vibration. Chopra (1995) indicated that for structures exhibiting a low to moderate period of vibration, the principle of conservation of energy should be used. In Canada, the principle of equal displacement is utilized to determine the seismic reduction factor. This can be described as an elastic perfectly plastic system and the reduction factor can be described as:

$$R = \mu_{\Delta} = \frac{\Delta_u}{\Delta_y} \quad (1.1)$$

where:

$$\mu_{\Delta} = \text{Displacement Ductility}$$

$\Delta_y =$ Yield Displacement (mm)

$\Delta_u =$ Ultimate Displacement (mm)

After examining the NBCC (2010) provisions for calculations of R_d , it can be seen that there is no specification for overall system ductility. Uang (1991) pointed out that while research in specific structural elements has defined their strength reduction factors experimentally, there is no agreement in the engineering profession about how the concept of ductility factor should be applied at the structural system level. He concluded that establishing reduction and overstrength factors for multistory building structures that exhibit significant strength and stiffness degradations is still a major obstacle. However, as will be shown from literature, the fact that reinforced masonry can incur deflections beyond yield without suffering significant strength losses makes it comparable in ductility to other building materials such as reinforced concrete.

1.5.4 Masonry Codes

The current Canadian standard for masonry design is CSA S304.1 (2004). In this design standard, provisions are made for the design of masonry shear walls. It outlines specific detailing requirements that are necessary to achieve certain levels of ductility related force reduction factors. First, any unreinforced masonry wall is assigned a force reduction factor, R_d , of 1.0, that is, the elastic design force is not reduced. Conventionally reinforced masonry walls are assigned an R_d value of 1.5.

Similarly, limited ductile shear walls are allowed an R_d of 1.5. These walls must have a height to length ratio of greater than one. The strain limitation for these walls is

satisfied when the length of the compression block, c , is less than 20% of the length of the wall. The wall height to thickness ratio, $h/(t+10)$, should also not exceed 18 in that compression zone. Finally, the compressive strain is limited to 0.0025 in the plastic hinge zone.

Moderately ductile shear walls are assigned an R_d value of 2.0. These walls must meet the requirements of walls with limited ductility as outlined in the previous section but also have more strict limitations. The unsupported section of the wall in the compression zone should satisfy the equation $h/(t+10) \leq 14$ where h is the height of the wall and t its thickness. Furthermore, the compressive strain limitation is deemed satisfied if the length of the compression block, c , is less than 20% of the wall length for walls of height to length ratio of less than four and 0.15 times the length of the wall for walls with a height to length ratio more than 4 but less than 8. The final category of shear walls is squat shear walls with moderate ductility. These are also assigned the load reduction value of 2.0 and are separated from regular moderately ductile shear walls by their height and length ratio being limited to one. They also must have a height to thickness ratio, $h/(t+10)$, of less than 20.

These reduction factors are quite low when compared to those allowed by the NBCC (2010) for reinforced concrete. With special reinforcing provisions, R_d values of up to 4.0 are permitted (NBCC, 2010). As mentioned previously, the NBCC (2010) also allows for an overstrength factor (R_o) in addition to the ductility-related force modification factor R_d . For reinforced masonry, R_o is defined to be 1.5 while a factor of

1.7 is permitted for reinforced concrete. The resulting total seismic reduction factors are 3.0 for reinforced masonry ($R = R_d \times R_o = 2.0 \times 1.5 = 3.0$) and 6.8 for reinforced concrete. Furthermore, ASCE 7 (2008) provides the same seismic reduction factors of 5.0 for specially reinforced masonry or reinforced concrete shear wall buildings.

The conservative nature of CSA S304.1 is also illustrated when examining the Masonry Standards Joint Committee Code (MSJC, 2008), where much greater R values are sanctioned for reinforced masonry walls which are comparable to reinforced concrete elements. This standard contains three categories of reinforced masonry shear walls including, ordinary, intermediate and special walls corresponding to load reduction factors of 2.0, 3.5 and 5.0 respectively. Ordinary walls are to be used in areas of low or moderate seismic risk and this level of performance is reached by designing a wall which has a strain gradient such that the strain in the extreme tensile reinforcement is at least 1.5 times the yield strain when maximum compressive strain in the masonry is reached. For intermediate level walls which are also only applicable to low and moderate seismic zones, this ratio should be 3.0 or more. Finally, for special walls which are permissible in all seismic zones, it should be at least 4.0. To achieve these strain gradients, guidelines for horizontal and vertical steel along with their spacing are given (MSJC, 2008). These large differences noted for seismic reduction factors along with the literature presented earlier suggests that the values for masonry construction as allowed for by the NBCC (2010) are quite conservative.

1.5.5 Reinforced Masonry Shear Wall Behaviour

As mentioned before, reinforced masonry shear walls exhibit two general failure modes namely; shear and flexure. Shear failure is characterized by diagonal cracking caused by tensile failure of the masonry (Shing et al. 1989b). Paulay et al. (1982) demonstrated that, even in squat shear walls, this failure mode can be prevented through proper detailing of the horizontal reinforcement. Proper detailing of shear reinforcement can improve the failure mechanism by preventing brittle shear failure. Shear failure is well known as a brittle failure mode and is not desirable for seismic response. Similar to the intent of code design, shear failure was eliminated in this study through over-design of the horizontal reinforcement. Therefore, flexural failure was the intended failure mode for each wall in this study and as such, shear failure will not be examined here in great detail.

Since the flexural failure mode is the focus of this study, it will be examined in detail to present the current state of research knowledge at the time of this experiment. Flexural failure of reinforced masonry is characterized by tensile yielding of the reinforcing steel at one end of the wall followed by the crushing of the masonry at the compression end of the wall (Shing et al.1989a).

Shing et al. (1989b) performed a study in the area of flexural failure by testing 16 reinforced masonry walls with different reinforcing levels, aspect ratios and magnitudes of applied axial stress. They concluded that reinforced masonry panels could exhibit significant ductility levels and therefore were appropriate for seismic

resistance design provided that proper reinforcing guidelines were developed and followed. In this study, they noted that walls with a larger aspect ratio (height/length) exhibited a more ductile flexural response than their more squat counterparts. They also found that the failure mode of a wall can be changed from a brittle shear mode to a more ductile flexural mode through the addition of sufficient distributed shear reinforcement.

In this study, Shing et al. (1989b) also demonstrated that increasing the axial load on a shear wall increases both flexural strength and stiffness. They attributed this to the fact that increasing the axial load caused a larger compression zone in the wall which limited the flexural cracking. The increase in strength was also accompanied by a trend towards less ductility. In the extreme, increasing the axial loading could produce brittle failure by increasing the maximum compression stress in the toe of the wall resulting in premature crushing of the toe prior to yielding of the tensile reinforcement. Additionally, the higher compressive strain due to the axial load would increase the curvature and, subsequently, the drift observed at first yield. Conversely, at failure, lower levels of curvature and drift correspond to a more brittle failure mode. Therefore, increasing the axial loading would reduce a shear wall's level of ductility by reducing Δ_u and increasing Δ_y . This is not desirable for design in highly active seismic regions (Shing et al. 1989b).

In subsequent papers (Shing et al., 1990a; Shing et al., 1990b) they noted that the strength of wall panels could be quite accurately predicted using simple flexural

theory based on the plane-sections remaining plane assumption. They also suggested that the actual flexural strength of a wall may be greater under seismic loading due to strain hardening that would occur under cyclic loading. On the other hand, they also noted that including strain hardening on walls with low axial stresses would overestimate the flexural strength. Therefore, consideration should be given to limiting when one should include strain hardening. Nonetheless, through this study, they did still demonstrate that walls with high axial stresses could behave in a ductile manner by properly confining the toes of the walls.

1.5.6 Plastic Hinging

The flexural ductility demand required for shear walls is satisfied through inelastic deformations at the base of the wall. This so called plastic hinge zone in the wall provides large inelastic curvatures via plastic yielding of the vertical tensile reinforcement. This plastic region extends up to different heights of the wall depending on the configuration of the wall's design and loading condition. As such, the plastic curvature extending over the height of the wall is not uniform and a method needs to be adopted to idealize this curvature profile. Paulay and Priestley (1992) broke the wall down into two parts. They suggested using an equivalent plastic hinge zone with a length l_p having constant plastic deformation combined with an elastic zone over the full height of the wall. In this model, the assumed constant plastic rotation was defined to rotate about the mid-height of the plastic hinge. They related the height of the

equivalent plastic hinge region to the wall length and concluded that it varied from 30% to 80% of the wall length.

They presented empirical equations for equivalent plastic hinge length that did not match well with their following experimental results. They suggested that these discrepancies occurred because the formulations did not account for the tensile straining of the bars into the foundation or the spread of plasticity throughout the entire wall due to shear cracking. Diagonal shear cracking increases deflection therefore adding to the total deflection. Both of these behaviours add additional strains into the steel beyond those predicted by the equations.

In a later publication, Paulay and Priestley (1993) examined the stability of ductile structural walls. They noted that walls with no end elements that have undergone plastic deformations can become unstable as the loading is reversed. This is due to the fact that since the vertical steel has undergone plastic deformation, the flexural cracks will not close with removal of the lateral load. Therefore, as the loading is reversed, the vertical steel is the only material initially providing compressive resistance. Stability becomes a problem given that masonry shear walls only can house one line of reinforcing bars. They suggest a minimum wall thickness as the preventative measure for this problem.

Drysdale and Khattab (1995) performed biaxial stress tests on both unreinforced and reinforced masonry so as to examine the effects of the bed joint orientation and

amount of reinforcement on the failure modes of masonry. This test had the advantage of having very specific stress states and boundary conditions so that no idealizations had to be made. They concluded that for reinforced masonry, the bed joint orientation did not matter when the failure mode was tensile but was very important when the failure was compressive. They related this to the lack of confinement in reinforced masonry. Another conclusion made was that it is incorrect to relate the effectiveness of shear reinforcement solely to the percentage of reinforcement present. Rather, it also depends on the direction in which the reinforcement is oriented. Ensuring that there is shear reinforcement both parallel and perpendicular to the bed joints is essential implying that the vertical reinforcement in a shear wall must also be designed to accommodate some shear loading.

In another study, Kikuchi et al. (1999) performed experiments on eight full scale reinforced concrete and masonry walls each with varied levels of reinforcement including grouted masonry walls with the face shells removed. For walls with the face-shells removed, they noted that the presence of the webs did reduce the ultimate lateral strength and stiffness of the bearing walls. From this study they found that reinforced masonry walls have similar seismic capacity to the reinforced concrete specimens including almost the same ultimate strength, initial stiffness, deformation capacity and failure mode.

Most recently, tests on six full scale reinforced masonry walls were performed at McMaster University by Shedid et al. (2008). In these walls, the amount of vertical

steel, and applied axial stress were varied. This study was intended to examine how these parameters affected the ductility and energy dissipation characteristics of the walls. They concluded that as axial load increases, a slight reduction in ductility occurs and that the displacement ductility of the walls was highly dependent on the amount of vertical reinforcement present. As the amount of vertical reinforcement was increased, the yield displacement also increases thereby lowering the displacement ductility that can be achieved. Yield displacement also increased for walls under increased axial compressive stress. They also found that the zone of plasticity for these walls extended up to a height of half the length of the wall but less than 150mm into the foundation. Displacement ductility's ranged from 1.9 to 4.6. It was noted that ignoring the compression reinforcement in the analysis of the walls yielded conservative results while including it gave a closer prediction of the onset of yield as well as the ultimate capacity especially for walls subjected to high compressive stress. This test program illustrated that masonry walls can behave in a ductile manner up to and beyond usable drift levels.

1.5.7 Testing of Building Systems

Fully reinforced masonry system behaviour is an area that is relatively uninvestigated. Most studies in this area do not gather data or present data that involve modern ductility philosophy. Furthermore, because studies in the area are rare, an extensive search was performed to find as much information as possible on previous

reinforced masonry system testing. Therefore, studies of confined masonry are included as well as those related to reinforced masonry.

The testing of reinforced masonry building systems for the purpose of examining energy dissipation was performed by Abrams (1986). The experimental program, 'Measured Hysteresis in a Masonry Building System' involved subjecting a full-scale symmetric reinforced masonry structure to repeated, reversed cyclic lateral loading. The information available for this experiment was quite limited but a significant usable conclusion from this test study was that the reinforced masonry structure lost a significant amount of stiffness while undergoing reversed cyclic loading. Essentially, the ductility of the system was poor because of the inability of the structure to maintain its strength while undergoing repeated loading cycles.

In addition to the conclusions drawn from this paper, it should be noted that the type of loading this building underwent was load controlled; not displacement controlled. As such, with three cycles at each load level being performed, the deflection of the third load cycle under the same load would have been much greater than the first (not presented). Therefore, the displacement ductility characteristics of the structure cannot be discerned accurately from the given information.

In the early 1990's at the University of California, San Diego, a five-story full-scale reinforced masonry building was constructed and tested. The test was part of the Technical Coordinating Committee for Masonry Research (TCCMAR) program for

furthering the understanding of reinforced masonry. The goal of the experiment was to confirm new design guidelines that had been implemented in highly active seismic regions.

This study examined the effects of coupling structural walls, the effective width of the floor slab contributing to seismic response and the effects of T and L shaped flanges on the ends of structural walls. This test was aimed at examining new design philosophies in the masonry field including; uniformly distributed vertical reinforcement for ease of construction, reduced vertical reinforcement and increased horizontal reinforcement to more evenly distribute small diagonal cracks, no lap splices in the first story to prevent brittle bond failure, decoupled doorway lintels and confined coupling elements between the two walls of the test specimen creating reliable local ductility. The building was subjected to 75 different tests including General Sequential Displacement, Quasi-static Inverse Triangular load, stiffness and shakedown tests (Seible et al. 1993 and 1994).

This test showed that higher mode effects can have a significant impact on the level of base shear that the building experiences. However, as plastic hinges develop in the structure, these higher modes have less of an effect while the first mode shape dominates the system behaviour. The structure exhibited significant displacement ductility in both directions; $\mu_{\Delta} = 9$ in the push direction and $\mu_{\Delta} = 6$ in the pull direction. This result far exceeded the desired displacement ductility of 4 and the calculated ductility's of 5.5 and 2.2 in the push and pull directions respectively. This test shows

clearly that ductile design of masonry building systems is possible and that, with some study and modified parameters, improvement is also possible (Sieble et al. 1993 and 1994).

In a paper published in 1994, Tomazevic and Weiss examined the seismic behaviour of plain and reinforced masonry buildings. This study included the testing of 1/5th scale parts of two buildings under simulated seismic ground motions on a simple earthquake simulator. It is unclear from the literature as to what extent the building was grouted or if the specimens were of confined masonry. Either way, the horizontal steel was placed in the mortar joints and the vertical steel was concentrated at the ends of the wall. It also was noted that the strength of the model materials was significantly different from normal material strengths. While the full scale and model masonry strengths were comparable at 6.3 MPa versus 5.3 MPa, the strength of the model steel was less than a quarter that of normal reinforcing bars only having a yield strength of 93 MPa. However, even with this factor considered, the results are still valid given the positive effects of the presence of the steel; if the steel had been more representative, the test results would have been enhanced. Tomazevic and Weiss (1994) noted that, if the walls are not reinforced, the flexural capacity of their sections above and below the walls was too low to activate the flexural capacity of the tie beams and floor slabs they interacted with. On the other hand, reinforced structural walls behave like vertical cantilevers coupled with the horizontal structural elements. This led to the conclusion that even with this light reinforcement, this type of masonry building could withstand

repairable damage up to a peak ground acceleration of 1g. The force reduction factors calculated from the data gathered for the reinforced and unreinforced buildings were equal to 3.74 and 2.84 respectively demonstrating significant ductility capacity.

In a follow up study, Tomazevic and Klemenc (1997) examined similar models of confined masonry and found that these structures could withstand repeated shakings at levels of 1.3g. Both of the models tested, M1 and M2, were identical in configuration. However, M1 was tested longitudinally while M2 was tested transversely. The test along the transverse axis was to examine the effects of torsion for unsymmetrical confined masonry buildings. While the actual torsional behaviour of the model M2 was not discussed, they did note that the reduction factor for the transversely loaded, and therefore unsymmetrical model, was lower than its symmetric counterpart. They calculated values of 2.91 and 2.47 for models M1 and M2, respectively.

Zonta et al. (2001) performed a study on a reinforced masonry structure for the purposes of identifying the ductility reinforced masonry and the effects of using a reduced scale model. They subjected a 1/3 scale model to scaled accelerations so as to examine the dynamic behaviour of the structure. They found that the structure achieved displacement ductility of approximately 7.5 at the ultimate state and declared this definitively satisfactory (Zonta, 2001).

Kelly (2007) performed a shaking table test of a slice of a 7 story full scale reinforced concrete structure. The structure was subjected to white noise tests as well

as four earthquake loadings. The challenge was to invent a blind prediction test to try and predict the response of the structure. It was found that with regular analytical techniques that ignored so called secondary elements of the wall, namely the column and orthogonal flange wall, the model gave reasonable displacement predictions but significantly underestimated the base shears and moment of the structure for all excitation levels. In fact, the model underestimated the base shear and moments of the structure by 30% for the moderate level earthquakes. However when these components were included, the model predicted the displacements, accelerations, shears and moments to within 10% of the actual response. This study showed the importance of including all elements of a system when attempting to model its response. From this it is noted that utilizing these parameters in design will also improve structural response.

1.5.8 Testing of Diaphragm Influence

Tena-Colunga and Abrams (1996) examined the seismic behaviour of structures with flexible diaphragms. The data for this project was collected from in-situ buildings that were instrumented and withstood the Loma Prieta Earthquake in 1989. While two of the three structures only contained unreinforced masonry, one of the structures in this test program contained grouted and reinforced clay-unit masonry shear walls. The data collected clearly showed that structures with flexible floor diaphragms behave in a much different manner than those with rigid diaphragms. This real world study showed

that torsional effects could be reduced considerably as the flexibility of the diaphragm is increased.

As mentioned before, most of the testing in the area of masonry systems has been performed on structures with highly irregular plans. The level of complexity involved makes it difficult to assess the effects that different parameters have on the structure. One exception to this norm is a study performed by Cohen et al. (2004a, b, 2006). This study examined the behaviours of two half-scale reinforced masonry structures; one with a diaphragm of diagonal sheathed lumber and the other with a welded metal deck diaphragm. These buildings were representative of buildings owned by the United States Army that were deemed to be seismically vulnerable and were subjected to earthquake ground motions on the Tri-axial Earthquake and Shock Simulator at the United States Army Construction and Engineering Research laboratory. Following the shaking table tests, the diaphragms of each specimen were then tested quasi-statically in their own plane. Cohen et. al. (2004a) noted that, unlike previously thought, buildings with flexible roof diaphragms do not behave as single degree of freedom systems but rather as at least two degree of freedom systems. One degree of freedom would be associated with the in-plane response of the shear walls while the other would be associated with the in-plane behaviour of the diaphragm. This study also concluded that the potential seismic damage in walled structures with flexible roof diaphragms (one story buildings), cannot be completely characterized by inter-story drift, but that it must be characterized also by a measure of the in-plane deformation of

the horizontal diaphragms themselves (Cohen et al. 2006 and 2008). The shaking table tests caused cracking in the masonry but led to a failure of the diaphragm rather than the masonry. However, extensive cracking was noted in the out-of-plane walls and yield lines emerged on the in-plane walls. No data was collected in terms of ductility or curvature in any direction for any of the masonry walls. As such, the dynamic tests did not yield results relevant to this current study.

Rigid diaphragms on the other hand, distribute the lateral load between the in-plane walls of a structure according to their corresponding stiffness. The diaphragm also distributes the developed torsion to the out-of-plane walls (Drysdale and Hamid 2005). Given the significant behavioural differences between rigid and flexible diaphragms along with the special slab design provisions found in this study, extreme care must be taken to ensure that the slab maintains its rigid behaviour.

1.5.9 Torsional System Behaviour

Torsion in a building system occurs when the system centre of rigidity does not coincide with the centre of mass. Therefore, under seismic excitation, the inertia forces which act through the centre of mass cause a torsional moment about the centre of rigidity (Drysdale and Hamid 2005). The NBCC (2010), dictates that an additional $\pm 10\%$ eccentricity be added to the calculated value due to the uncertainty of the location of the centre of mass. Drysdale and Hamid (2005), present a method for calculating and redistributing the torsional moment developed in an unsymmetrical structure based on the stiffness of each wall and its distance from the centre of rigidity.

Bertero (1995) presents an equation based on classical plastic theory to account for inelastic torsion in a structure. This equation is only useful for Coaxially Coeccentric Elastic-Perfectly Plastic buildings and he also suggests that this equation should be used for preliminary design. However, some of the conclusions drawn from his study are relevant for design. He presented a method to reduce the effects of inelastic torsion since it has been shown that torsion reduces the seismic resistance of a structure. These steps include; locate the centre of rigidity as close as possible to the centre of mass, increase torsional redundancy, locate torsion resisting planes as far from the centre of rigidity as possible, select the ratio of strength between the x and y axes to be as close as possible to one and select the torsional capacity to be at least 20% larger than the relative torsional demand.

Paulay (1996) performed an investigation into the behaviour of torsionally unbalanced systems. He defined two categories of structures, those that were torsionally restrained as the result of having transverse torsion resisting elements that remain elastic during earthquake motions and those that were torsionally unrestrained in which there are no torsion resisting elements or all these elements yield during earthquake motions. For the torsionally unrestrained structures, he makes the argument that, if the centre of rigidity of the building deviates slightly from the location of the centre of mass, the resulting eccentricity would cause massive ductility demand from the weaker side of the building. The logic behind this statement is that, without torsional restraint and under the elastic perfectly plastic behaviour assumption, the

weaker wall will yield while the stronger will not. With no residual stiffness or prevention of twist, the stronger wall will not yield while the weaker will deflect without restraint. The result is a system with a reduced ductility level. This led to the conclusion that restraining buildings with elastic elements would produce more ductile structures since all in plane elements would reach full yield.

In a following paper, Paulay (1998) further examined these principles. He pointed out that while there is a good understanding and employment of capacity design whereby the lateral force resisting system is suitably designed and detailed for energy; there is no strategy in this area to deal with inelastic torsion. This publication attempts to present principles relevant to kinematically admissible torsional plastic mechanisms. These were established by the study of structural system response to static actions in order to clearly define mechanisms associated with story translation and story twist. He provides a method for design rather than analysis to ensure that when torsion induced displacements occur, the ductility demand, which would be greatest for elements having the smallest yield displacement, is not exceeded.

Humar and Kumar (1999), performed additional analytical studies on single story, torsionally unbalanced, that is unsymmetrical, structures to examine the effects of orthogonal in-plane elements on the torsional response of a structure. They noted that in the elastic range, it does not matter if the structure is unsymmetrical or not or if it has orthogonal torsion resisting planes. However, when a building is torsionally unbalanced and is pushed into the inelastic range, these orthogonal planes reduce the

ductility demand for the flexible planes, (referring to the relatively more flexible in-plane shear walls), but not significantly. They also pointed out that the ductility demand on the stiff end wall of the building might even be increased depending on the value of the frequency ratio of the uncoupled rotational frequency to the uncoupled translational frequency. From these studies, it can be seen that the presence of orthogonal elastic shear walls, while helping with overall torsional resistance, may not have much effect on the overall ductility demand of a structure.

In a recent study, Strathopoulos and Anagnostopoulos (2005) found that eccentric frame type buildings designed in accordance with EuroCode 8 and subjected to two-component earthquake excitations did not experience similar levels of inelastic deformation in all members. In fact, when comparing the response of an associated symmetric building, it was found that the frames on the flexible side of the building experience increased inelastic deformations while those on the stiff side underwent decreased deformations. The frames on the flexible side of the structure had ductility factors and damage indices that reached values of more than twice those of the stiff side. This imbalance of ductility demand can cause premature failure in the members on the flexible side and they suggest that this is not desirable for design. They also point out that their results are in opposition to those from investigations using simplified one-story shear-beam type systems. It is emphasized that such systems are not adequate models of multistory, frame-type buildings responding in the inelastic range and suggest that the basic assumptions used in these models be re-examined. These studies

highlight the fact that different structure types should be examined individually under torsion so as to properly identify their specific behaviours.

1.5.10 Effects of Scaling

In order to make the building test proposed in this thesis more feasible, a 1/3 scale sized block was chosen. While making the test easier to perform, it required an investigation into the effects of this scaling and how it could change the characteristics of the structural response.

Abboud et al. (1990) published a summary of their research findings related to the testing of reduced scale masonry. This research was performed at Drexel University in Philadelphia and spanned over 14 years. The authors concluded that the direct modeling of concrete block masonry techniques of fabrication, construction and testing is a viable and powerful method to study and improve, in an economical manner, the understanding of complex masonry systems. They have shown good correlation between the component materials and masonry assemblages to available prototype data (Abboud et al., 1990).

Tomazevic and Velechovsky (1992), performed tests on reduced scale masonry structures using a uni-directional earthquake simulator for the purpose of identifying whether or not small scale model testing would give representative data for their full-scale counterparts. Five models were tested; one full-scale model, two 1/3 scale models and two 1/5 scale models. They concluded that the correlation of experimental results

with the observed effects on masonry buildings indicates that reliable information related to the global seismic behaviour and failure mechanisms can be successfully obtained by testing small-scale models of buildings on simple earthquake simulators.

In 1996, Abrams published an article explaining the effects of scale and loading rate on the response of masonry structures. He compared results from tests performed on reduced scale and equivalent full scale specimens. He showed consistently that there were significant differences between the reduced scale and full scale tests when the tests were dynamic versus static. With slow strain rates he discovered a 21% decrease in strength and a 45% decrease in stiffness for a quarter scale building. This was attributed to increased crack propagation that occurred during the static test. For a dynamic test on a 3/8th-scale unreinforced brick masonry system, cracking and rocking of the pier elements governed the response. However, for a full scale system of the same configuration, sensitivities of the cracking pattern to variations in material properties and load application changed the dynamic characteristics of the large scale flexible diaphragm. This was due to the fact that inertial forces at the static rates were not being developed. An important finding from this study is that the shapes of the hysteresis relations for 1/12th scale reinforced concrete frame components were similar to those of large scale components with the same configuration and loading pattern. This would suggest that under static loading, the tests of scaled masonry for energy dissipation would be comparable to that of full-scale masonry.

1.6 Conclusion

When examining the NBCC (2010) and comparing it with other codes, it becomes evident that the load reduction factors used in Canada for reinforced masonry are excessively conservative. This is even supported by the fact that studies have shown reinforced masonry to behave similarly to reinforced concrete which is allowed much greater force reduction factors.

From the extensive research performed on masonry shear walls, it can readily be seen that reinforced masonry exhibits inelastic ductile behaviour. Further tests performed on masonry structures shows this principle even more clearly. However, more work in the area of masonry structures must be performed to better understand and quantify the system behaviour and ductility.

With proper understanding and analytical techniques to account for structural elements in their setting, proper load reduction factors can be established and used. If sufficient test results are presented, the design codes should be modified to more accurately reflect the true ductile response of reinforced masonry systems.

2 Experimental Program

2.1 Introduction

This experiment was designed to examine the inelastic response of a reinforced masonry structure constructed with a variety of shear wall shapes, each with its own load-displacement characteristics. The objective was to document the overall inelastic performance of the building as affected by the combined actions of the individual walls as some of the walls yield and lose stiffness at lower displacement levels than other walls. As a result of the changing relative stiffnesses of the walls, the influence on location of the centre of resistance and thus torsion was also of major interest. The test was part of a larger experimental program of testing seismic performance of 1/3rd scale reinforced masonry shear walls. Assemblage tests, cyclic tests of individual walls as well as additional buildings are being performed.

The assemblage testing was carried out to establish scaling factors for the 1/3rd scale masonry as well as to ensure that comparisons can be made between the 1/3rd scale results and full scale design. Some of the walls tested in isolation were designed to provide individual wall characteristics of those found in the 1/3rd scale structure to be tested in this research program. This information will allow conclusions to be drawn as to the legitimacy of methods used to analyze structures based on predicted properties of individual walls. As such, a more in-depth analysis of the complete masonry structure will be undertaken to provide advice on future analyses to determine design forces.

This chapter includes sections documenting the design and construction of the shear walls chosen for the building as well as the test setup. It also includes the masonry assemblage test results as well as the individual material properties determined by testing. A section will also be dedicated to documenting the instrumentation setup for the building. The chapter will conclude with the documentation and reasoning behind the test procedure.

2.2 Design and Construction of the Test Building

2.2.1 Introduction

This section contains documentation of the design process as well as the method of construction. Only 1/3rd scale 20 cm blocks were used for this experiment because it is the most common block size used in Canada. The third scale size was used to permit testing of a practical sized building aimed at providing reasonable representation of actual construction.

Only three types of blocks were used; end units without frogs, regular stretcher units, and half end units also without frogs. These are shown from left to right in Figure 2.1.

Special modifications were made to some blocks to accommodate the designed shear reinforcement. For each course with horizontal shear reinforcement, the webs or face shells of the blocks were notched to a depth of 25mm to allow the horizontal

reinforcement to be completely enclosed within grout via a horizontal passage. This is common practice in industry as blocks with knockout or depressed webs are available.

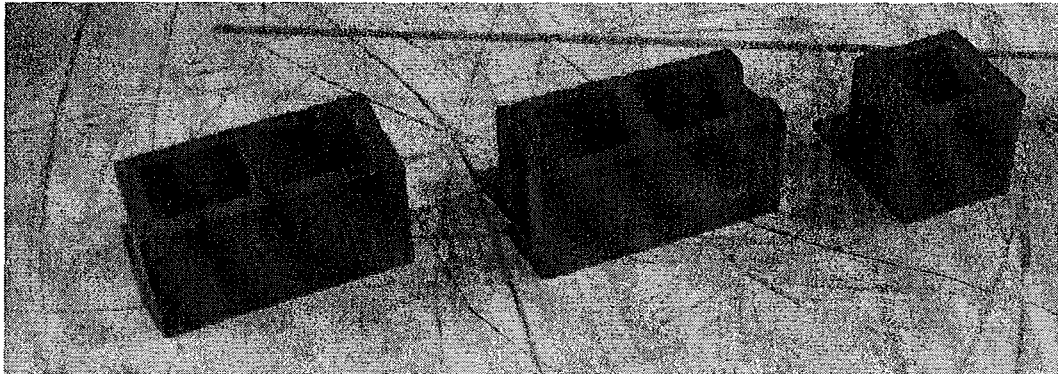


Figure 2.1: Blocks Used for Construction

2.2.2 Selection of Wall Dimensions

Initially, the intent of the design process was to create a building design based on seismic loading found in Victoria British Columbia. This location was chosen since the seismic provisions represented maximum loading for Canada. However, after examination of this option, it became apparent that, given the restricted layout and general experimental nature of the project, designing a building for actual seismic provisions would yield a building with very few shear wall elements and therefore would produce limited data. Therefore, in order to maximize the effectiveness of the test, an experimental layout was adopted that would incorporate a reasonable complex arrangement of walls and varied wall geometry.

The walls selected for this structure were chosen in conjunction with a colleague, (Wierzbicki, 2010), who would test the same walls in isolation. Given

restrictions in the setup for testing individual walls and the building test setup, the limitation of a reasonable building layout as well as the out-of-plane strength requirements resulted in the chosen layout after many different proposals had been considered. The decision was based on having the layout provide sufficient useable system data featuring a wide range of wall shapes and aspect ratios as well as having a general simplicity of the wall arrangement.

The goal of this building test was to examine reinforced masonry walls with flexure controlled capacities. Hence, the aspect ratios (height/length) of the walls were chosen to be greater than one. Based on previous work in this research area (Shedid, 2006), a minimum practical length of 600mm, corresponding to 1.8m length in full scale, was selected. Other wall lengths were selected based on achieving similar steel arrangements within the bounds of the aspect ratio limitation.

The rectangular walls (walls with no end elements) were all constructed with special block units at the end so as to have flat ends without any frogs. The middle units were regular stretcher units. A typical rectangular wall layout is illustrated in Figure 2.2.

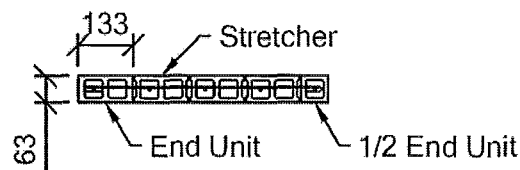


Figure 2.2: Typical Rectangular Wall

The C-Wall shown in Figure 2.3 was constructed similarly so as to have flat ends at the end of the wall as well as at the ends of the flange portion of the wall. All walls were built in a running bond pattern.

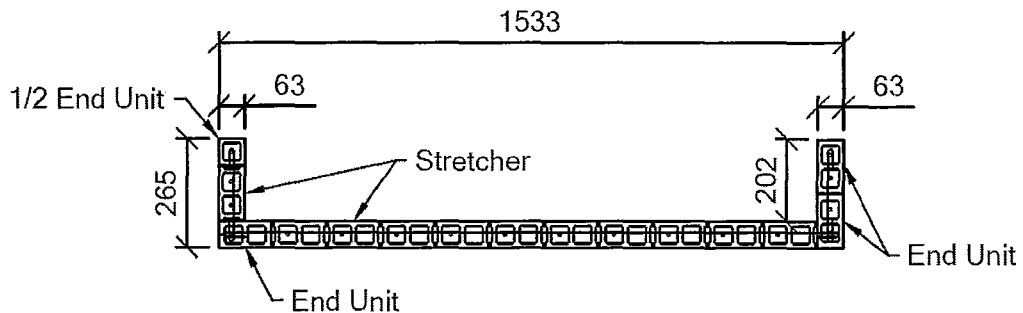


Figure 2.3: C-Wall (Wall 8) block layout

2.2.3 Building Layout and Dimensions

Given the laboratory area available for this test program, the building size was limited to 2.5 m by 2.5 m. For the first test in this program a slightly smaller size of 2 m by 2 m was chosen so as not to push the limits of the test setup with the first trial. The layout of the structure also was designed to be torsionally unbalanced in the plane of loading to include the effects of torsion on reinforced masonry structures. On the other hand, the building was designed to be balanced in the plane orthogonal to the loading plane so as to simplify the analysis of the torsional response. The full building layout can be seen in Figure 2.4.

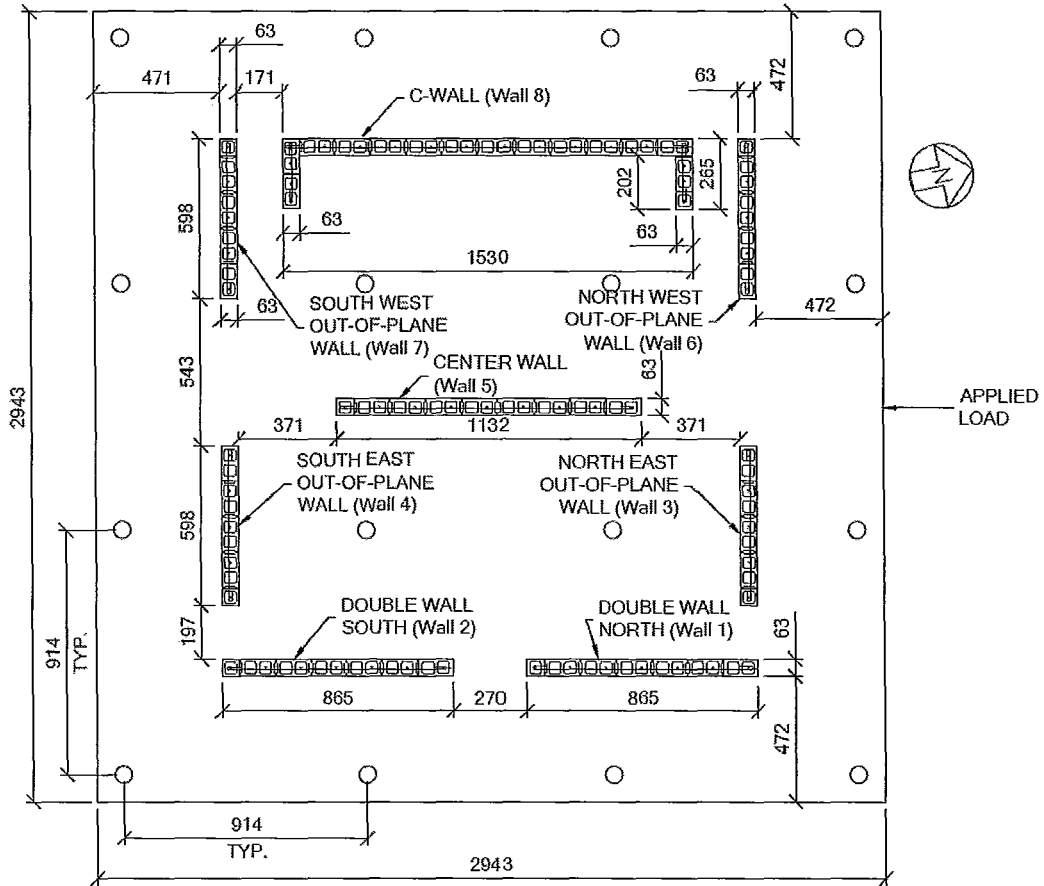


Figure 2.4: Final Layout of Experimental Building

The building layout had a torsional eccentricity of about 27% of the building width based on elastic gross uncracked section properties. The out-of-plane walls were designed to remain elastic while the in plane walls behaved plastically. This design characteristic was in response to literature suggesting that buildings that were torsionally unrestrained were very susceptible to seismic loading damage (Paulay, 1996).

Since the building was experimental in nature, the goal was not necessarily to design a realistic structure in terms of layout but rather a practical structure that would permit gathering of as much data as possible regarding inelastic structural response of reinforced masonry. That being said, the layout was chosen to be as realistic as possible given the dimensional and wall shape restrictions.

2.3 Construction

2.3.1 Foundation

The foundation for the structure was designed to not only fit into the test rig but also to provide a stable base for the structure. The foundation slab was designed to be 150 mm thick with top and bottom layers of No. 10 reinforcing bars spaced at 200 mm horizontally. This reinforcement was chosen based on a rough calculation of the moment that would be developed in the base due to the strongest wall. The calculated moment required No. 10 bars spaced at 400 mm to resist the loading but a spacing of 200 mm was chosen to avoid any possibility of foundation flexibility and also to accommodate the bolt grid in the strong floor of the laboratory. Orthogonal bars were added to resist any moment developed by the torsional response of the structure. Figure 2.5 shows the layout of the foundation slab reinforcement and how it fits in with the grid of bolt holes in the laboratory floor.

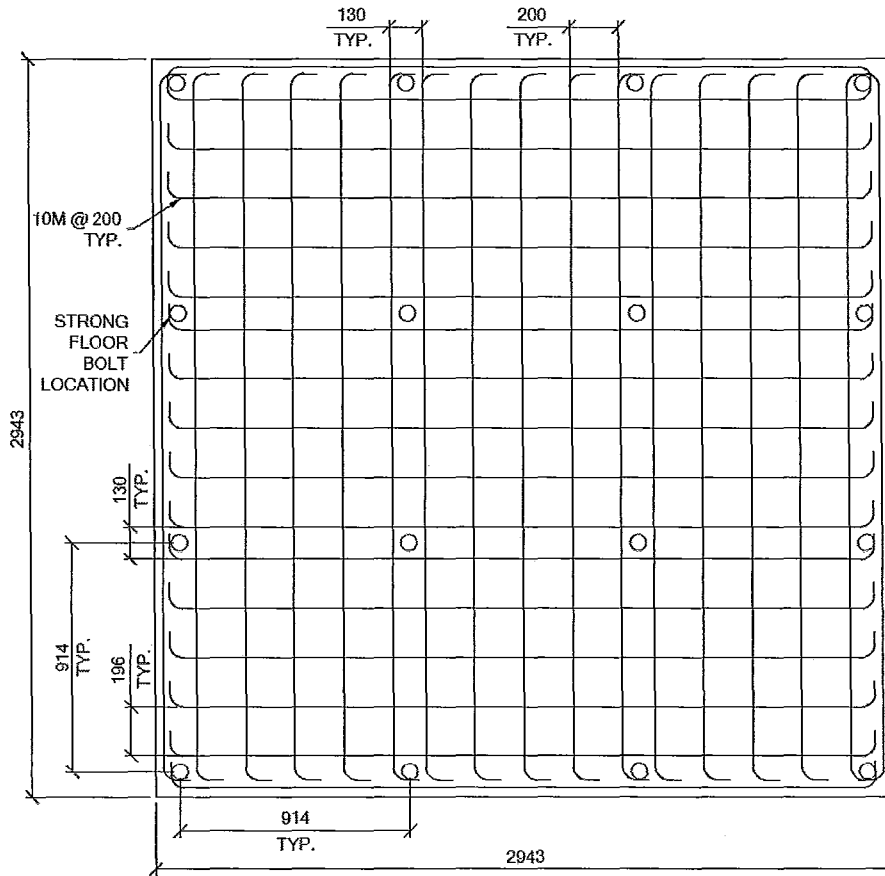


Figure 2.5: Reinforcing Bar Locations in the Foundation Slab

Figure 2.6 shows the vertical bars terminating in a 90 degree bend in the bottom of the foundation slab where they were tied to the slab reinforcing bars to help hold them in place during the pouring of the slab concrete. These bars extended up to over the entire height of the building to avoid any need for splicing of the vertical reinforcing bars. In effect, the foundation slab was over designed so that it would not become a factor in terms of deflections or vertical bar pullout.

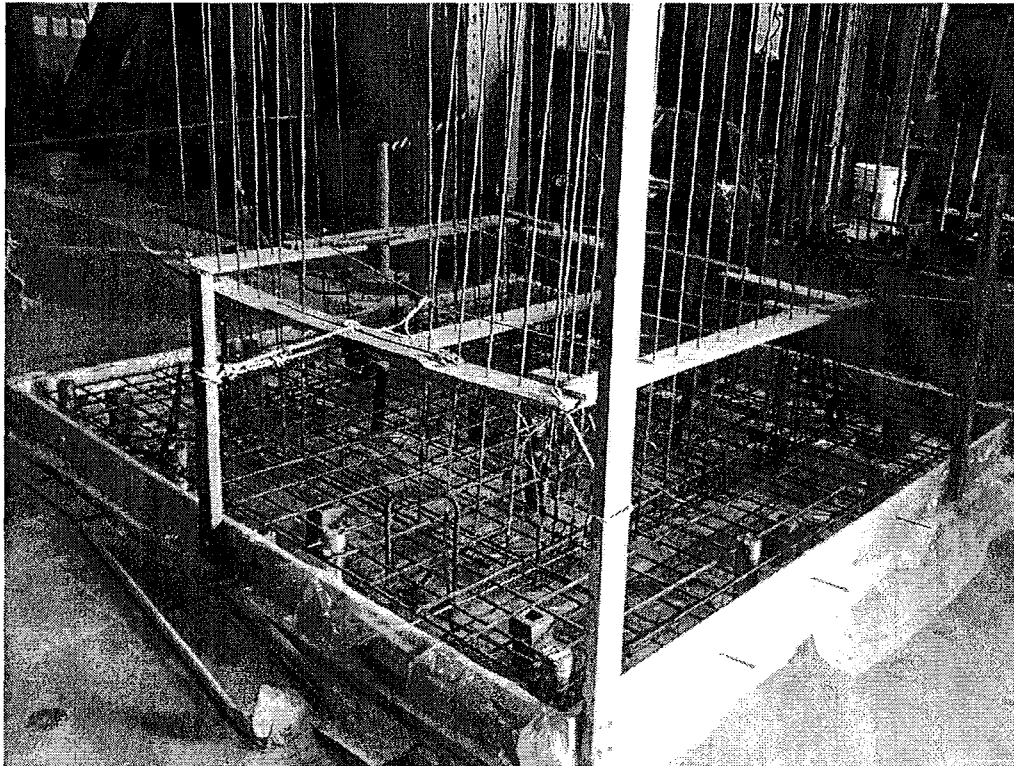


Figure 2.6: Photograph of Reinforcement Prior to Placing the Slab Concrete

In order to fasten the building into the test rig and the laboratory strong floor, a grid of holes was required for anchoring bolts to pass through. Since the slab was being poured on site, a grid of steel pipes was mounted in the floor to keep the holes open. The dimensions of the grid can be seen in Figure 2.5.

Great care was taken using surveying equipment to square the foundation and, more importantly, to accurately position the vertical reinforcing bars. The photograph also shows the wooden templates used to properly space the bars at levels above the foundation slab so that they would be formed in the proper arrangement. These templates were screwed together with wooden struts to hold the vertical bars in place.

This was an essential step in making sure the building was positioned properly on the foundation and had the same dimensions as given in the design drawings. The major effort required during this part of the construction process ensured that the rest of the construction process could proceed without difficulty.

2.3.2 Construction of Block Walls

The construction of the walls of the building was performed over the course of a six week period. Initially the process was quite slow due to the fact that the mason had to square the walls and work with some vertical bars that had shifted slightly during the placement of the foundation concrete. Furthermore, the blocks needed to be lowered from over a 2.5 m height corresponding to the entire length of the vertical bars. This was the only way to have vertical bars positioned in the walls without reverting to bar splices or using open-ended block.

The walls were constructed in a running bond pattern with 3-4mm mortar joints corresponding to the third scale construction. This was representative of equivalent full scale wall construction. The blocks were kept dry by being kept inside the climate controlled laboratory starting from a month prior to the beginning of construction as well as during the entire construction phase. The mortar properties were consistently maintained throughout the construction process by the drying of the materials prior to mixing. This was combined with precise material weights taken to arrive at consistent mixing ratios. Proper workability was monitored by performing flow tests on each batch shortly after mixing. Figure 2.7 shows the walls part way through the construction

process. The moisture showing in these walls was from the grouting process which will be described later.

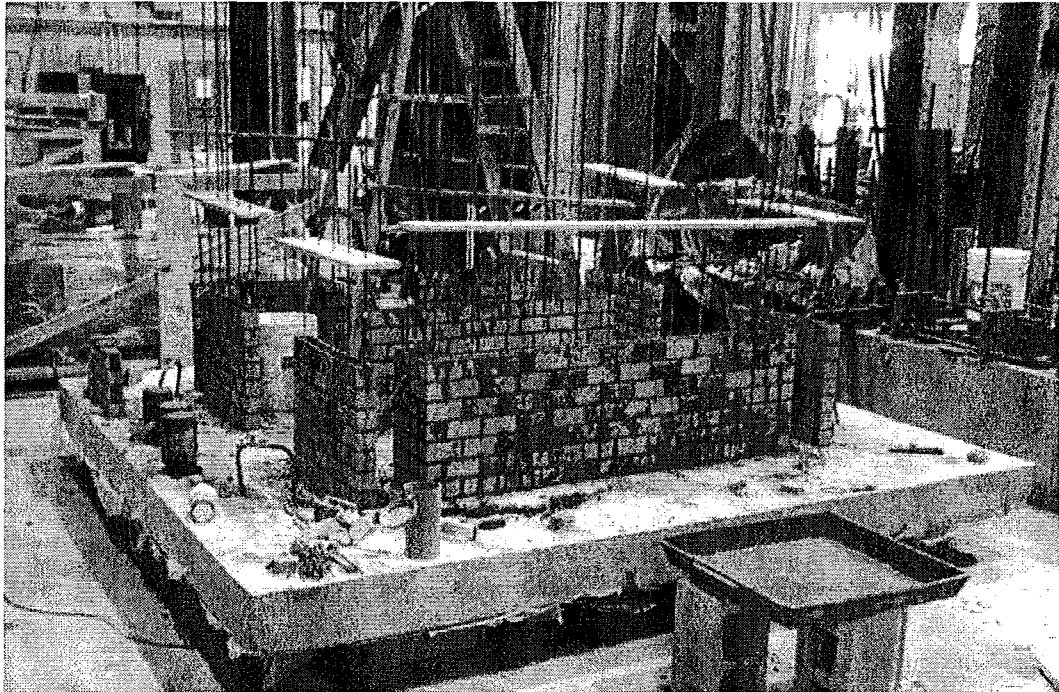


Figure 2.7: Partially Completed Wall Construction

2.3.3 Grouting of the Block Walls

Due to the small size of the cells in the $1/3^{\text{rd}}$ scale blocks combined with the large amount of horizontal steel, grouting of the walls was performed in four separate lifts to ensure complete filling of the cells. Each building story was 15 courses high. Therefore, the grouting of the wall for each story took place in two lifts; the first seven courses were grouted followed by building and grouting the remaining eight courses. Since the first floor of the structure is most critical in the flexural response of the building, greatest care was taken in grouting the lower half of the first floor. Even so,

the rest of the building was also very carefully grouted so as to avoid any voids in the wall that would adversely affect the system response.

The grout was designed and mixed in-house and poured by hand into the cells. (The small amount of grout required did not justify the use of ready mix grout and the 1/3rd scale blocks were much too small to accommodate any form of industrial pouring device.) The size of the blocks forced the use of an extremely fluid grout with an average slump of 275 mm. Placement of the grout was aided by the use of a regular pencil type concrete vibrator. Since the block cells were too small and access was blocked by reinforcement, the vibrator was used to vibrate the reinforcing bars as well as an additional bar used as a probe down the empty cells. The knockout webs in the walls that were cut to accommodate the horizontal reinforcing wire formed a horizontal column of grout that fully encased the horizontal shear reinforcement.

2.4 Design Details

This section contains information on the basic characteristics and layout for each of the walls found in the structure. The building consists of eight walls of four types. Each wall type shares some design similarities yet is unique in shape or dimension. Most testing in reinforced masonry has focused on rectangular walls. Yet, it is known that even structural walls intersect with other walls. As such, linear walls are, in fact, not the only type that needs to be tested for seismic performance. (Current testing at McMaster University includes masonry walls with end elements with several

different end element reinforcing and geometries.) This study extends the idea of testing the walls in isolation to testing these wall configurations in a system setting.

2.4.1 General Wall properties

The walls contained within this structure have many common design characteristics. All the walls contain shear reinforcement consisting of a W1.2 in every course in the first story and in every other course in the second story. This shear reinforcement is a 4 mm diameter drawn wire having a cross sectional area of 11 mm^2 . The vertical reinforcement consists of a 7.6 mm diameter D7 deformed wire resulting in a cross sectional area of 45.2 mm^2 . All linear walls are reinforced vertically with these bars in every other cell of the masonry blocks resulting in a bar spacing of 133.3mm. The only exception to this is in the end element of the so-called C-Wall where there are bars in every cell resulting in a spacing of 66.7mm. All walls were fully grouted using the procedure previously described. The following figures show the individual layout and detailing of each type of wall.

2.4.2 The C-Wall (Wall 8)

This wall was the strongest of the in-plane walls but the most squat with an aspect ratio of 1.44 and had the largest reinforcing ratio at 0.66%. It was located at the West end of the building and oriented in the plane of loading. It had a calculated ultimate moment capacity of 332 kN-m which required a lateral load of 150.9 kN at its top. The calculated yield moment for this wall assuming elastic behaviour was found to be 247 kN-m. This yield moment capacity was calculated using the material properties

gathered from the prisms and tensile tests of the vertical reinforcing bars. In this regard, the masonry strength was taken as 22.94 MPa while the steel properties used were yield strength of 540 MPa at 0.0027 strain. The layout and elevation of this particular wall are shown in Figure 2.8.

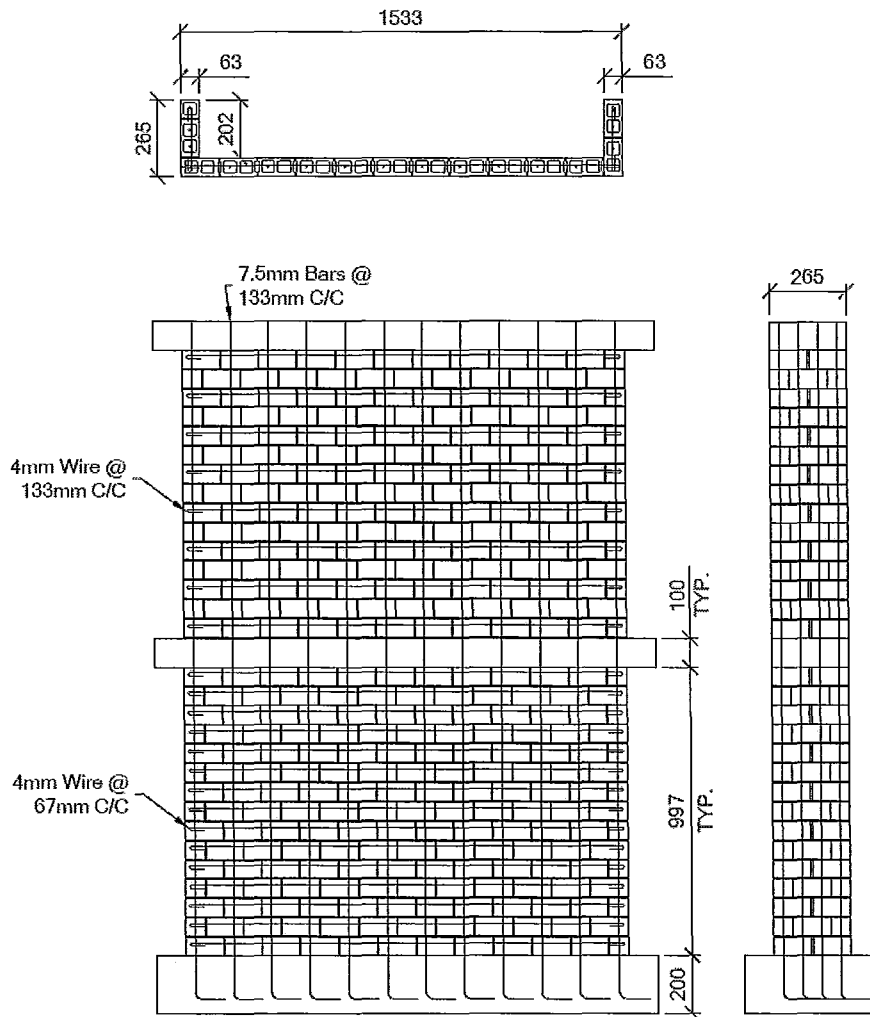


Figure 2.8: Plan Side and End Views of C-Wall (Wall 8).

2.4.3 The Double Wall (Walls 1 and 2)

The Double Wall (Walls 1 and 2) shown in Figure 2.9 was located on the East end of the building and was oriented in the plane of loading. It was designed into the layout of the structure so as to examine the effects of coupling of the in-plane walls in close proximity to each other connected only by the floor slab. For the purposes of the initial analysis, the slab between the two walls was considered to be ineffective in creating coupling behaviour. This wall was therefore treated as two separate in-plane walls in which case the flexural strength of each wall was calculated. However, as shown by Wierzbicki (2010), coupling was present and this will be looked at in the analysis of the test results.

Each part of the wall measured 865 mm long and the two walls positioned in line with each other formed a total length of 2000 mm. The aspect ratio of a single wall was 2.54. The walls were reinforced vertically with D7 bars in every other cell resulting in a reinforcing ratio of 0.58%. This Double Wall (Walls 1 and 2) had a calculated ultimate moment capacity of 66.4 kN-m for each wall which required a lateral loading of 30.2 kN for a single wall and therefore a required lateral loading of 60.4 kN for two of these walls acting together in plane. The calculated yield moment for this wall assuming elastic behaviour was found to be 42.7 kN-m.

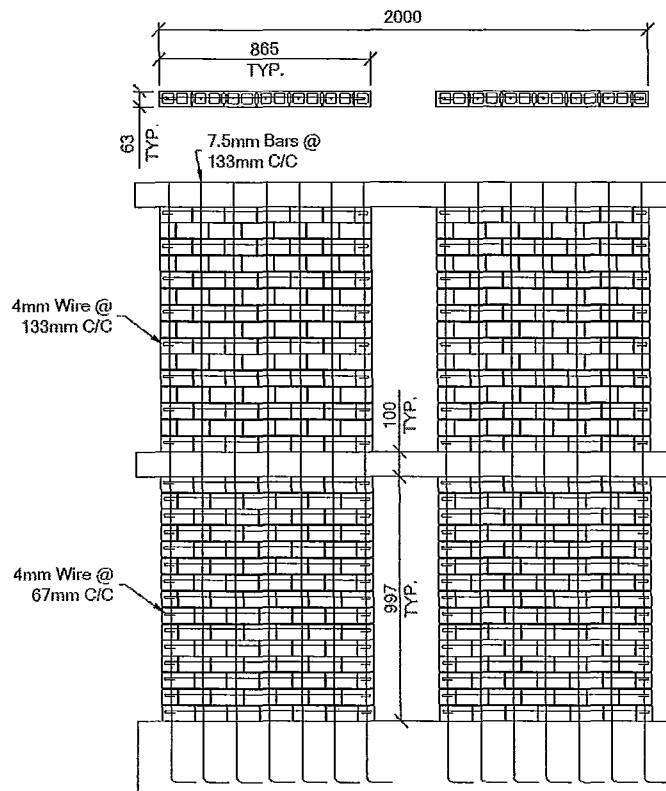


Figure 2.9: Plan and Elevation of Double Wall (Walls 1 and 2).

2.4.4 Centre Wall (Wall 5)

This wall, shown in Figure 2.10, was located at the geometric centre of the building. It was initially designed into the structure at the central location as a way to help load the structure through its geometric centroid. However, after the final loading mechanism was designed not to require the wall for the load transfer, it was retained as the only internal wall within the structure and created a larger degree of redundancy for resistance of the lateral load.

The wall measured 1132 mm long and was reinforced with vertical D7 bars in every other cell. It had an aspect ratio of 1.94 and a vertical reinforcing ratio of 0.57%. This wall had a calculated ultimate moment capacity of 114.4 kN-m corresponding to a required lateral load of 52.2 kN. Assuming elastic behaviour, the calculated yield moment for this wall was found to be 70.4 kN-m.

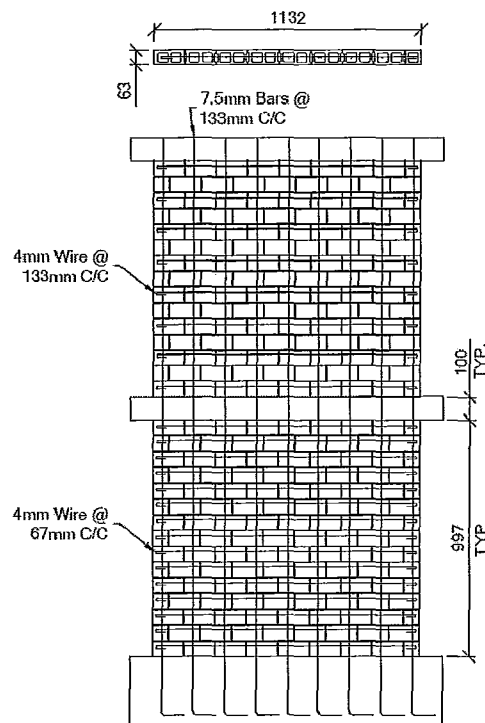


Figure 2.10: Plan and Elevation of Centre Wall (Wall 5).

2.4.5 Out- of-Plane Walls (Walls 3, 4, 6, and 7)

A total of four 4.5 unit long walls were located within the structure and oriented perpendicular to the direction of loading. These out-of-plane walls were added to the structure to provide lateral and torsional stability.

These walls were 600 mm in length and were reinforced with five vertical D7 bars distributed evenly. The resulting aspect ratio was calculated to be 3.67 with a reinforcing ratio of 0.59%. These walls had a calculated ultimate moment capacity of 33.1 kN-m which required a lateral load of 15 kN. The calculated yield moment for this wall assuming linear elastic behaviour was found to be 22 kN-m. Figure 2.11 contains the reinforcement configuration for this wall.

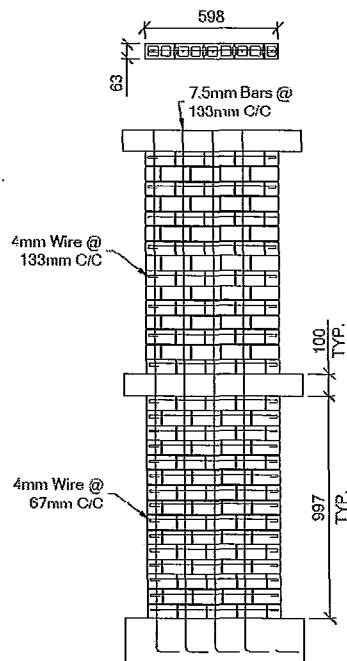


Figure 2.11: Elevation of Out-of-Plane Walls (Walls 3, 4, 6, and 7).

2.4.6 Overview of Structure

Table 2.1 contains a summary of the geometric and reinforcing characteristics of each wall.

Table 2.1: Geometric and Reinforcing Ratio for Each Wall

Wall	Wall Length (mm)	Vertical Reinforcing Area (mm ²)	Reinforcing Ratio (%)	Aspect Ratio (h_w/l_w)
4.5 Block Rectangular	600	226.0	0.59	3.67
6.5 Block Rectangular	867	316.4	0.58	2.54
	867	316.4	0.58	2.54
8.5 Block Rectangular	1133	406.8	0.57	1.94
C-Wall (Wall 8)	1533	813.6	0.66	1.43

For visualization purposes, a three dimensional model is presented in Figure

2.12.

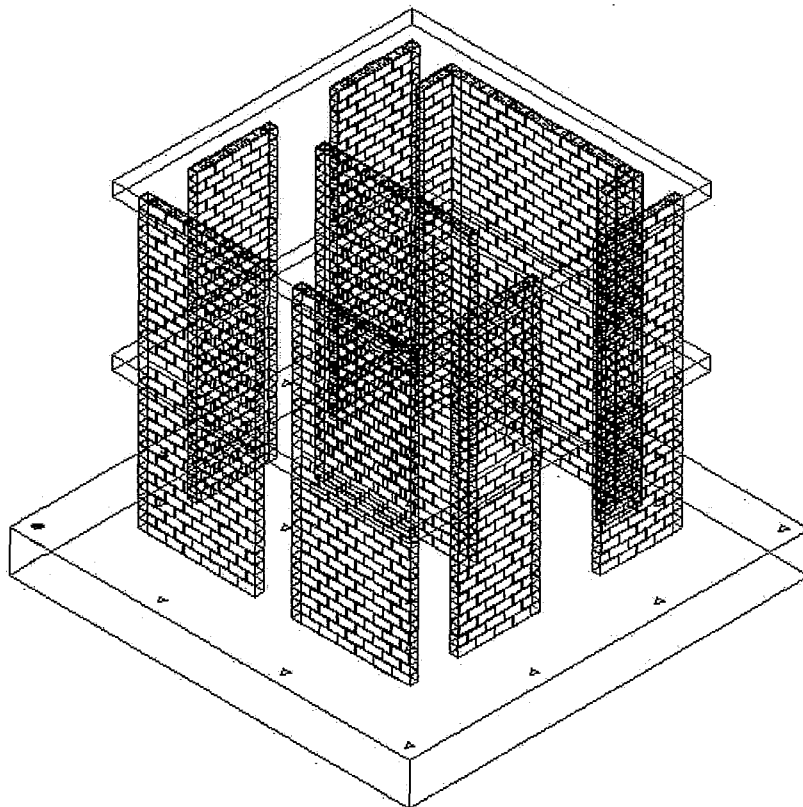


Figure 2.12: 3D Model of Specimen

2.5 Details of Design

2.5.1 Design for Flexure

As previously stated, all walls were designed to fail in a flexural manner. The walls were analyzed mainly using the equations found in CSA S304.1 (2004). However, the material reduction factors were removed from the equations so that the values calculated would be a close prediction of those found during the test. An extreme masonry strain of 0.0025 was employed as per the code value for ductile design. The equivalent rectangular stress block method was also used to idealize the compression zone of the walls. The inclusion of compression bars for flexural strength has been shown to more accurately reflect the actual wall strength (Shedid, 2006). Therefore, as a deviation from the masonry design standard, the compression bars were included in the strength calculations.

The material properties used in the calculation of wall strength were found using assemblage and standard material testing processes. Yield strengths of 540 MPa and 749 MPa were used for the vertical and horizontal reinforcing bars, respectively. Masonry compressive strength of 22.94 MPa was used along with a calculated self weight at the base of the wall equivalent to 0.1 MPa including the weight of the slabs. The equations used to calculate the flexural strength of the walls can be reviewed in Appendix A.

Table 2.2 contains the calculated yield and ultimate strengths of each of the walls in the structure. Also listed are the predicted steel strains at the ultimate load for each wall; this will become significant later on in this thesis in the discussion of ductility.

Table 2.2: Flexural Ultimate and Yield Strengths for all Walls

Wall	Yield Moment (kN-m)	Ultimate Moment Capacity (kN-m)	Associated Lateral Loading (kN)
4.5 Block Rectangular	22.03	33.08	15.0
6.5 Block Rectangular	42.69	66.42	30.2
8.5 Block Rectangular	70.39	114.36	52.0
C-Wall (Wall 8)	246.96	332.03	150.9

2.5.2 Design for Shear

The shear design for this structure involved mainly the elimination of possible shear failure. As such, the shear reinforcement was chosen after the flexural strengths of the walls were established. Maximum shear values were found for each wall based on the ultimate flexural capacity of each wall. With this design shear force in hand, the required amount of horizontal reinforcement was calculated based on design equations found in CSA S304.1 (2004). After the required amount of reinforcement was established, the amount of steel was increased so as to eliminate any possibility of shear failure.

2.5.3 Floor Slab Design

For analysis, the floor slab was assumed to be an infinitely rigid diaphragm. Due to the special provisions allotted to simplify the building's response, which will be discussed in Section 2.5.4, the slab mesh was required to transfer the loading to each of

the walls within the structure without significant in-plane slab deflection. A simple analysis was performed to ensure that the amount of steel reinforcement would be sufficient to transfer the loading from the slab into the walls without deformation of the slab. The analysis was based on bars being fully supported and unable to bend (since they were embedded in the concrete) and only the cross sectional area would be relevant. The resulting design is shown in plan in Figure 2.13 and in cross section in Figure 2.14 which also includes the special design provisions outlined in Section 2.5.4.

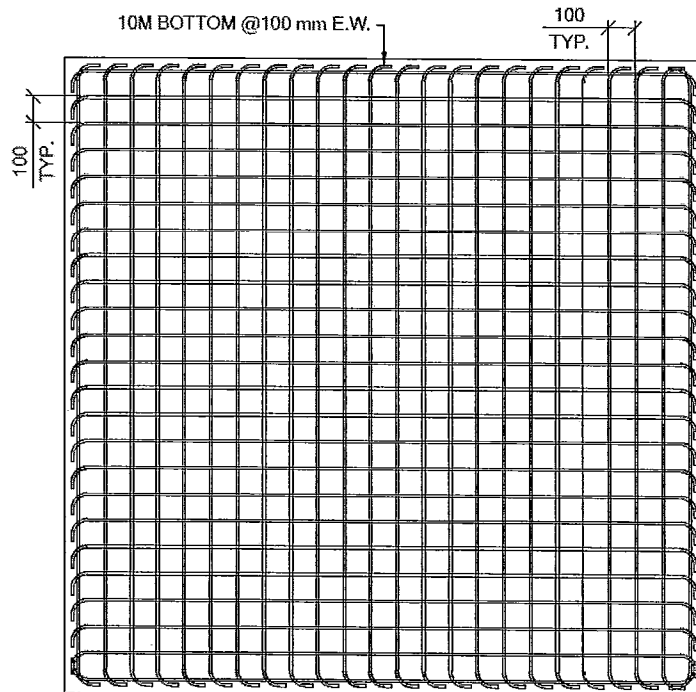


Figure 2.13: Floor Slab Reinforcing

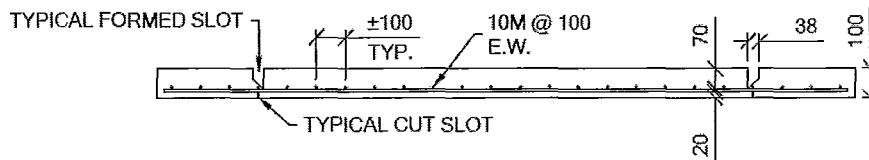


Figure 2.14: Slab Cross Section

2.5.4 Special Provisions for Floor Slabs

As mentioned previously, extending the understanding of inelastic reinforced masonry behaviour from the element level to the system level is a large step involving many variables. In order to look at torsion as the primary system parameter some other parameters had to be designed out of the building system or controlled in some manner using special provisions. Initially the intent of these provisions was to enable the slab to act as only a link member between the two walls in order to eliminate as much inter-wall coupling as possible. However, during the construction process, it was not possible to reduce the section of the slab at both ends (locations of maximum moment), while retaining the structural rigidity of the slab to ensure proper load distribution while also maintaining constructability. This was due mostly to the limited size of the specimen which only provided a small length of slab between the shear wall elements. However, the importance of diaphragm behaviour was anticipated and it was decided, therefore, to define a hinge location in the slab between each of the walls. This created a well defined hinge within the diaphragm between the wall elements for the eventual

coupling action. This hinging action was achieved through grooves formed into the slab during construction as shown in the Figure 2.15.

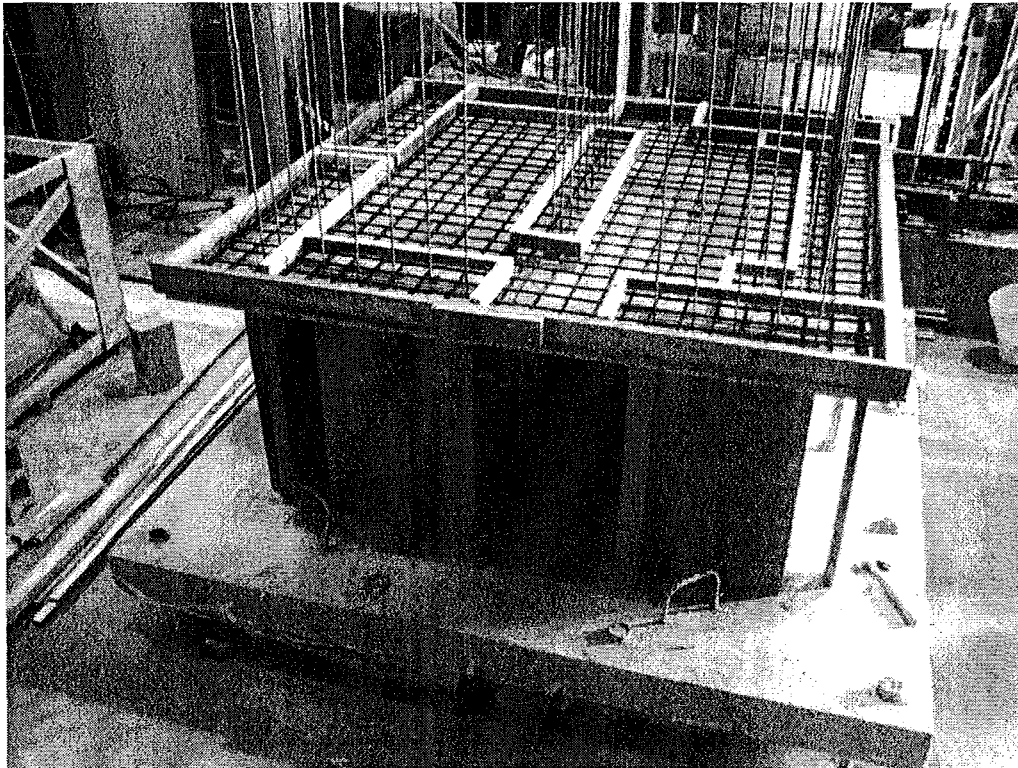


Figure 2.15: Formation of Hinges Using Grooves in the Concrete Slab

As can be seen in Figure 2.15, the steel mesh in the floor slabs is quite dense with No. 10 reinforcing bars spaced at 100 mm. In addition to the grooves formed at the top of the slab, slots were cut on the underside of the slab using a concrete saw so as to further reduce the moment capacity of the slab at this 'hinge' point. This resulted in a better defined hinge point normally associated with the inflection point of a coupling beam. As per the design calculations, this left the reinforcement alone to carry the shear and axial force through these joints. Figure 2.16 shows a close up of the slots

cut into the slab. These slots were cut in the same pattern as the formed depressions (grooves) in the top of the slab.

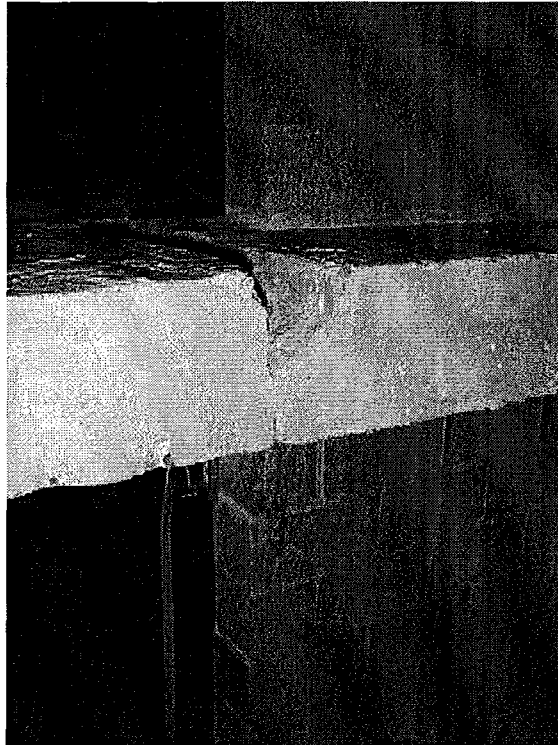


Figure 2.16: Close Up of Groove and Slot at the Hinge Location

As can be seen in this figure, the section of the slab has been reduced to about 25mm in depth. Considering the crossing pattern of the mesh of 10 mm bars, 20 mm of this cross section is made up of the steel mesh. This leaves the slab with a negligible moment capacity effectively creating hinges to define the points of inflection.

2.6 Material Properties

2.6.1 Steel Properties

Two sizes of reinforcing steel were used in the construction of the shear wall elements in the structure. For both sizes of steel, three 600 mm long samples were tested under tensile axial loads. For the vertical reinforcing, the D7 bars were a 7.6 mm diameter deformed wire representing a full scale bar size that fell between standard No. 20 and No. 25 reinforcing bars. The samples were tested under tensile loading until rupture in a Tinius Olson machine utilizing self-tightening jaws to grip each specimen. The data from a 100 mm long extensometer was collected via data acquisition software on a nearby computer. The average yield strength of these bars was found to be 540 MPa using the 0.2% offset method with an associated idealized yield strain of 0.0027. This was the strength used in the design calculations. Figure 2.17 contains a plot of the stress strain data for the bar tests.

From Figure 2.17 it can be seen that there is no definite yield point for this steel. It reaches approximately 8 times the yield strain at fracture. Unfortunately, as discussed in Section 2.9 on test procedure, this limited straining property has specific implications for the method required to test the structure.

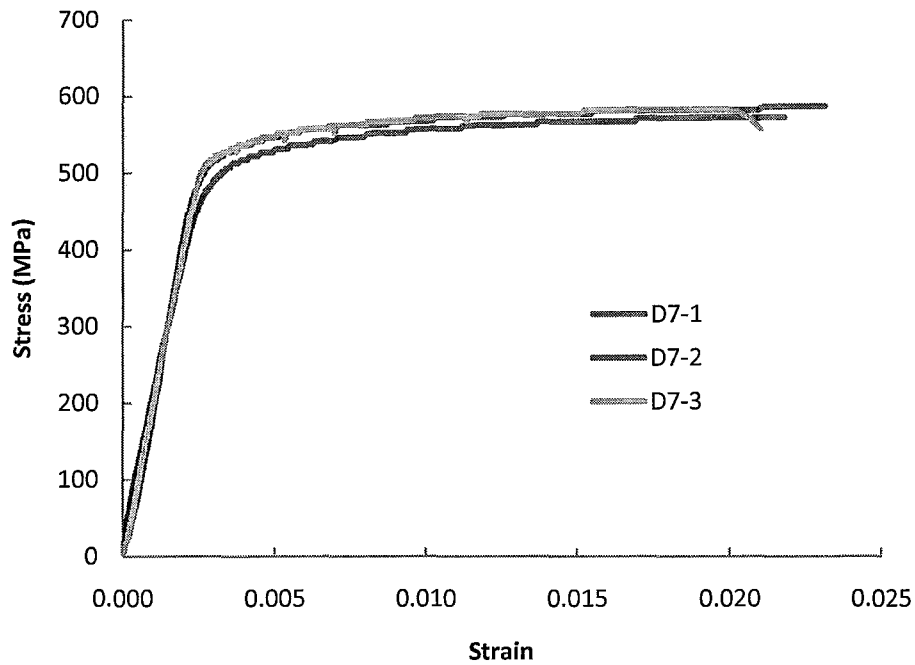


Figure 2.17: Stress Strain Relationship for D7 Reinforcing Bars

The horizontal steel was an undeformed W1.7 drawn wire with a 3.8 mm diameter. Due to the method of manufacturing, the resulting characteristics are quite different from regular reinforcing steel. The modulus of elasticity was quite normal at 200 000 MPa but the average nominal yield strength of the steel was found to be 679.8 MPa while not even reaching four times the yield strain at failure. Figure 2.18 illustrates the stress-strain relationship of the deformed wire. The effects of the stress-strain characteristics of the vertical reinforcement on the building behaviour will be discussed later during the discussion of the building test results in Chapter 4. A summary of the steel test results is presented in Table 2.3.

Table 2.3: Reinforcing Steel Yield Strength

Test #	Tensile Yield Strength of Steel (MPa)	
	D7	W1.7
1	542.3	689
2	530.8	670
3	546.8	680.5
Average	540	679.8
C.O.V. (%)	1.53	1.4

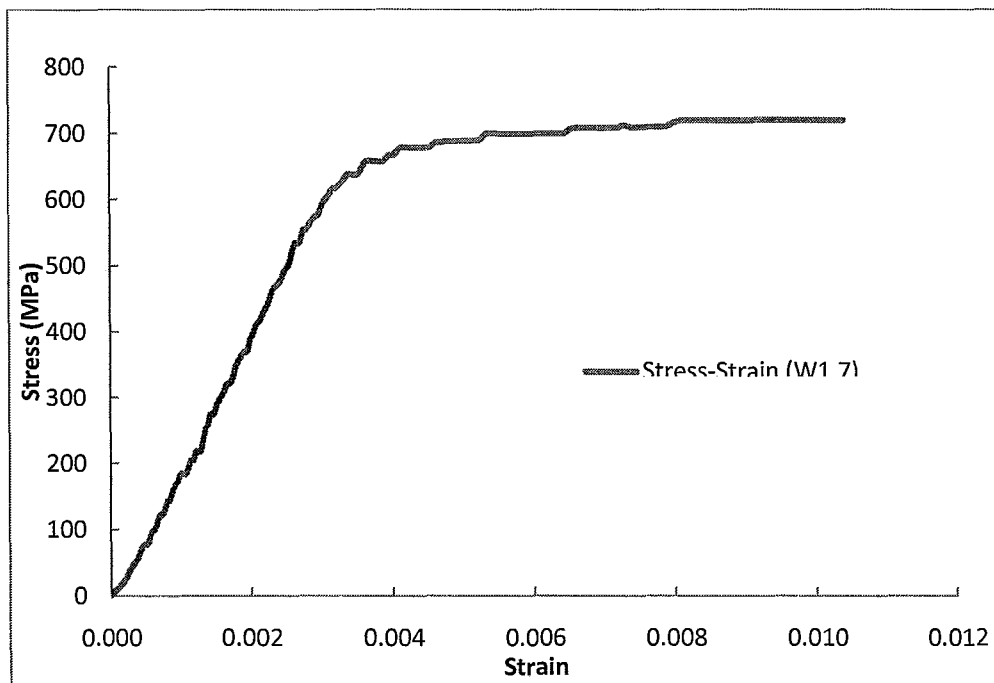


Figure 2.18: Stress-Strain Relationship for the W1.7 Wire Reinforcing

2.6.2 Foundation Slab Concrete Properties

The foundation slab concrete was tested for compressive strength by testing three standard 150 mm diameter cylinders. The test was performed using a Tinius Olsen hydraulic machine with a loading range of 0 – 300 000lbs. The average strength of the cylinders was found to be 34.6MPa (C.O.V. = 5.3%) at approximately five months

after pouring. This strength is quite normal for concrete used for general construction purposes. This concrete was provided by a local ready mix supplier.

2.6.3 Slab Concrete

Concrete for the first and second floor slabs was mixed in-house using a typical mix design. The slab concrete mix design was proportioned by weight of materials in the ratio of 1:2.73:1.36:0.63 of type 10 cement, coarse aggregate, sand and water respectively with a maximum coarse aggregate size of 10 mm. Each constituent material was dried before preparation and weighing of the proportions of the mix.

This mix resulted in an average compressive strength of 38.43 MPa (C.O.V. = 2.6%) which is a fairly high strength for this type of construction. However, due to the special load transfer design provisions included for this slab, this over-strength was welcomed. Table 2.4 contains the data collected from these cylinders. Due to some spilling of the grout during construction, only one usable cylinder was formed to be tested for the second floor slab.

Table 2.4: Floor Slab Concrete Compressive Strength

Specimen	Failure Load (kN)	Stress(MPa)
S1.1	716.1	39.73
S1.2	693.9	38.49
S1.3	691.7	38.12
S2.1	302.5*	37.38
Average		38.43
COV (%)		2.55

*- 100x200 mm Cylinder

2.6.4 Mortar Properties

The mortar used in this project was mixed at the laboratory due to its specialized nature. Although regular material proportions were used, the sand was sieved to remove any particles larger than 2.5 mm. This was to prevent any of these particles from causing problems in forming the 3.3 mm mortar joints of the walls or with the resulting masonry strength. Due to the small size of the mortar joint, large particle sizes could cause construction and performance problems.

A target flow of 125 was selected to ensure that a highly workable mix was produced. This was confirmed on a standard flow table set-up and facilitated an easy formation of the thin mortar joint. The mortar was mixed by hand in a dampened wheelbarrow using regular hand tools. The proportions of the materials used in each mortar batch were 1:0.2:3.53 of Type 10 Portland cement: lime: sand by weight. The sand was air dried and each batch was mixed immediately prior to its use to ensure consistent quality control. Water was added on occasion to retemper the mortar and ensure satisfactory performance as per the mason's request. For each of the nine batches, a set of three 50.8 mm cubes were formed and later tested to examine their compressive strength. All three cubes were tested from each mortar batch yielding an average compressive strength of 26.5 MPa with a COV of 12.1%. Appendix B contains a listing of all the mortar cube strengths obtained from the collected specimens.

2.6.5 Grout Properties

As stated earlier, the grout was mixed in house and poured into the walls in four separate lifts as the walls were being built. The grout had an average slump of 275 mm and for each grout pour; three 100 mm diameter cylinders were cast. These cylinders were tested in the Tinius Olsen machine used to test the concrete cylinders.

The grout was prepared according to dry material weights proportioned as 1:0.04:3.9 of type 10 Portland cement: Lime: Sand. The resulting compressive strengths are listed in Table 2.5. The average strength of the grout was 20.1 MPa (C.O.V. = 15.33%) which was a very reasonable strength as seen in common masonry construction.

Table 2.5: Grout Strength

Specimen	Failure Load (kN)	Stress(MPA)	Average
G1.1	195.7	24.19	24.12
G1.2	175.7	21.50	
G1.3	215.7	26.66	
G2.1	169.0	20.89	20.25
G2.2	175.7	21.71	
G2.3	146.8	18.14	
G3.1	133.4	16.49	17.26
G3.2	144.6	17.87	
G3.3	142.3	17.42	
G4.1	140.1	17.32	18.84
G4.2	169.0	20.69	
G4.3	151.2	18.51	
Average		20.12	
COV (%)		15.33	

The strongest of the mixes was found in the first pour. This was due to the fact that this was the grout with the lowest water content which resulted in a lower water to cement ratio thereby yielding a higher strength. This was also the least workable grout and took the most effort to place in the walls.

2.6.6 Block Properties

As part of the assemblage testing performed by a colleague (Hughes, 2010), many compressive tests were performed on many blocks. As mentioned previously, the blocks were 1/3rd scale of common 20 cm hollow concrete block. The blocks measured 130 mm in length and 63.3 mm in height and depth. The face shells were 10.7 mm thick and the resulting area of the block was approximately 4280 mm². The compressive tests were performed in the same Tinius machine mentioned earlier. The blocks had an average compressive strength of 54.8 MPa with a COV of 4.7%. This strength is unusually high for concrete block masonry (target of 30 MPa) and can be attributed to the manufacturing process (Wierzbicki, 2010). Table 2.6 contains the compressive strengths collected from the block testing.

Table 2.6: Block Compressive Strength

Specimen	Compressive Strength (MPa)
1	56.5
2	53.4
3	57.6
4	55.2
5	51.1
Average	54.8
C.O.V. (%)	4.70

2.6.7 Prism Properties

Twelve unreinforced grouted prisms were constructed to examine the properties of the grouted masonry. These prisms were built by the same experienced mason at the same time as the walls were constructed. They were also grouted with the same grout as the walls and at the same time. The grout was compacted using a rodding technique which proved quite successful. These assemblages were constructed to give an experimentally determined strength of masonry for this construction.

The prisms were four courses high and one block in length. The running bond pattern was simulated by stacking two half end units on top of a stretcher. The webs at the ends of the stretchers were mortared to prevent any grout from escaping during its placement. Each prism cross section measured 133mm by 63mm resulting in a gross area of approximately 8380 mm².

Testing was performed when the age of the prisms was approximately six months. This was just prior to the testing of the completed structure to give a realistic masonry strength for analysis. The prisms were capped using a gypsum cement to provide a level bearing area and compressive loading was supplied again using the Tinius Olsen test machine. Data was collected via the same data acquisition software and hardware as mentioned earlier from two extensometers on either side of the prism. Table 2.7 contains a listing of the strengths found for each of the four phases of construction.

Table 2.7: Prism Compressive Strengths

Prism	Compressive Strength (MPA)	Average Strength (Mpa)
1.1	22.70	22.94
1.2	23.10	
1.3	23.02	
2.1	22.05	22.80
2.2	22.26	
2.3	24.09	
3.1	24.26	24.33
3.2	23.39	
3.3	25.35	
4.1	19.15	17.42
4.2	17.35	
4.3	15.76	
Average (Phase 1 to 3)		23.36
C.O.V. (%)		4.50

On initial inspection, it is obvious that the masonry compressive strength is quite high. This is mostly due to the effect of very high strength of the concrete blocks.

It also can be seen that the prism strength for the fourth phase of construction is much lower than the others. The photograph in Figure 2.19 shows that this reduction in strength is due to incomplete grouting of the specimens. This happened during the last phase of construction where some of the grout was spilled during its placement causing very little to be left for the filling of the prisms. As such, only a small amount of stiff grout was left to grout the prisms. Even with vigorous rodding, voids still remained in the grout of the prisms.

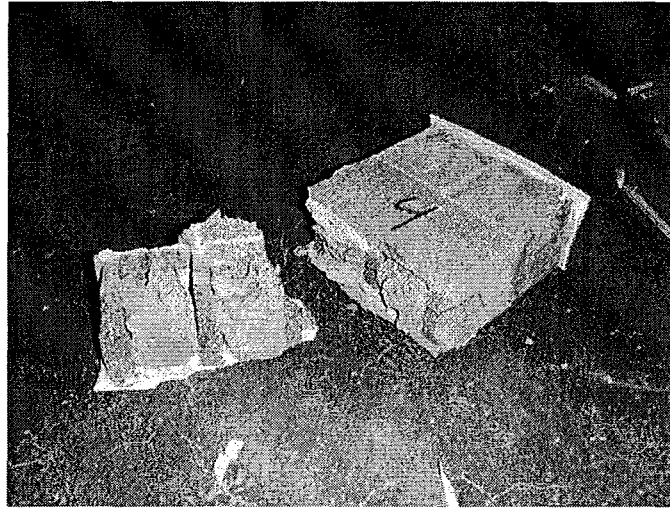


Figure 2.19: Void in Prism from Fourth Stage of Grouting

Since this problem did not occur until grouting of the final prisms, this was not a problem for the building walls and no voids were found in the top portion of the second story. The most critical portions of the wall in terms of curvature and stresses occur at the base of the wall. As such, the more meaningful average masonry strength of the first nine prism strengths was 23.36 MPa (C.O.V. = 4.5%); omitting the results from the fourth phase prisms.

It can be seen that the most variability was shown in the prisms that contained some voids while the fully grouted prisms show very consistent results. Table 2.8 contains the observed results for the stress and strain at maximum stress data collected from each of the prisms. The measured masonry modulus elasticity (E_m) was taken as the slope of the line between $0.1 f'_m$ and $0.5 f'_m$. Again using the results of the first nine prisms, the stiffness of the masonry was found to be 13,217 MPa. Figure 2.20 contains

the typical stress strain relationship noted for the prisms from the first phase of construction.

Table 2.8: Prism Stiffness Characteristics

Prism	Maximum Strain	Modulus of Elasticity (MPa)		C.O.V. (%)
		Individual	Average	
1.1	0.00187	13856.41	13193.18	4.7
1.2	0.00257	13104.70		
1.3	0.00221	12618.44		
2.1	0.00224	14121.37	13394.71	9.8
2.2	0.00244	11885.37		
2.3	0.00211	14177.39		
3.1	0.00256	14712.34	13063.49	21.7
3.2	0.00262	9786.62		
3.3	0.00226	14691.50		
4.1	0.00227	11352.96	10657.74	7.7
4.2	0.00184	10868.92		
4.3	0.00286	9751.33		
Average (Phase 1-3)	0.00232		13217.13	12.07

The values used for the strength and deflection calculations were selected as the data from the first phase of construction since this is the location of the greatest moment.

2.7 Building Test Setup

This project represents a new research area at McMaster University and, as such, a new test rig had to be designed and constructed.

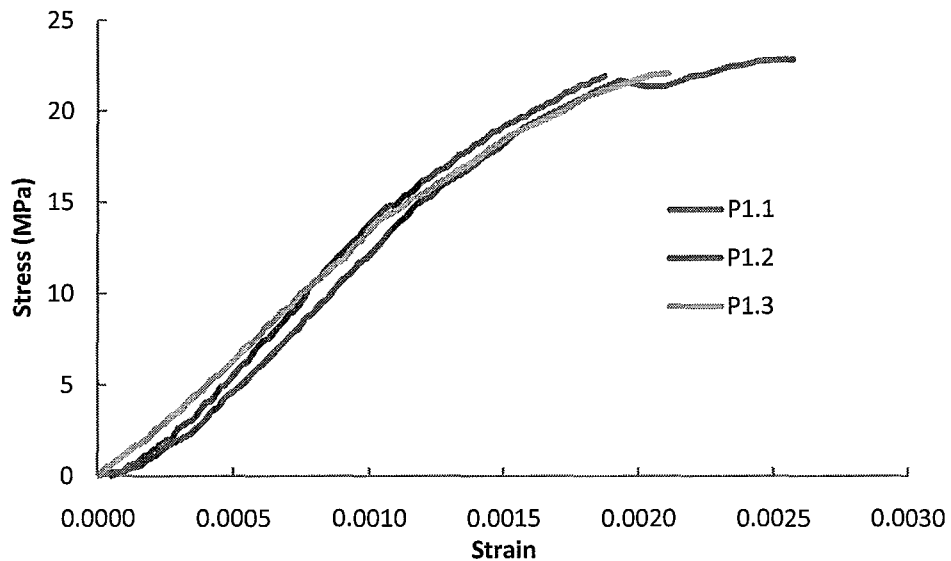


Figure 2.20: Stress-Strain Relationship for Prisms from Construction Phase 1

2.7.1 General Configuration of Test Setup

A large truss frame was initially designed to accommodate a lateral loading of 1000 kN to accommodate testing of potential structures measuring a maximum of 3m by 3m in plan to a maximum height of 3m. The frame was also designed to be self-contained for loads up to 500 kN so as to improve the flexibility of where the tests could be performed within the structures laboratory.

As adequate laboratory space became available, the design of the frame was modified to carry its loads into the strong floor of the laboratory. This allowed for smaller section sizes and reduced deflections. The frame was designed in the widely used SAP2000 structural analysis program. Linear elements with their material and geometric properties were inserted into the program to obtain elastic member loads

These Figures show the general characteristics of the frame. The plan view of the setup in Figure 2.22 shows that the two parallel frames are the main lateral load resisting system. This view also shows the five Hollow Structural Steel (HSS) cross beams that connect these two frames by being bolting to the base beams of the two frames. The elevation shows the positioning of these cross beams along the length of the base beams. This view also shows the grid of holes existing in the strong floor of the laboratory. Holes were cut into the cross beams in this exact pattern so that the specimen could be bolted to the frame and to the strong floor of the lab simultaneously. In other words; the bolts would pass through the foundation slab, the cross beams and the strong floor, effectively tying the whole system to the laboratory floor.

The elevation view also shows the position of the actuator reaction beams on the columns of the frame. These two HSS beams span the gap between the two frames. This is also where the hydraulic actuator was mounted to push horizontally against any specimen mounted on the four cross beams at the other end of the test setup. From this description, the load path can be deduced.

For a push force on the specimen, the resultant force would travel through the actuator back onto the HSS actuator beams. This force would then flow into the vertical columns causing tension in the main strut of the actuator beam and negative moment in the base beam. The loading in the base beam would be resisted by the base beam itself internally but also would flow partially into the strong floor of the laboratory via the bolted connections to the cross beams which in turn were bolted to the floor. This

moment would also be resisted in part by the bearing of the single cross beam located directly below the columns of the frame. At the other end of the test setup, the force exerted on the specimen itself would flow directly into the strong floor of the laboratory.

For a pull action, the exact opposite load path would be noted with the exception of the bearing of the cross beam found below the columns of the frame. The reversed loading of the actuator would cause a positive bending moment in the base beams of the frames thereby tending to lift that cross beam off the floor. This could not be prevented since the grid of holes in the strong floor did not extend beyond the four crossbeams found in the location of the specimen. Therefore, some additional deflections were anticipated for the reversed cycle of loading. However, these deflections would not affect the structure since the structure and the support part of the test frame were bolted directly to the strong floor and, therefore, would not move.

Each member in the frame was designed according to the loads found from the elastic analysis performed. The structural members were chosen from beam loading tables found in CSA S16-01, the Limit States Design of Steel Structures (2003). Shop drawings for all the elements comprising the frame can be seen in Appendix C.

The connections between each of the members were significantly over-designed. The connections were based on the critical slip condition according to CSA S16-01. Following the design, the number of bolts required was increased by 30-40% to

ensure that no possible failure could occur at the connections of the frame. All connections were formed using a 25mm thick steel plate with holes drilled for bolting. With the exception of the actuator beam to column connection, all other connections were designed to form rigid moment connections between members. This created a frame that could be dismantled, moved or adjusted for future use while still developing the required strength and stiffness.

Overall, the frame was designed for a lateral loading of 1000 kN while remaining in the elastic range with top displacements of the columns and, therefore, at the actuator location of approximately 15mm. The frame can accommodate specimens with dimensions up to approximately three meters in height, length as well as width. The original design was for a specimen measuring two meters square and, therefore, the frame was constructed in this manner. However, the frame can be easily reassembled to accommodate larger specimens. The elements of the frame were fabricated by Aldershot Structural LTD located in Aldershot Ontario Canada. The elements were shipped to McMaster University where they were assembled on site. The specimen was held down by sixteen 2.5 inch diameter steel bolts that were hand tightened according to CSA S16-01. Since the frame was essentially self-reacting these bolts did not require any prestressing load.

Figure 2.23 shows the test setup and details as built in the laboratory.

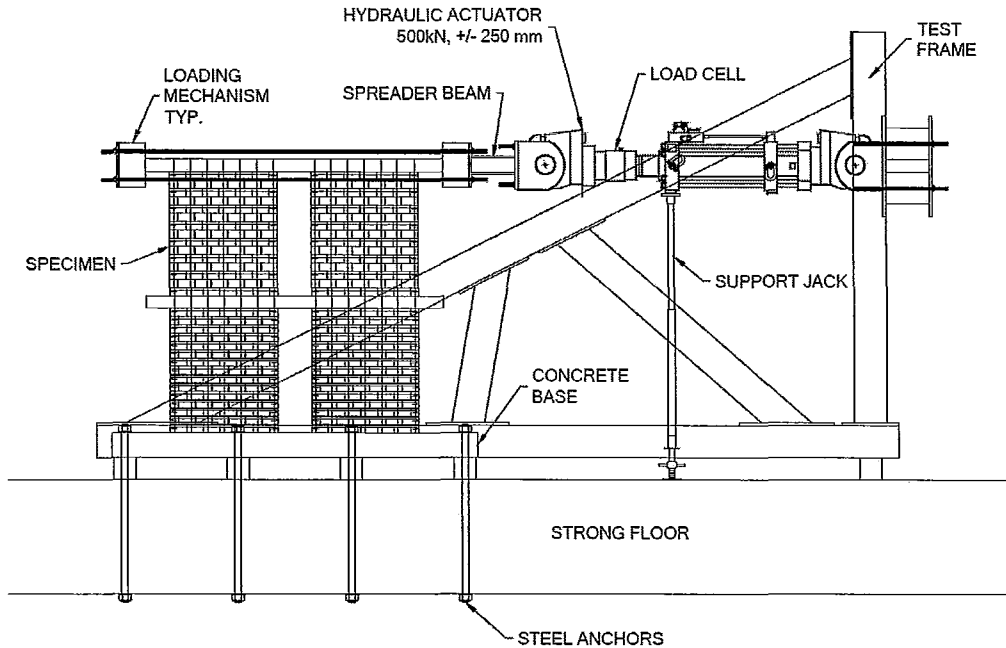


Figure 2.23: Detailed Test Setup

The lateral load was applied using a displacement controlled MTS hydraulic actuator. This actuator was capable of 500 kN in both the push and pull directions with a maximum stroke of 500 mm. This actuator pushed on the top slab of the building where a specially formed concrete loading block had been poured in conjunction with the top slab. This loading block was constructed of reinforced concrete measuring 350mm by 350mm. It had holes formed into it that allowed one inch diameter threaded rod to be passed through to the other end of the building where a similar loading block had been constructed. Therefore, when the actuator pushed on the specimen, the load would pass directly from the actuator through the short loading beam onto this loading

point. However, when pulled, the load would be carried by the high strength threaded steel rods to the opposite end of the building effectively pushing on the structure from the other side. This allowed for a symmetrical loading of the building for both directions without the need for two independent hydraulic jacks.

Figure 2.24 shows this loading block, its position on the slab, and the location of the holes where the threaded rods were used to carry the load across the building for the case of pull type loading.

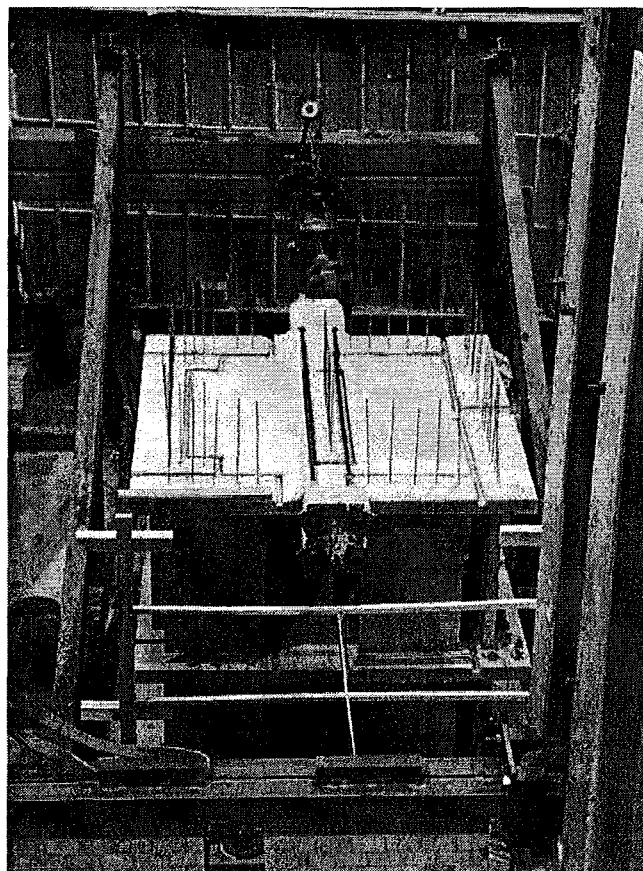


Figure 2.24: Loading Mechanism Plan

2.8 Measurements and Instrumentation

Due to the large size of the test building, a large number of data acquisition channels were used. In total 172 channels of data were collected. Of these channels, 82 were quarter-bridge strain gauges to measure reinforcement strains, 80 were Linearly Varying Displacement Transducers (LVDT's) externally measuring deformations between two points on the surfaces of the walls, 8 were String Displacement Transducers measuring the global slab displacement and the remaining two were load and displacement readings from the hydraulic actuator. All of these channels were read at 10 second intervals by controlled data acquisition software.

2.8.1 External Instrumentation

During testing, displacements were measured at key points along each of the walls in the structure. The in-plane walls were more heavily instrumented due to the fact that they were designed to go well beyond the yield displacement.

A total of thirteen LVDT's were used to monitor the more heavily instrumented walls. All of the instruments were mounted on the first floor of the structure where the displacements would be most critical (Shedid, 2006). Five LVDT's were mounted on each end of the wall to measure vertical movement of the wall relative to the foundation slab. The data collected by these instruments would be used to calculate average curvature values over different segments of the wall height. One LVDT was used to check for base slip of the wall relative to the foundation slab. The remaining two were diagonally mounted in a cross formation creating a strain rosette that could

potentially be used to distinguish between flexure and shear deformations. Figure 2.25 illustrates the position of each of the instruments that could be found on each of the in-plane walls while Figure 2.26 shows the positions for the out-of-plane walls.

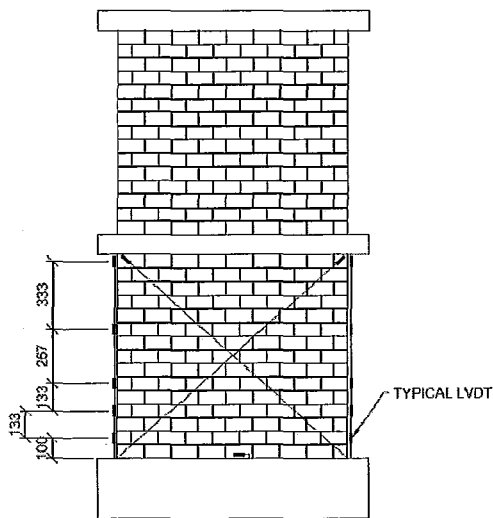


Figure 2.26: LVDT Position for the In-Plane Walls

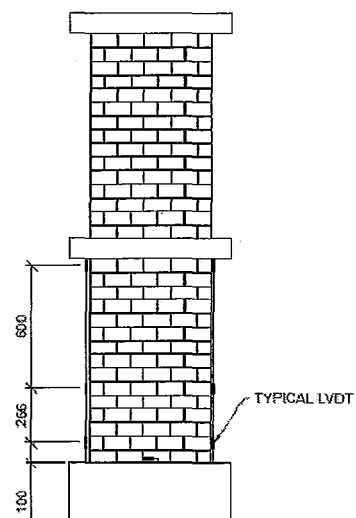


Figure 2.25: LVDT Position for the Out-of-Plane Walls

2.8.2 Internal Instrumentation

As mentioned earlier, 82 electrical strain gauges were used in Quarter Bridge to measure strains in the reinforcing bars. These gauges were mounted to the bars using a delicate procedure. First the ribs of the bar were removed with a grinder outfitted with an abrasive pad. The pad was used to prevent excess removal of material that would in turn weaken the bar itself. Even with this careful grinding, the area of the bar was reduced by a small amount. The bars were then cleaned with alcohol and the gauges were fixed to the bars using strong glue. The foil gauges were then coated with a sealer

for waterproofing, covered with thick tar tape to protect them from physical damage and finally wrapped with electrical tape to hold everything together. Figure 2.27 shows a typical gauge on a typical reinforcing bar.

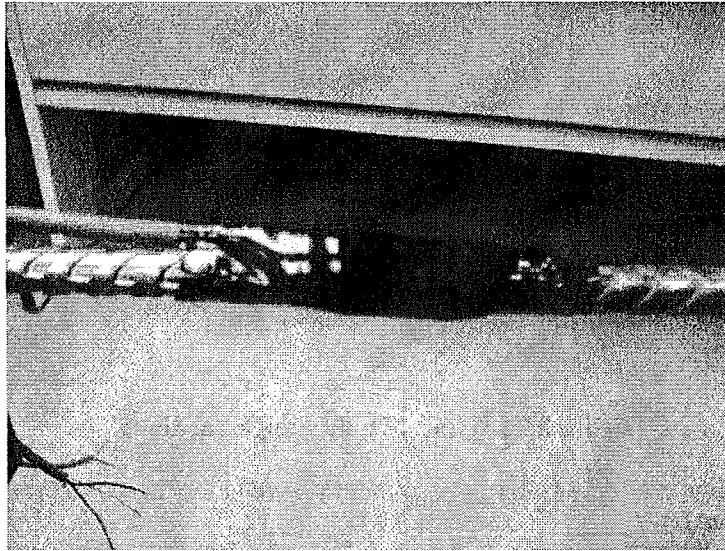


Figure 2.27: Typical Strain Gauge on a Vertical Reinforcing Bar

The electrical strain gauges were mounted on the two end bars in each wall. Three gauges were mounted to the extreme end bar while one gauge was mounted to the next nearest bar from the end. This accounted for eight gauges per rectangular wall. This configuration was common to all rectangular walls (both in and out-of-plane). For the C-Wall (Wall 8), all four end bars contained three gauges with the same single gauge on the first bar inside the linear web portion of the wall. This accounted for a total of 26 electrical gauges for this wall alone. Positions of the gauges on a typical wall are shown in Figure 2.28.

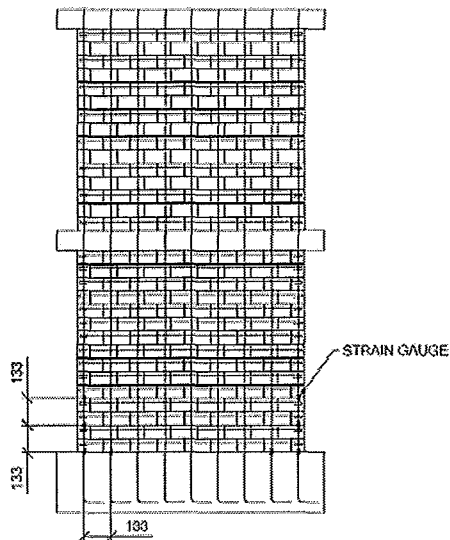


Figure 2.28: Typical Strain Gauge Positions

One gauge was mounted at the foundation-wall interface with two more gauges located at 150 and 300 mm above the foundation slab. For bars with a single gauge, it was mounted at the interface of the wall and the foundation slab.

All of these sensors were wired through an Ethernet cable board as a point of connectivity between the sensors themselves and the data logging software. Data was logged using three Agilent 34970A Data Acquisition/Switching Units and stored on a nearby computer.

To capture the global change in position of the building, String Displacement Transducers, commonly known as string pots, were employed at the corners of both floor slabs in the building. The readings from these sensors were utilized to triangulate

the position of the slab and the resulting displacements. Figure 2.29 illustrates the position of these string pots in plan, relative to the position of the building.

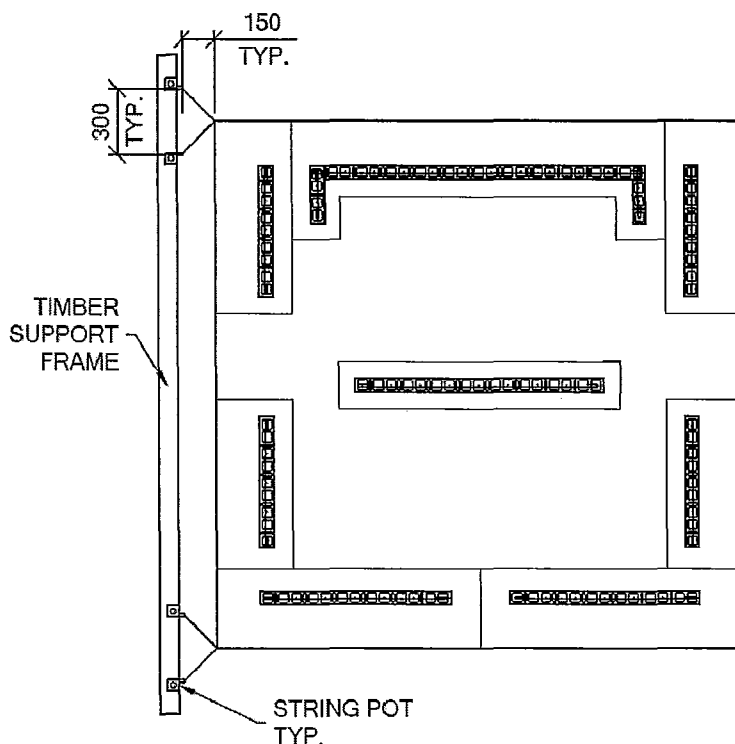


Figure 2.29: String Pot Locations in Plan

2.9 General Test Procedure

The specimen was tested under displacement control using the aforementioned MTS hydraulic actuator. Due to the lack of ductility in the vertical reinforcement as seen in the stress-strain diagram, multiple reversed loading cycles could not be performed. The logic behind this decision was confirmed by premature failures observed by Wiersbicki (2010) who used similar reinforcement. As such, only two loading cycles were performed at low displacements prior to the final monotonic push of the structure

to failure. Due to the unsymmetrical nature of the building, the chosen pre-cycling of the structure were based on percent of predicted total building strength.

The initial loading cycles were chosen to be well under the yield point of any of the walls to avoid damage to the bars which might have resulted in premature bar rupture during the final pushover test. The two cycles chosen for pre-pushover testing were selected to avoid having any bar in any wall reach half of its yield strain. After some analysis, it was noted that this limitation would occur at approximately 40% of the predicted first yield loading of the structure. This corresponded to a load of approximately 60 kN.

A total of four loading cycles were performed on the building. The first was a full push-pull cycle reaching 20% of the predicted first yield strength of the building or 32 kN. The second was a full push-pull cycle reaching 40% of the predicted buildings first yield load or 64 kN. The main test for data collection was a push until failure.

2.10 Conclusion

In this chapter, the selection of the building layout and wall geometry was presented along with their design considerations. Construction methods and details for the foundation slab, floor slabs, loading mechanism and walls were presented. The results of the material and assemblage testing were also presented. Further, the design of the test setup and instrumentation was also described along with the loading procedure.

3 Test Results

3.1 Introduction

The results of the test program are presented in this chapter. In total three phases of loading were performed. First, two complete push-pull cycles were carried out. The first cycle reached a load corresponding to 20% of the anticipated yield loading while the second cycle reached 40% of this anticipated loading.

The main lateral loading test cycle to be examined is the push cycle with monotonically increasing lateral displacement until failure. As mentioned in Chapter 2, the poor performance of the reinforcing under cyclic loading led to the decision not to perform cyclic loading on the building after initial yield. A full description documenting the building response along with photographs showing wall cracking and other effects of loading are presented. Then the general load-displacement response of the structure is presented in simplified fashion. The displacement in this case is the displacement of the geometric centroid of the top floor slab in the direction of loading. For clarity, the push direction mentioned in this thesis was directed towards the south of the building and will be the positive convention for both loading and displacement. Furthermore, in-depth analysis will be presented in Chapter 4. For clarity purposes Figure 3.1 contains the building layout with the walls numbered for reference.

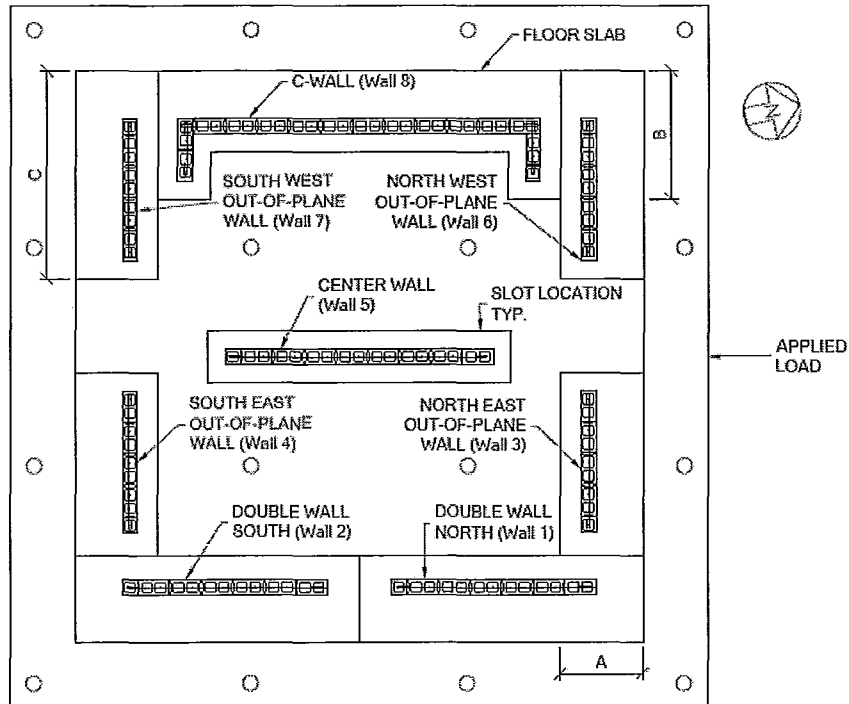


Figure 3.1: Wall and Slot Layout

3.2 Preliminary Cyclic Loading

The above mentioned pre-yield cycles performed prior to the push to failure were considered to be of an exploratory nature so as to iron out any potential problems with the test rig and electronic measurements. In this regard, it is worth noting that, due to the small scale of the structure, some of the displacements measured for these two preliminary cycles had such low magnitudes that in this range the noise in the signal of the instruments could significantly affect the accuracy of the data collected. The nominal yield loading used for these tests was defined as the level of loading at which the first vertical reinforcing bar in any wall oriented in the direction of loading reached

the yield strain. General load displacement diagrams will be presented but no other significant results were observed and no analysis was performed on the data collected during these two cycles at low loads.

3.2.1 20% of Yield Load Cycle

Prior to the start of this cycle, the actuator was attached for the first time to the specimen. Small incremental displacements were applied until the actuator head mated with the small spreader beam. Loading was then increased via displacement input increments of approximately 0.3 mm. This value was chosen arbitrarily as these small loading cycles were primarily performed for equipment testing. The maximum load reached for this cycle was 32.3 kN at a centroidal deflection of 0.35 mm.

No significant visual observations were made during this cycle. No visible cracks were observed in any of the walls of the building. Figure 3.2 contains the load displacement diagram for this entire cycle.

From Figure 3.2, it can be seen that the building showed similar stiffness in the push and in the pull direction. The slope of the load displacement diagram is similar for both. It is noted that the associated displacement for the same loading in the pull direction was significantly less than in the push loading direction. This can be attributed to the fact that during the push cycle, hairline cracks may have opened which had to close, and may not have closed perfectly, before the pull cycle could commence. This

Wall (Wall 8) remained uncracked at this juncture of testing. Figure 3.3 shows the load-displacement response of the structure for this cycle.

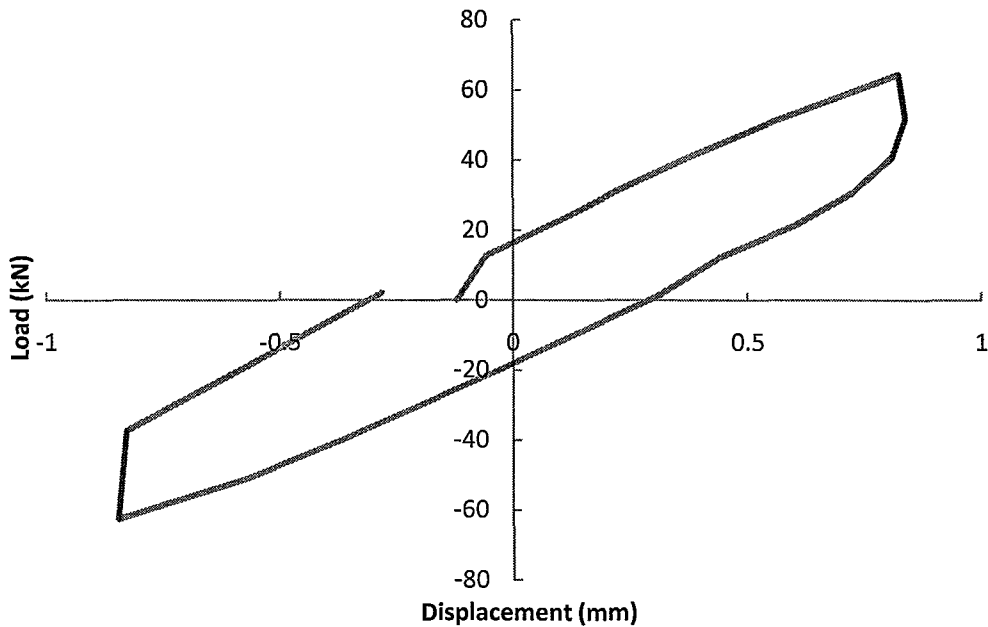


Figure 3.3: Load-Displacement Plot for 40% of Yield Loading Cycle

Again the building showed very symmetric response in terms of its stiffness characterized by similar slopes for the push and pull directions. The maximum push and pull displacements again were slightly different. Once more, this can be attributed to the push cycle preceding the pull cycle. Further discussion of this data will be presented in Chapter 4.

3.3 Pushover Test of Shear Wall Structure

The pushover test of the shear wall structure was performed by monotonically increasing the lateral displacement of the structure until failure occurred. As was

mentioned earlier, due to the brittle nature of the vertical reinforcing bars, significant cycling of the structure could not be performed without causing a premature failure and producing relatively worthless information. Therefore, a pushover test was performed to peak lateral resistance and beyond until only 80% of the peak strength remained. Data up to this amount of strength degradation has been suggested as useful in ductility analysis (Shedid, 2009).

Figure 3.4 is the resulting pushover curve of the building plotted as the total applied lateral load versus the corresponding top of building displacement in the direction of the applied load at the geometric centroid of the structure.

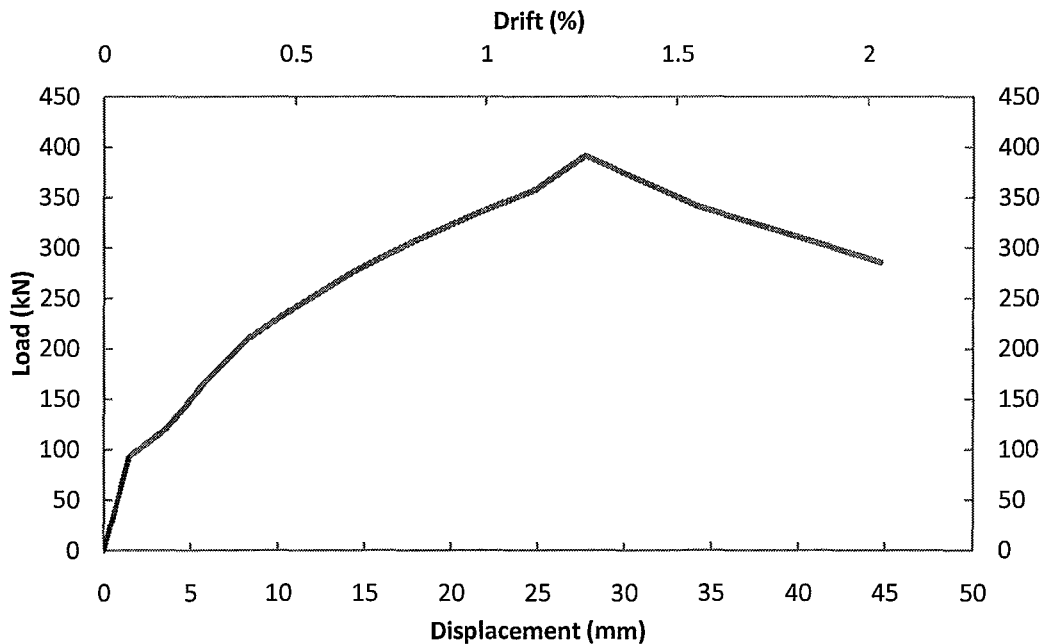


Figure 3.4: Pushover Curve for the Shear Wall Structure

As can be seen in Figure 3.4 rupturing of the vertical reinforcing bars in the Northern portion of the Double Wall (Wall 1) took place at approximately 29 mm deflection corresponding to approximately 1.3% drift. Continued displacement resulted in gradual reduction of strength with negative stiffness corresponding to additional rupture of bars in both portions of the Double Wall (Walls 1 and 2) and culminating in rupture of the extreme tensile bar of the centre wall (Wall 5). At this point, the test was terminated since the strength of the structure had decreased to 80% of its peak strength.

Here the large stiffness of the structure at the onset of loading can be seen as well as how this stiffness dropped off as increased loading causes increased cracking. The load reached a peak of 392 kN at a drift level of 1.26%. As mentioned above, the test was terminated when building strength degraded to 80% of the peak loading.

3.3.1 General Observations

The overall behaviour of the structure during the test was governed by the flexural response of the in-plane walls. This predominant in-plane behaviour was ensured by the stiffness of the out-of-plane walls (Walls 3, 4, 6 and 7) which controlled and limited the twisting behaviour of the structure. The flexural response of the in-plane walls was noted by observing significant bed joint cracking in all of the in-plane walls. These cracks propagated and widened as the load increased. Diagonal shear cracking developed in all in-plane walls in addition to the cracking along the bed joints. However, these cracks did not widen significantly as the test progressed. Flexure cracks

had already been noted at a loading of 64 kN. Further, documentation of the cracking pattern for each wall was made at regular intervals throughout the test. As mentioned earlier, the load was increased using displacement control and increments of the predicted first yield displacement of the structure. Observations at each of these displacement levels are described in the following sub-sections.

3.3.1.1 Definition of First Yield

The calculated in-plane displacement for the structure at yield was 4.3 mm based on the cracked stiffness of the walls calculated in accordance with the transformed elastic section. Therefore, it was assumed during testing that at a displacement of 4.3 mm, the extreme flexural reinforcing in the C-Wall (Wall 8) would reach yield strain. Normally, the strain gauge data would be used to identify when this actually occurred. However, due to strain gauge malfunction, this was not possible. Furthermore, the displacement data collected during the test required triangulation calculations to determine the in-plane and lateral components of the actual slab movement. Consequently, no yield point could be directly identified during the test. Accordingly, the Hydraulic Actuator displacement was the indicator of the in-plane movement of the building and was used as the basis for the applied displacements during testing for control purposes. The applied 4.3 mm displacements resulted in the building drift increasing in steps of 0.1 to 0.16% drift for each push increment. However, the building's, rather than the actuator's, displacement values were used throughout the analysis as detailed in the following sections and in Chapter 4.

3.3.1.2 0.07% Drift

At drift level of 0.07%, a load of 96 kN was attained. This was much less than the anticipated yield loading of 161 kN. Since the strain gauges were not providing reliable data, this anticipated yield loading could not be confirmed. At this loading level, no visible cracks were apparent beyond those noted for the pre-yield load cycling.

3.3.1.3 0.17% Drift

The structure was displaced again, reaching a drift of 0.17% with the load reaching a peak of 140 kN. During this displacement controlled push, the load dropped suddenly by approximately 15 kN. This could be attributed to sudden cracking of the C-Wall (Wall 8) which had not cracked prior to this loading. This decrease in load occurred near the completion of this push increment and the loading remained at approximately 125 kN.

Examination of the structure after reaching 0.17% drift showed that the existing cracks had propagated. The cracking of the bed joints in the out-of-plane walls had lengthened as was the case with the flexural cracks of the in-plane walls. There was no visual evidence of flexural cracking of the C-Wall (Wall 8). Figure 3.5 shows the cracking pattern of the Centre Wall (Wall 5) at this loading level.

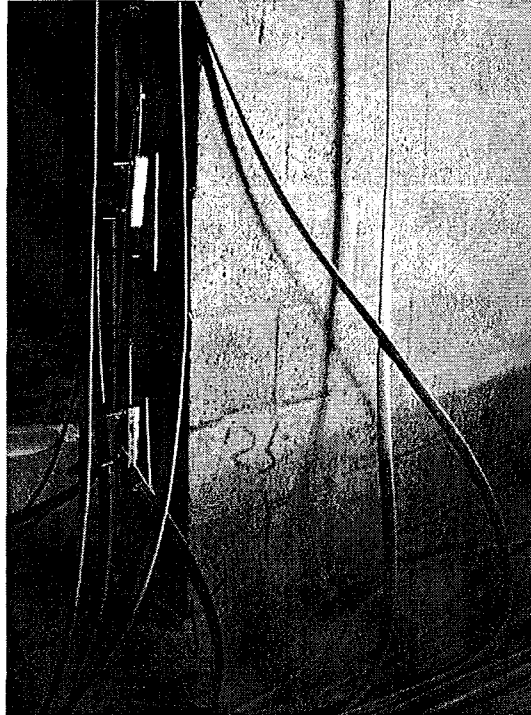


Figure 3.5: Flexural Cracking in Centre Wall (Wall 5) at 0.17% Drift

At this time, it was noted that all cracks marked on the in-plane walls (Walls 1, 2, 5, and 8) were concentrated at the North ends of these walls. Since the loading was not reversed during the course of the final push-to-failure cycle, the crack patterns marked on these walls were concentrated at their North end and therefore the photographs capture those ends of the walls.

3.3.1.4 0.26% Drift

Following another push increment, the drift reached 0.26% and the load reached 170 kN. At this load the flexural cracks in the in-plane walls lengthened again. This continuing crack propagation was evident in all of the in-plane walls. This was the

first loading where cracking of the C-Wall (Wall 8) was visually documented. This cracking included flexural cracking, evident from horizontal cracking of the bed joints at the first and second courses, as well as shear cracking consisting of stepped cracking through head joints at the fourth and fifth courses.

Further to the observed increasing length of the flexural cracks displayed by the in-plane walls, the slab also began to crack at specific locations. The first area was in the span between the two portions of the Double Wall (Walls 1 and 2) at the location where the thickness of the slab section had been reduced. Figures 3.6 to 3.12 document the observed cracking patterns which are marked in blue.

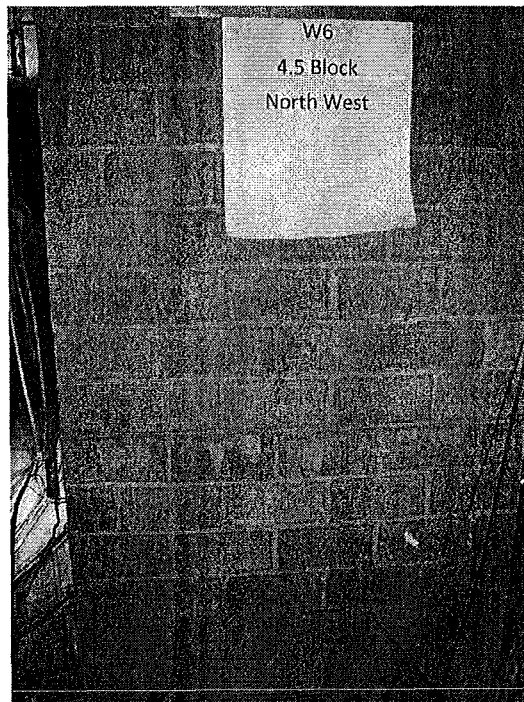


Figure 3.6: Cracking on North West Out-of-Plane Wall (Wall 6)

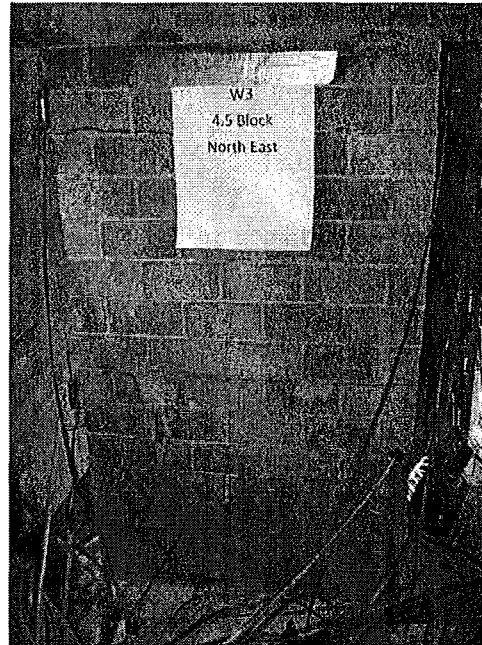


Figure 3.7: Cracking on North East Out-of-Plane Wall (Wall 3)

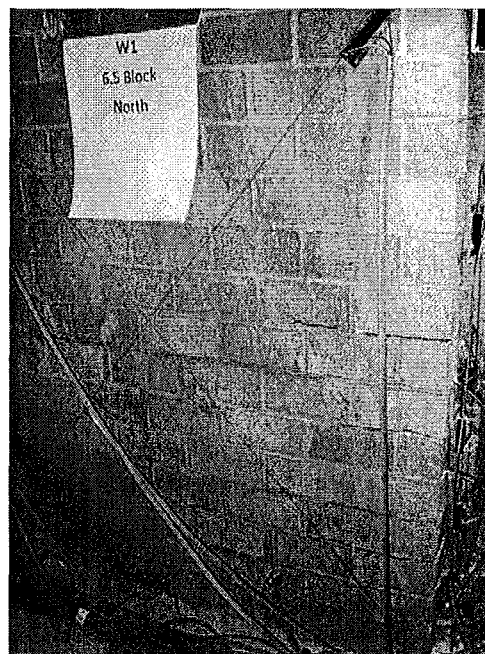


Figure 3.8: Cracking on North Portion of the Double Wall (Wall 1)

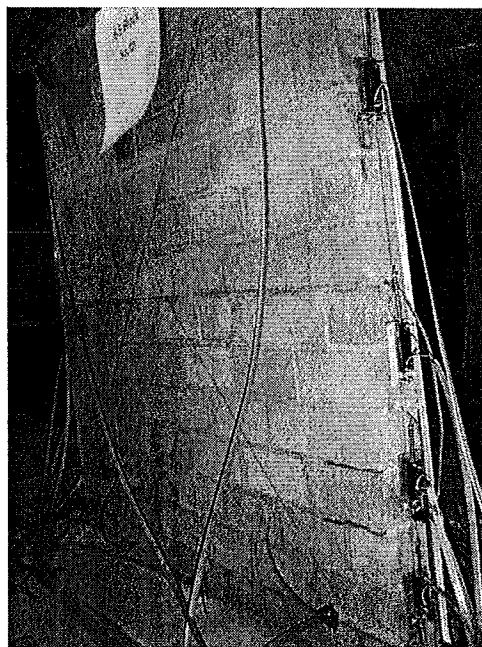


Figure 3.9: Cracking on South Portion of the Double Wall (Wall 2)

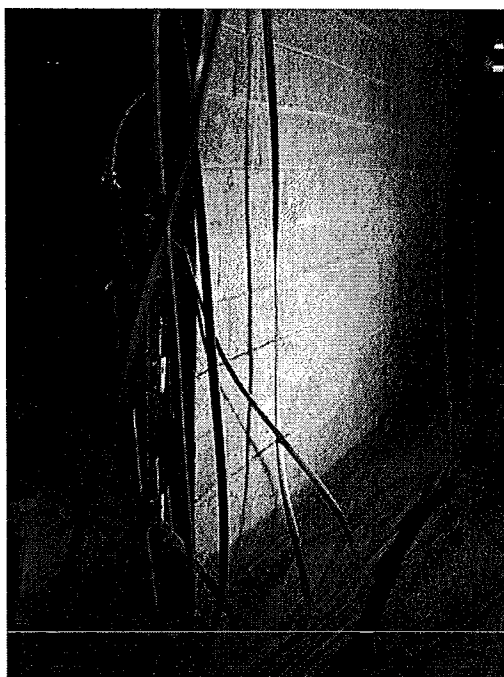


Figure 3.10: Cracking on Centre Wall (Wall 5)

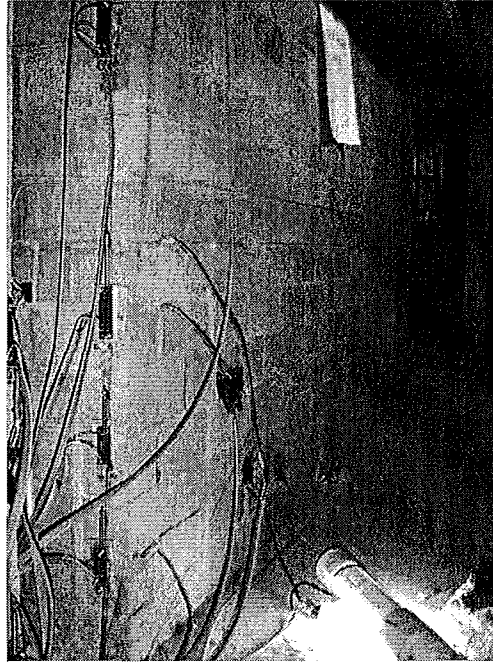


Figure 3.11: Cracking on C-Wall (Wall 8)

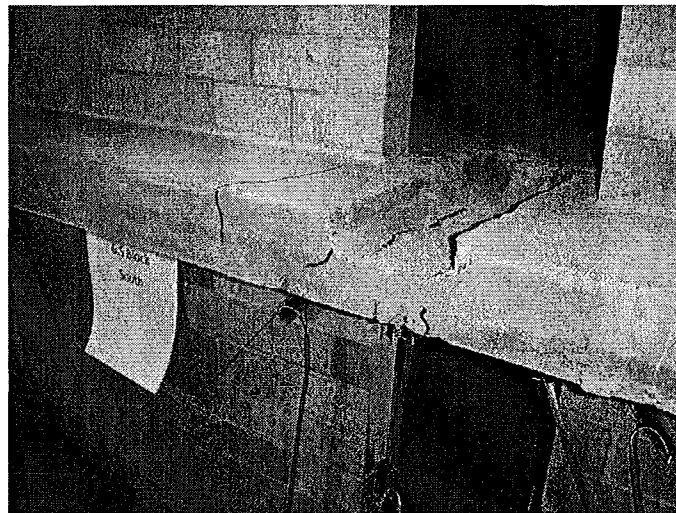


Figure 3.12: Cracking of the First Story Slab between Portions of the Double Wall (Walls 1 and 2)

3.3.1.5 0.38% Drift

After documenting the cracks at 0.26% drift, the building was pushed through to 0.38% drift. This drift level resulted in a corresponding load of 214 kN. The flexural cracks in the in-plane walls lengthened and also increased in number. The new cracks were confined to the bed joints.

During this push load increment, additional cracks opened up in the out-of-plane walls; specifically in the North West Out-of-Plane Wall (Wall 6). Considering the overall direction of rotation of the structure, these cracks could not be attributed to flexure caused by the out-of-plane walls resisting torsional loading. Since the cracking had propagated along the entire length of the bed joints of this wall, it appeared that the cracking could be related to coupling between the C-Wall (Wall 8) and this nearby out-of plane wall which was acting in tension. It could also be attributed to some out-of-plane behaviour of the wall. Figures 3.13 to 3.17 show the progression of the cracking at this load level which is marked on the wall in brown.

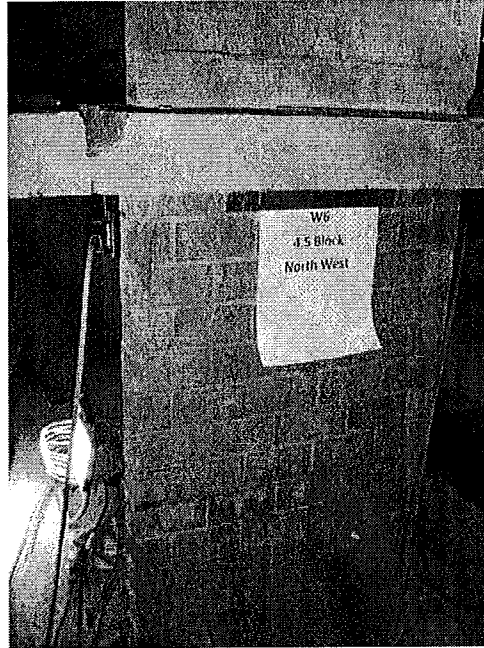


Figure 3.13: Cracking on North West Out-of-Plane Wall (Wall 6)

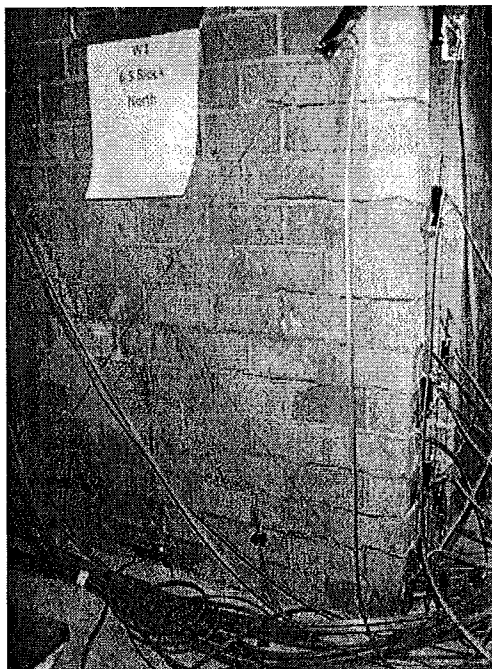


Figure 3.14: Cracking on North Portion of the Double Wall (Wall 1)

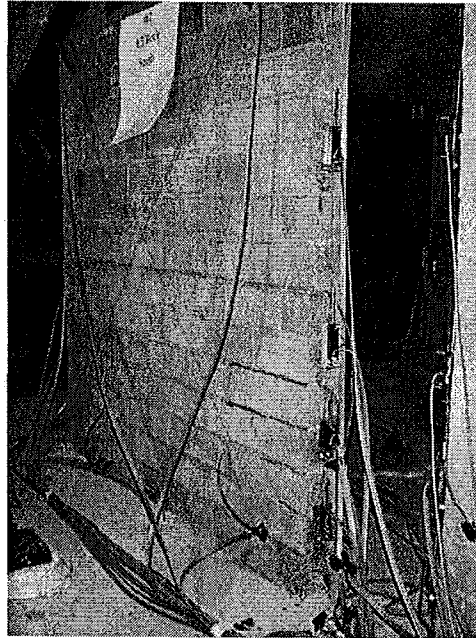


Figure 3.15: Cracking on South Portion of the Double Wall (Wall 2)

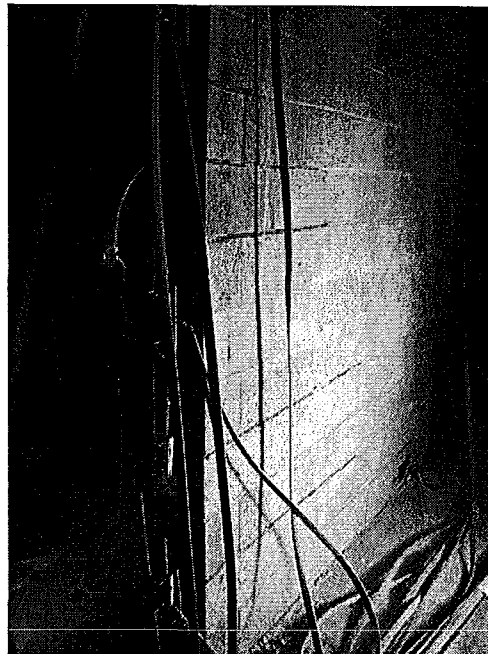


Figure 3.16: Cracking on Centre Wall (Wall 5)

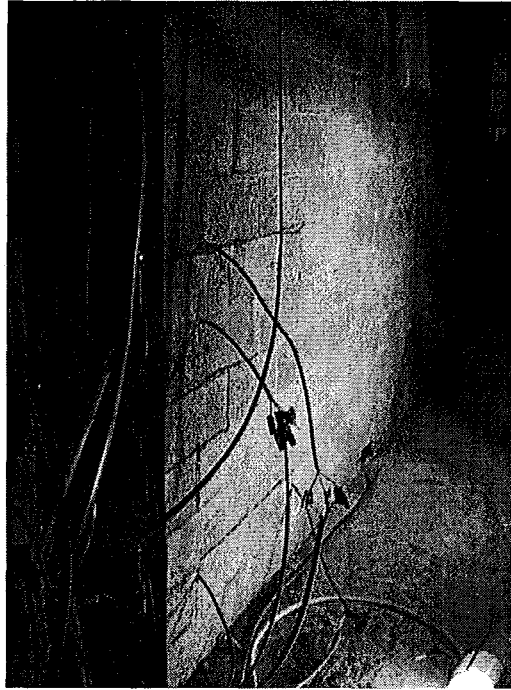


Figure 3.17: Cracking on C-Wall (Wall 8)

3.3.1.6 0.51% Drift

Another push increment resulted in a building drift of 0.51%. This corresponded to a load of 247.7 kN and the opening of a significant number of new cracks in all the walls as well as in the concrete floor slabs. The cracks in the slab started mainly at the reduced slab section between the two portions of the Double Wall (Walls 1 and 2) at the first floor level and extended inwards towards the Centre Wall (Wall 5). Other cracks were noted in the slab at the top floor level in this same area but were not as wide as those observed at the first floor level.

As noted during the previous displacement increment, the flexural cracking of the in-plane walls extended in length and increased in number. The existing cracks had

yet to significantly open with the highest cracks occurring at the eighth course of the first story.

Further cracking of the out-of-plane walls took place spanning the entire length of the walls. Some of these cracks started to propagate upward through head joints. Figures 3.18 to 3.23 illustrate the cracking pattern following this push increment which is marked in pink with hatching.

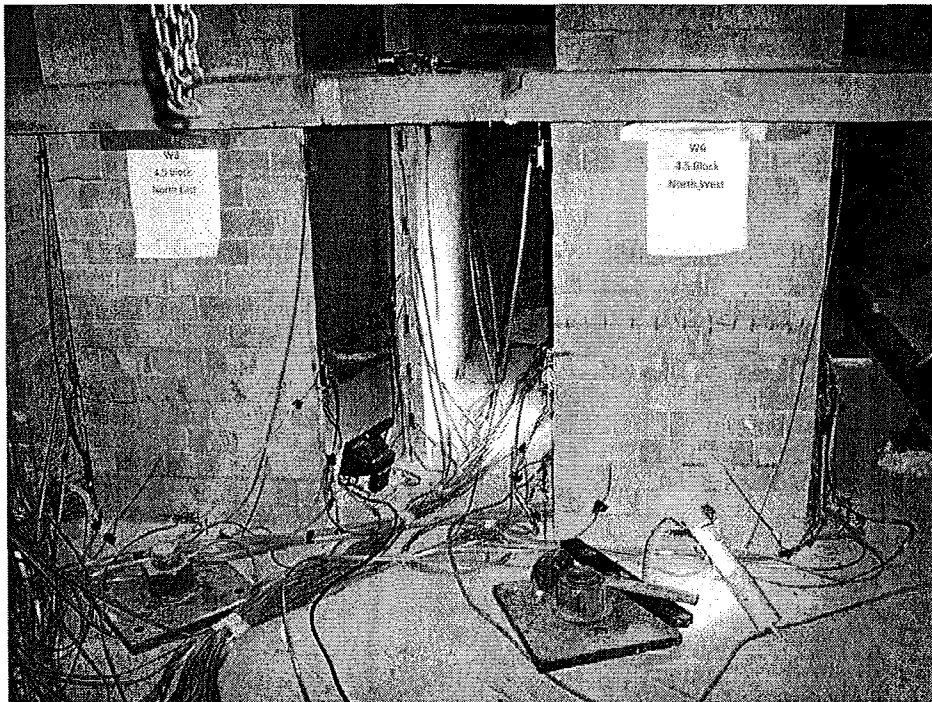


Figure 3.18: Cracking on North East and West Out-of-Plane Walls (Walls 3 and 6)



Figure 3.19: Cracking on North Portion of the Double Wall (Wall 1)



Figure 3.20: Cracking on South Portion of the Double Wall (Wall 2)

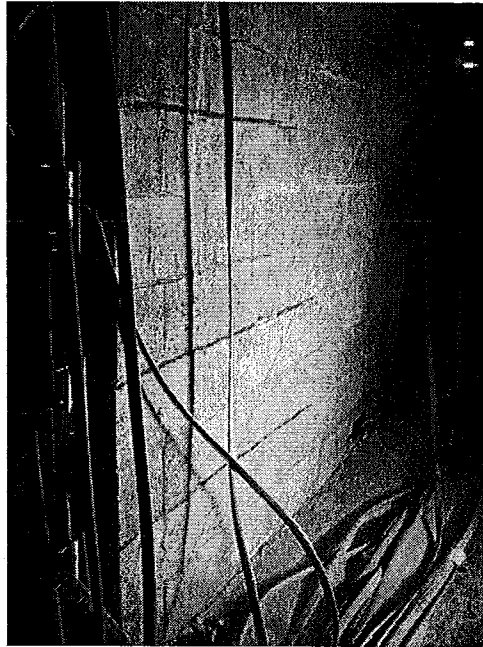


Figure 3.21: Cracking on Centre Wall (Wall 5)

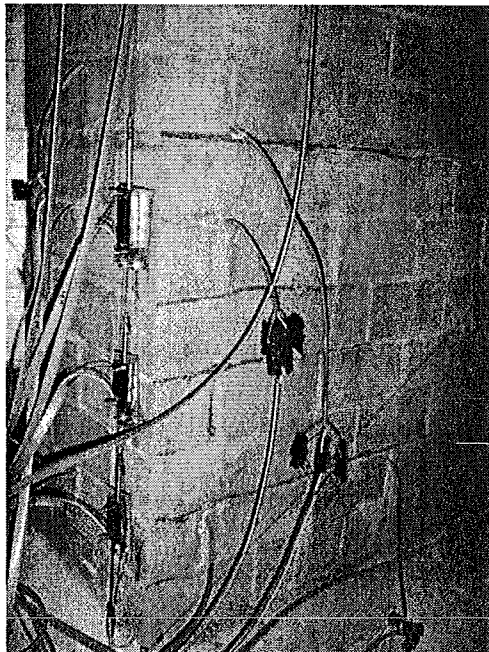


Figure 3.22: Cracking on C-Wall (Wall 8)

3.3.1.7 0.65% Drift

Following another displacement increment, the building drift reached 0.65% and the load reached 280 kN. At this point during the test, some typical diagonal shear cracking began to develop. This occurred in three of the in-plane walls. The first was documented in both portions of the Double Wall (Walls 1 and 2) which showed inclined cracks even through the blocks of the first story. The Northern portion of the Double Wall (Walls 1 and 2), which was the closer of the two to the application of load exhibited significantly less diagonal cracking which was isolated more towards the lower courses of the theorized compression side of the wall while the south portion had more diagonal cracking that extended almost the entire story height.

The Centre Wall (Wall 5) showed some shear cracking in the form of head joint cracks at the tenth course of the first story. The cracks remained isolated to the head and bed joints creating the beginning of a stepped crack. The C-Wall (Wall 8) did not show any inclined cracking at this time. Again, the length of the flexural cracks increased in all in-plane walls. New cracking occurred just below the top slab of the south end of the North portion of the Double Wall (Wall 1) near the gap between it and South portion (Wall 2). Furthermore, the cracks in the out-of-plane walls also extended along the bed joints. Cracks were also noted in the floor slabs at the locations where the sections had been reduced as well as outside these areas. Figures 3.23 through 3.27 illustrate the cracking pattern which is marked on the walls in blue with hatching.

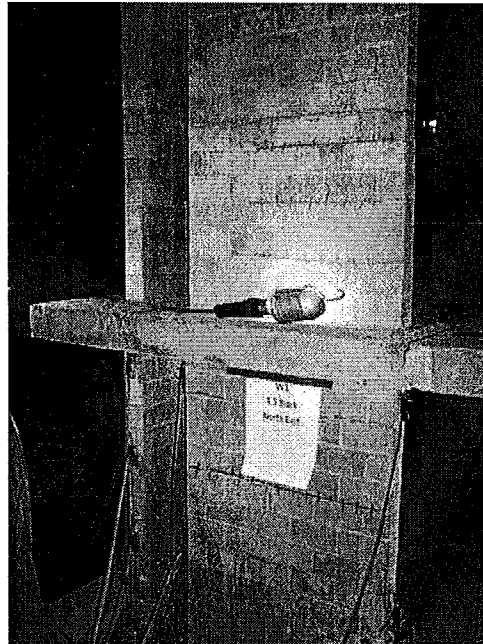


Figure 3.23: Cracking on North East Out-of-Plane Wall (Wall 3)

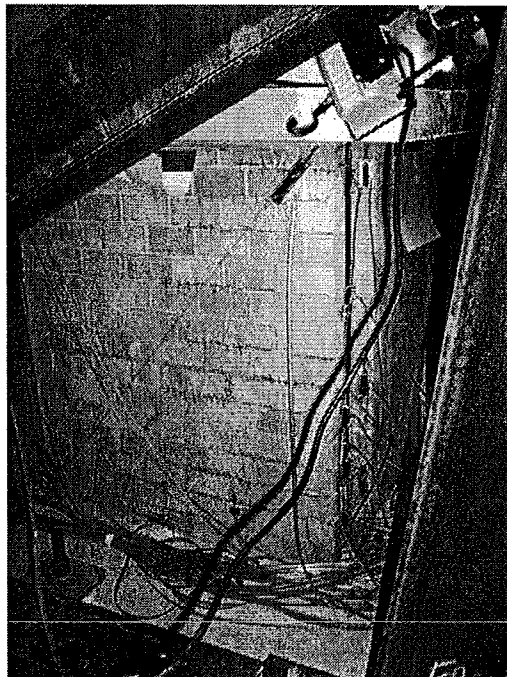


Figure 3.24: Cracking on North Portion of the Double Wall (Wall 1)

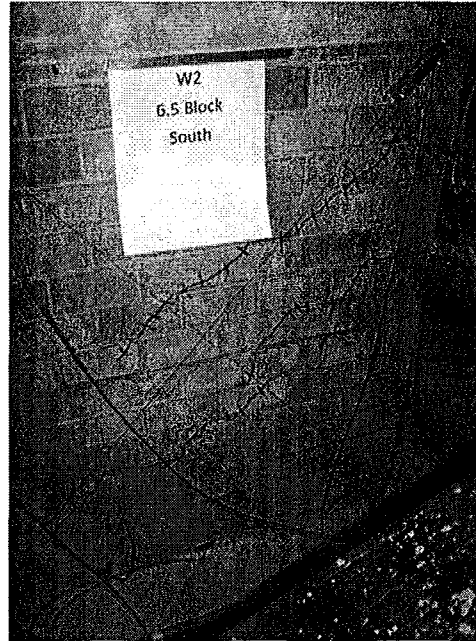


Figure 3.25: Cracking on South Portion of the Double Wall (Wall 2)

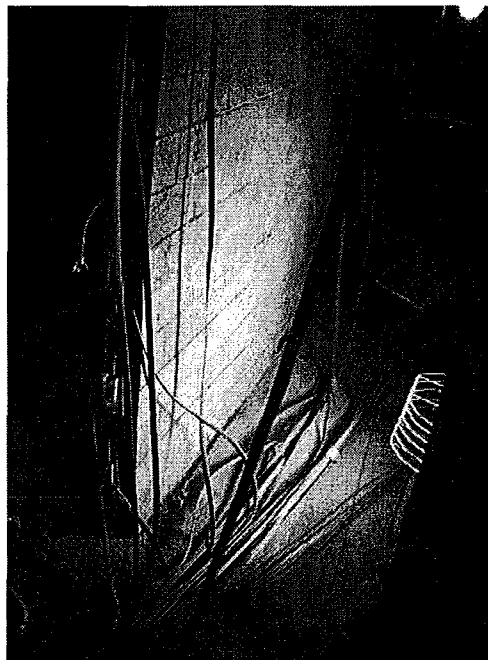


Figure 3.26: Cracking on Centre Wall (Wall 5)

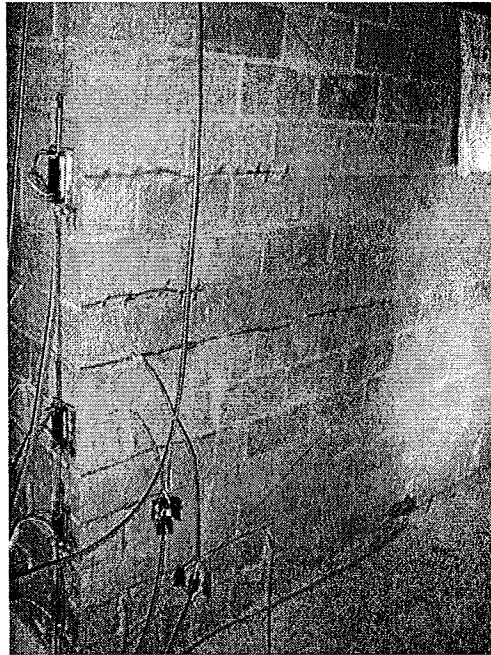


Figure 3.27: Cracking on C-Wall (Wall 8)

3.3.1.8 0.80% Drift

After seven push increments the building drift reached 0.8% drift while the loading had reached 309 kN. At this load level, the C-Wall (Wall 8) also began to show inclined shear cracking while all other in-plane walls also showed increased shear and flexural cracking. All of the cracks remained very narrow with more cracks occurring rather than existing cracks widening. Additional cracking also appeared at the top of the Northern portion of the Double Wall (Wall 1) and extended four courses below the top slab.

Cracking also continued throughout both slabs concentrated primarily between the two portions of the Double Wall (Walls 1 and 2). The out-of-plane walls began to

show more cracking throughout their height along their bed joints. Figures 3.28 to 3.34 document the cracking patterns at this drift level and are marked in green with hatching.

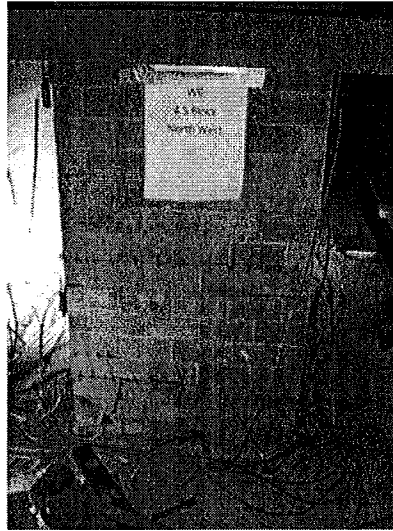


Figure 3.28: Cracking on North West Out-of-Plane Wall (Wall 6)

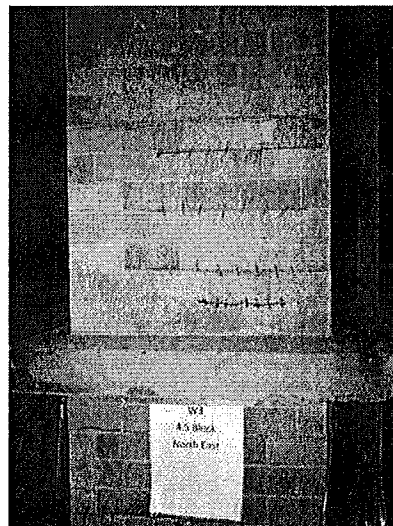


Figure 3.29: Cracking on North East Out-of-Plane Wall (Wall 3)



Figure 3.30: Cracking on North Portion of the Double Wall (Wall 1)

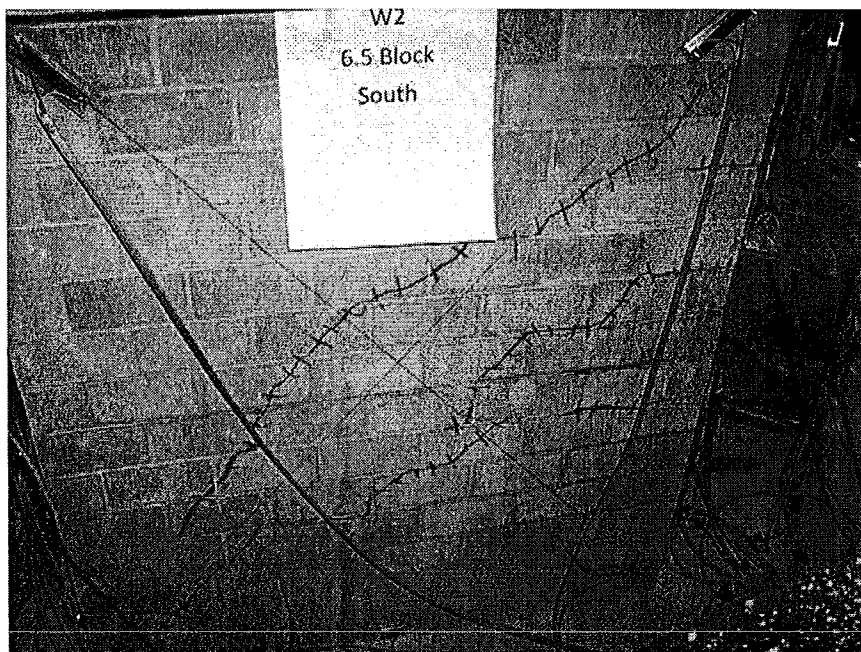


Figure 3.31: Cracking on South Portion of the Double Wall (Wall 2)



Figure 3.32: Cracking in Second Story of the Double Wall (Walls 1 and 2) and First Floor Slab

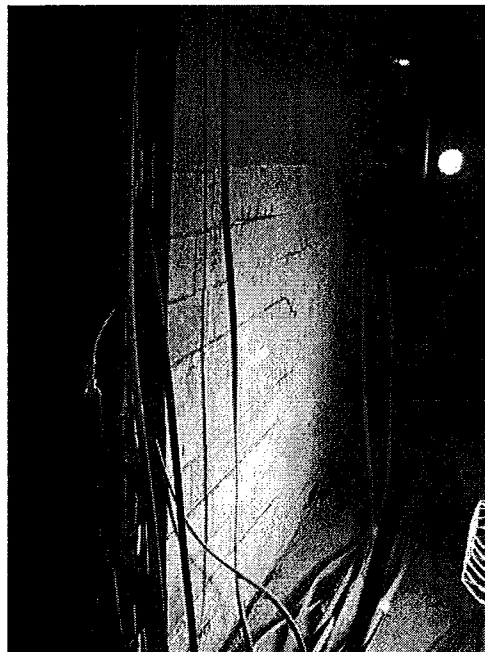


Figure 3.33: Cracking on Centre Wall (Wall 5)

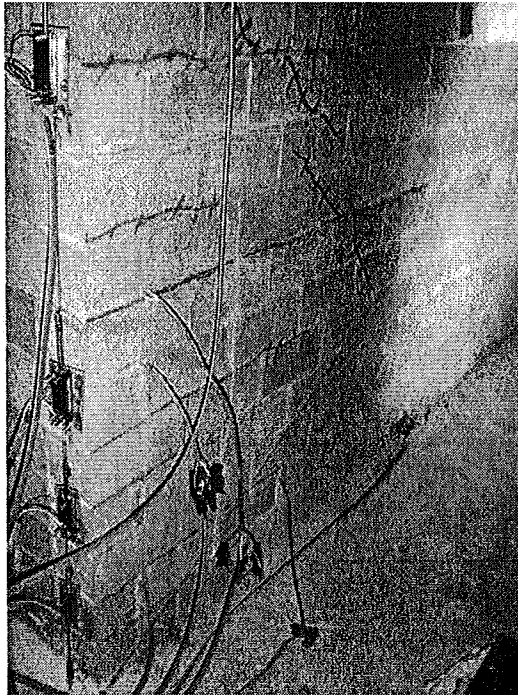


Figure 3.34: Cracking on C-Wall (Wall 8)

3.3.1.9 0.96% Drift

The loading reached 335 kN at a drift level of 0.96%. More significant shear cracking reached the second story of the in-plane walls at this load level. Cracks spread or lengthened on the first story of both the in-plane and out-of-plane walls. For this loading level, the visible cracks were marked in purple with X's and are contained in Figures 3.35 to 3.39.



Figure 3.35: Cracking on North East and North West Out-of-Plane (Walls 3 and 6)

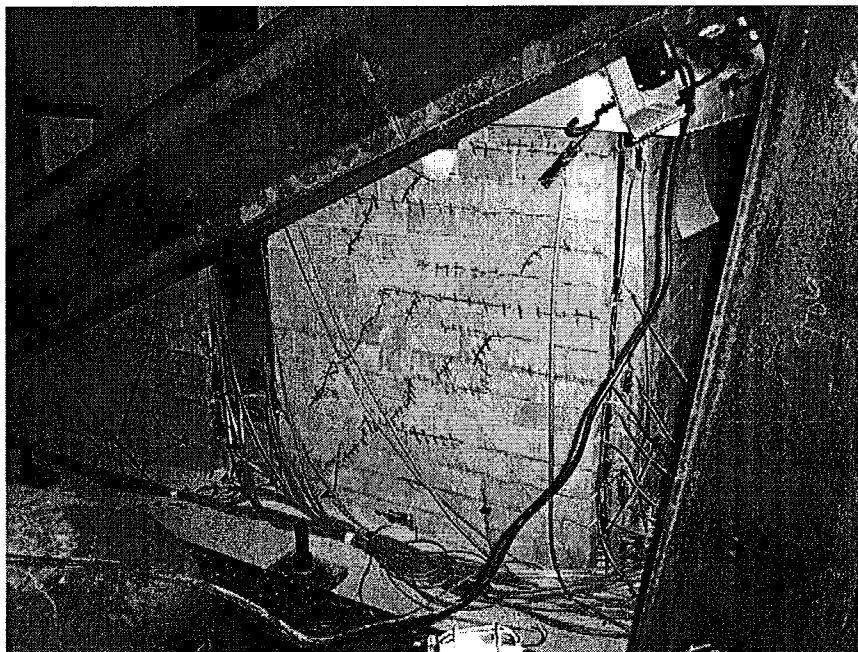


Figure 3.36: Cracking on North Portion of the Double Wall (Wall 1)

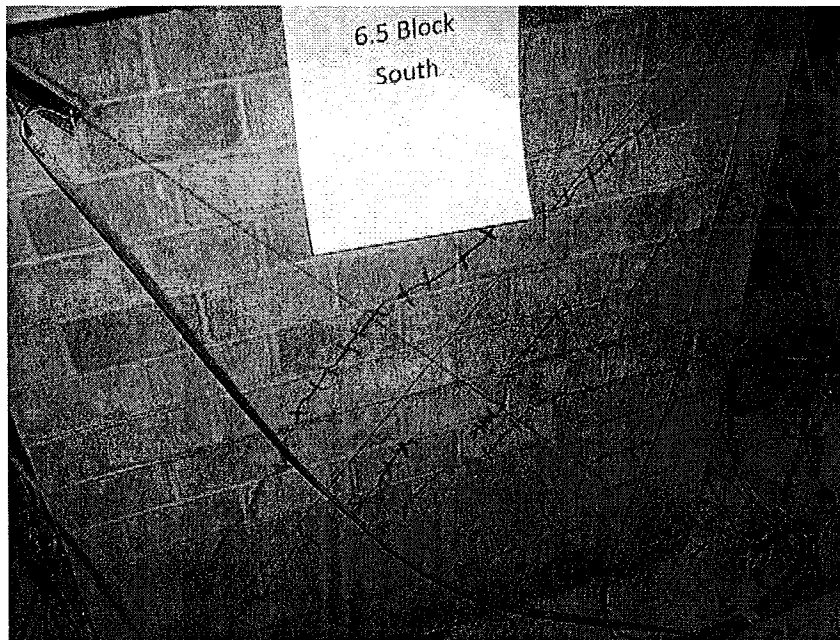


Figure 3.37: Cracking on South Portion of the Double Wall (Walls 2)

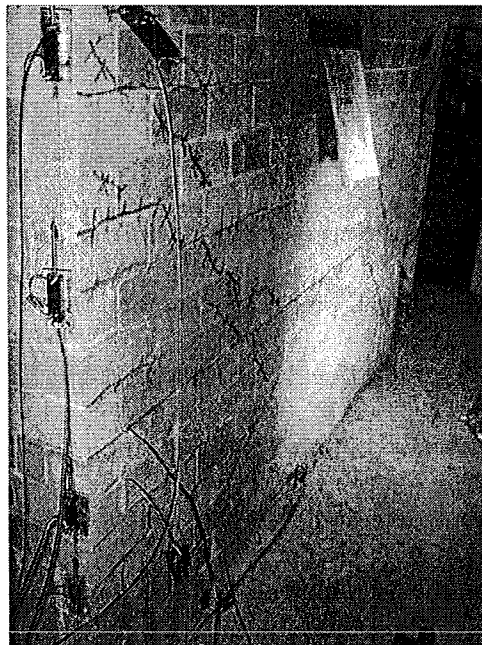


Figure 3.38: Cracking on C-Wall (Wall 8)

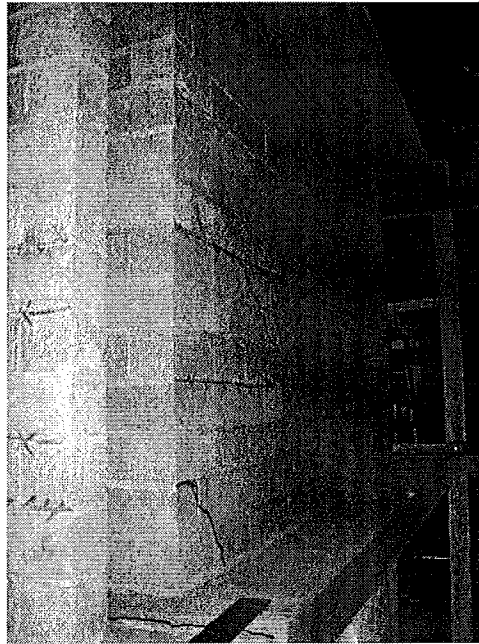


Figure 3.39: Cracking on Second Story of C-Wall (Wall 8)

3.3.1.10 1.13% Drift

Here, the load reached 361 kN at a drift level of 1.13%. Cracking patterns remained similar to the previous displacement increment with more cracking appearing on the second story level. Small pieces of concrete began to spall off of the slab between the two portions of the Double Wall (Walls 1 and 2). The cracking of all in-plane walls was quite extensive by this time. Yet, the cracks in the walls themselves remained narrow with more cracks developing rather than existing cracks widening. Figures 3.40 to 3.46 illustrate the extent of the cracking which is marked in black with circles.

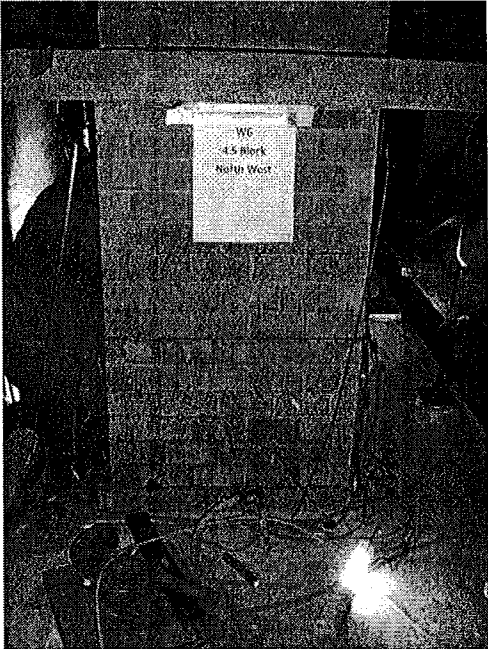


Figure 3.40: Cracking on North West Out-of-Plane Wall (Wall 6)

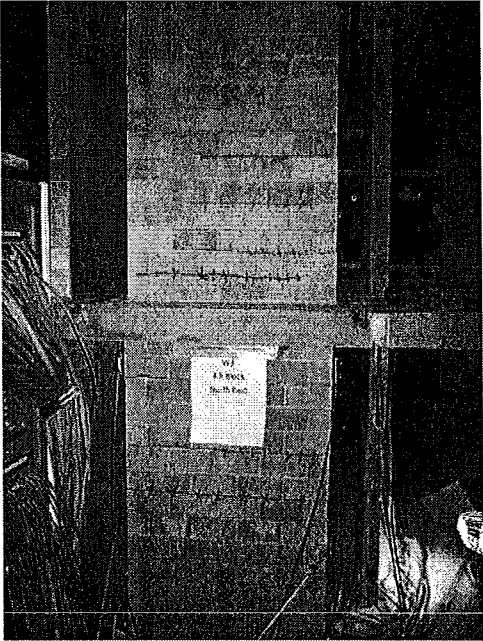


Figure 3.41: Cracking on North East Out-of-Plane Wall (Wall 3)



Figure 3.42: Cracking on North Portion of the Double Wall (Wall 1)

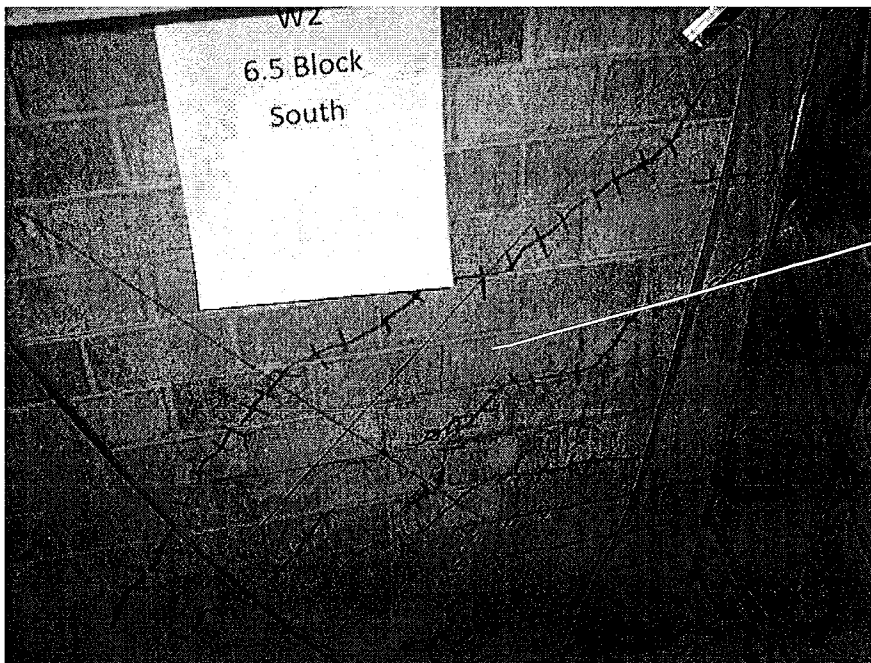


Figure 3.43: Cracking on South Portion of the Double Wall (Wall 2)



Figure 3.44: Cracking in Slab Between Double Wall (Walls 1 and 2) at First Story

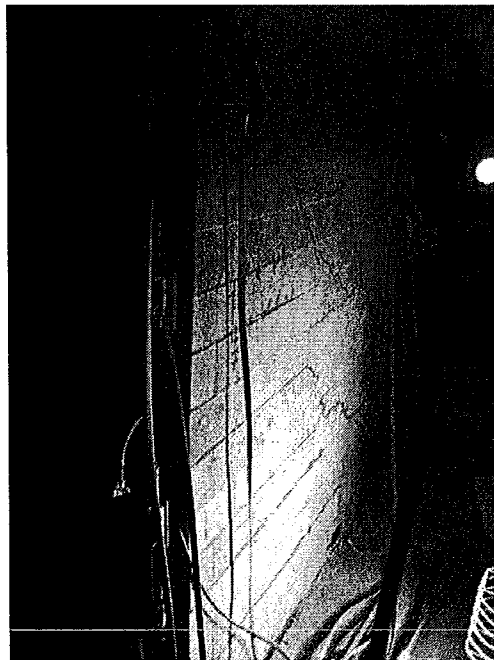


Figure 3.45: Cracking in Centre Wall (Wall 5)

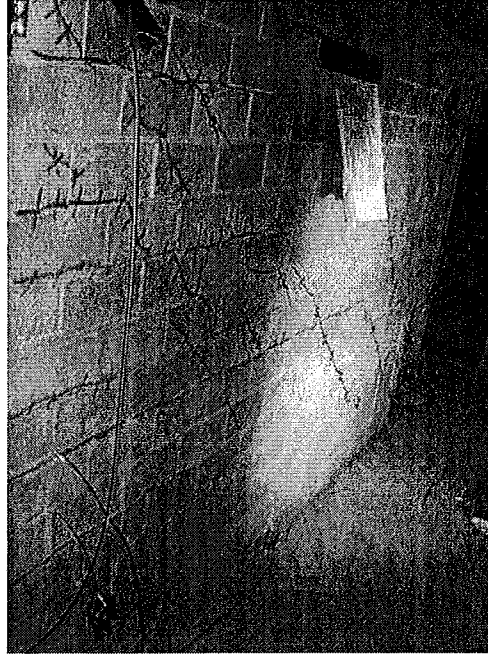


Figure 3.46: Cracking on C-Wall (Wall 8)

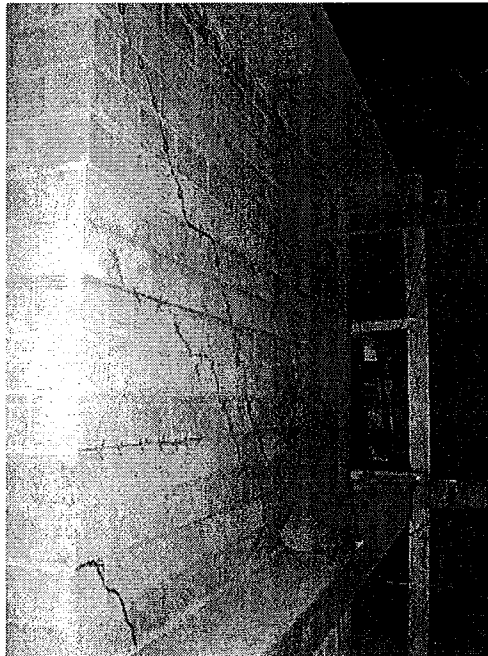


Figure 3.47: Cracking on Second Story of C-Wall (Wall 8)

3.3.1.11 1.26% Drift

During the tenth displacement increment, the loading reached 392 kN at a drift level of 1.26%. The cracking pattern remained similar for this push increment while the visible cracks increased in number as well as length. Further cracking appeared in the second story for all in-plane walls. This was especially true at the second story of the Northern portion of the Double Wall (Wall 1). Here, most new and lengthening cracks appeared at the top of the second story of the wall as shown in Figure 3.50 and radiated into the surrounding slab perpendicular to the wall. The South portion of the Double Wall (Wall 2) only exhibited minor flexural cracking on its upper level and did show lengthening of cracks in the first story. The floor slab at both levels between the Double Wall (Walls 1 and 2) showed significant shear cracks which continued to widen. Additional cracking throughout both the first and second floor slabs was noted at this displacement level. Figures 3.48 to 3.54 show the extent of cracking during this final push increment before the vertical reinforcing bars began to rupture. The visible cracks at this point during the test were marked on pink with circles.

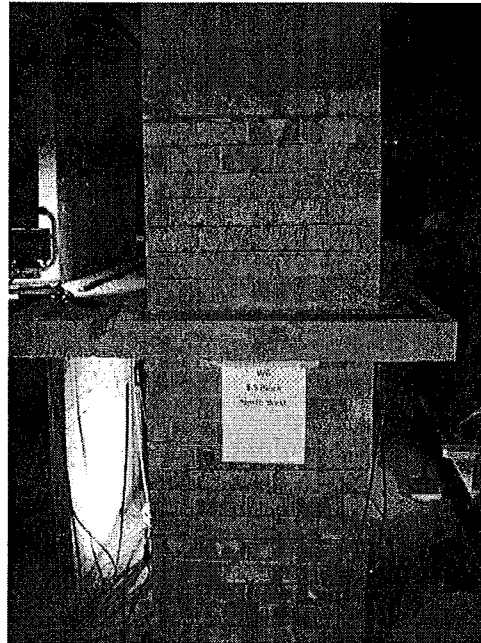


Figure 3.48: Cracking on North West Out-of-Plane Wall (Wall 6)



Figure 3.49: Cracking on North East Out-of-Plane Wall (Wall 3)

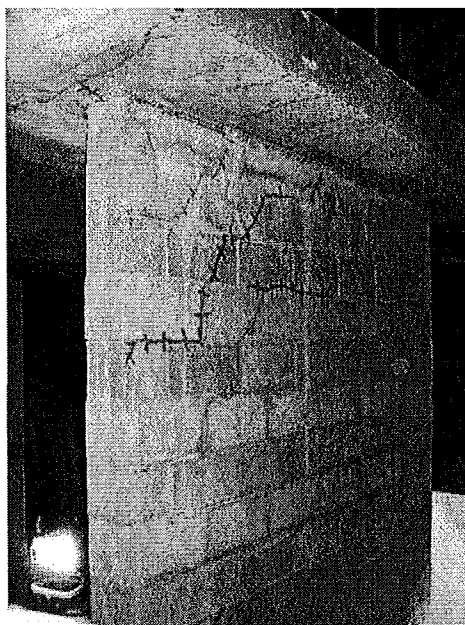


Figure 3.50: Cracking on North Portion of the Double Wall (Wall 1) at the Second Level

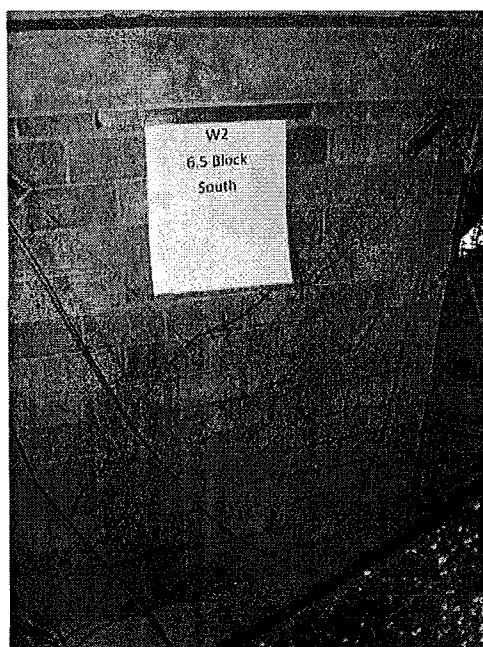


Figure 3.51: Cracking on South Portion of the Double Wall (Wall 2)

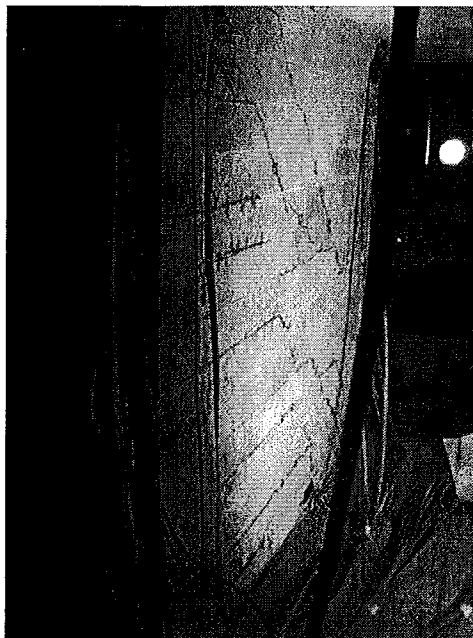


Figure 3.52: Cracking in Centre Wall (Wall 5)

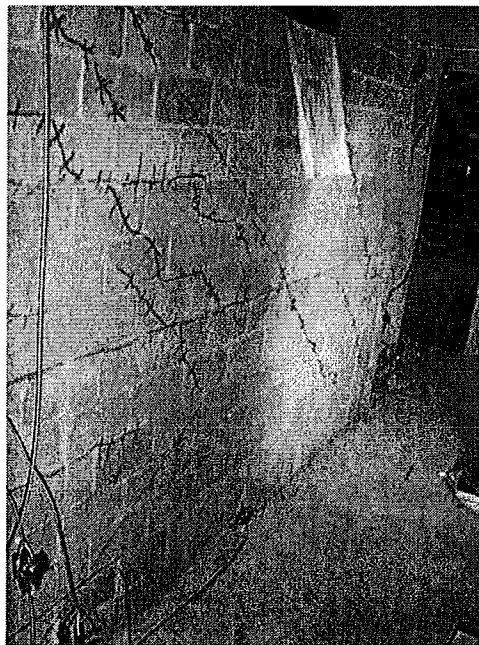


Figure 3.53: Cracking on First Story of C-Wall (Wall 8)

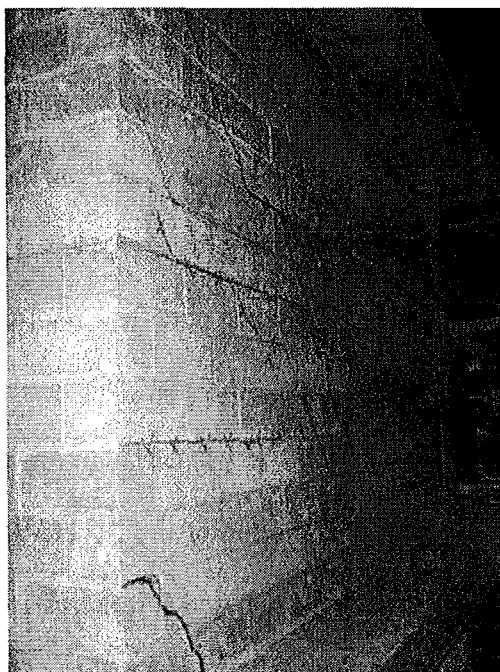


Figure 3.54: Cracking on Second Story of C-Wall (Wall 8)

3.3.1.12 1.55% to 2.03% Drift

Midway through the eleventh push displacement increment, bars began to rupture in the North portion of the Double Wall (Wall 1). This occurred at a load of 394 kN which was the highest load resisted by the structure. The extreme tensile bar of the North portion of the Double Wall (Wall 1) ruptured followed shortly thereafter by rupture of the extreme tensile bar in the South portion of the Double Wall (Walls 1 and 2). Following this, three bars that were difficult to pinpoint at the time then ruptured in rapid succession. At the location of the ruptured bars, a large gap opened up at the North ends of both portions of the Double Wall (Walls 1 and 2). After completing this push increment, the drift level had reached 1.55% and the loading had dropped down to 345 kN which corresponded to about 87% of the peak loading.

The cracking pattern in the walls at this load level had not changed significantly. Again, the length of the flexural cracks increased while more shear cracking occurred in the second story of the in-plane walls. Significant cracking also occurred in specific areas of the roof slab at this time. Wide cracks developed in the slab at the North West corner of the first floor slab between the North portion of the Double Wall (Wall 1) and the North East Out-of-Plane Wall (Wall 3). This crack initiated at the reduced section between these two walls and propagated at an inclination towards the bottom of the slab on the west side of the Northern portion of the Double Wall (Wall 1). This was similar to the crack appearing in the roof slab and first floor slab between the portions of the Double Wall (Walls 1 and 2). Cracks were observed as hairline cracks in many locations around the entire area of both slabs upon the completion of this displacement increment.

When the building was pushed through another increment, bars ruptured in so many locations that it was impossible to determine the sequence of rupture. The load steadily decreased as the displacement increased and bars ruptured. Upon completion of this push displacement increment, the loading had decreased to 295 kN and was steadily declining without further displacement input. Since the loading had fallen below 80% of the peak value ($0.8 \times 396 \text{ kN} = 317 \text{ kN}$), the test was stopped as per the predetermined test termination point. The test was completed at a drift level of 2.03%. Figures 3.55 through 3.62 illustrate the cracking patterns observed at the final stage of the pushover test. The visible cracks were marked in purple with circles.

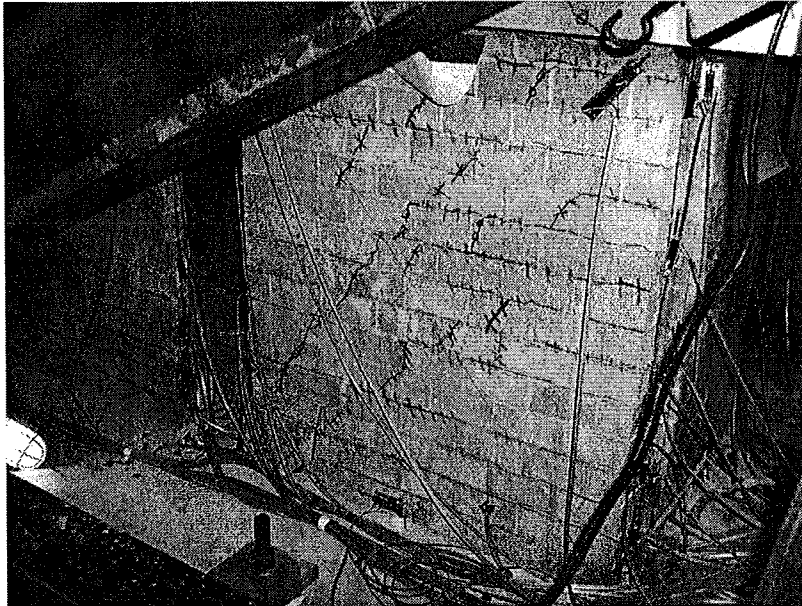


Figure 3.55: Cracking in North Portion of the Double Wall (Wall 1)

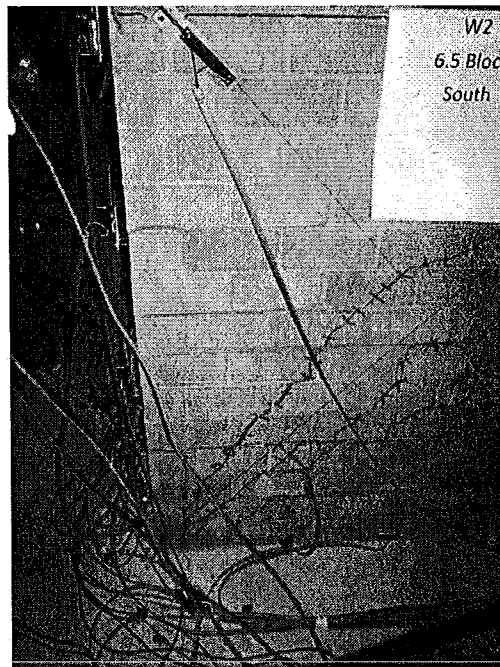


Figure 3.56: Cracking in South Portion of the Double Wall (Wall 2)

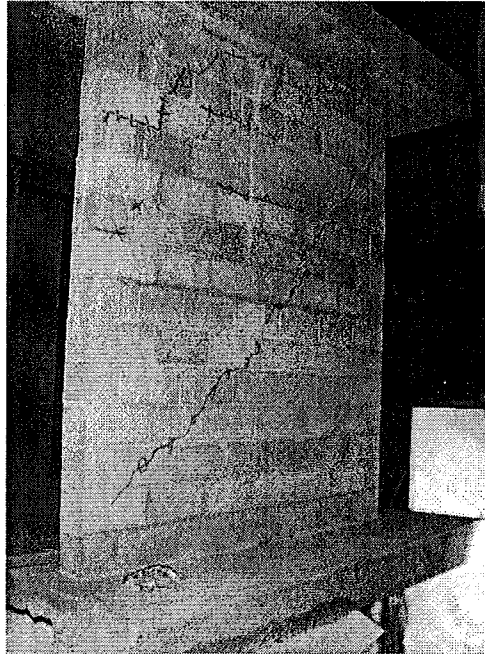


Figure 3.57: Cracking in Second Story of the North Portion of the Double Wall (Wall 1)



Figure 3.58: Cracking in Second Story of the South Portion of the Double Wall (Wall 2)

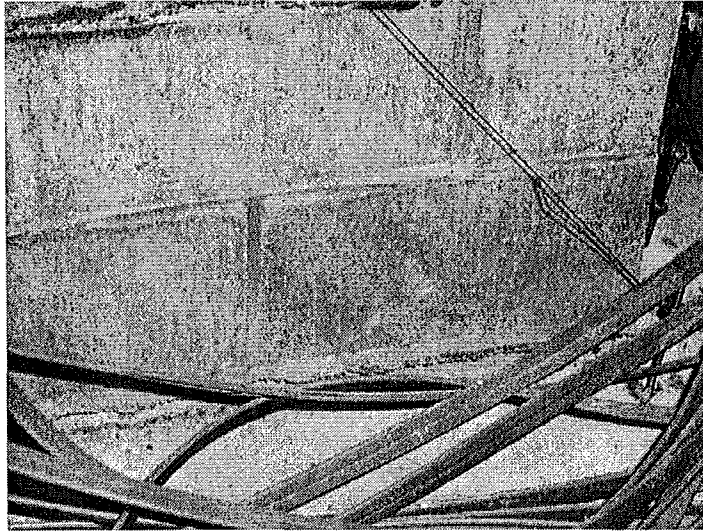


Figure 3.59: Uplift on North Portion of the Double Wall (Wall 1)

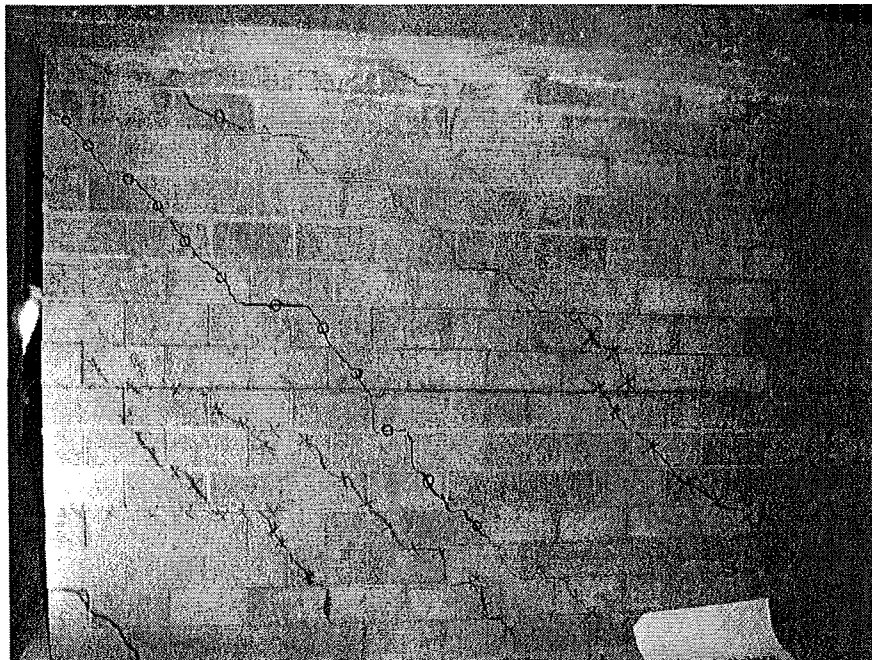


Figure 3.60: Cracking in Second Story of C-Wall (Wall 8)

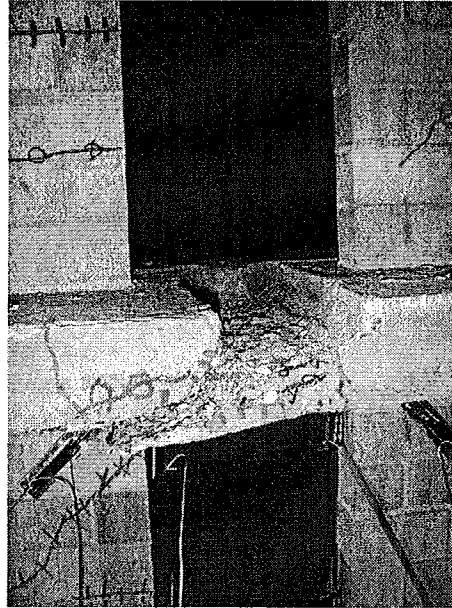


Figure 3.61: Slab Failure Between Portions of the Double Wall (Walls 1 and 2) after Bar Rupture

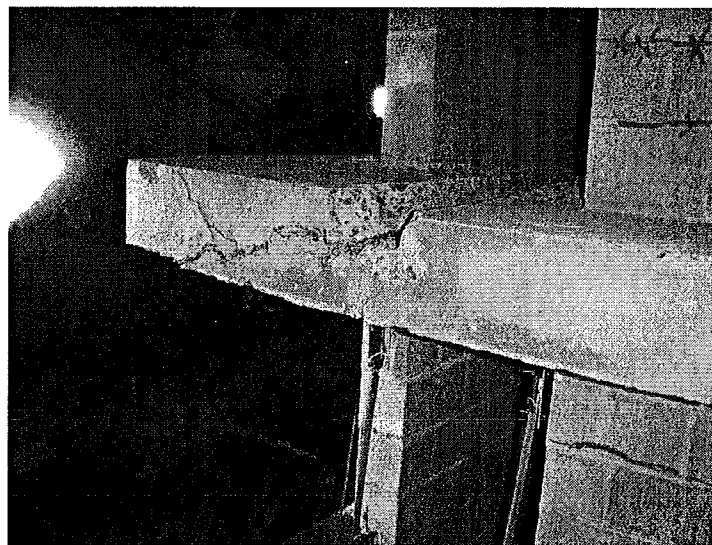


Figure 3.62: Slab Failure Between the North Portion of the Double Wall (Walls 1 and 2) and the North East Out-of-Plane Wall (Wall 3)

3.4 Conclusion

This chapter documents the overall behaviour of the individual walls along with the general structural response. This includes photographs, observations and graphical data. It was obvious that the structural behaviour of the building was limited by the brittle nature of the vertical reinforcing bars which ruptured before the masonry could crush in compression. This limited the ductile potential of the walls. Since the Double Wall (Walls 1 and 2) at the East end of the building was incapable of significant plastic deformation due to this, the input loading could not be completely redistributed to the other in-plane walls of the structure. Furthermore, flexural compressive masonry damage was not present even at the peak lateral loading condition, further limiting ductility (Masonry damage aids in energy dissipation capabilities of reinforced masonry shear walls). Since the masonry did not undergo large strains or exhibit any toe damage, only minor energy dissipation occurred prior to the reinforcement rupture. However, even with these limitations, the structure exhibited exceptional drift capability. The structure reached 1.26% drift without any significant damage. Even after some vertical reinforcing bars ruptured, the building still maintained over 70% of its peak strength up to 2% drift.

It is also obvious that the brittle nature of the vertical reinforcing bars eliminated the possibility of collection of much post-peak load displacement data. After the bars ruptured, the stiffness of the structure was compromised and the structure was unable to maintain the input displacement without sacrificing further lateral load

resistance. In this regard, the descending branch of the load displacement curve is slightly misleading. Since data scans only occurred every 10 seconds, the collected data did not capture the instant loss in stiffness that the rupture of the vertical reinforcing bars represented. The line connecting the peak and the residual strength is only the graphing software connecting two moments in time; a moment before peak loading and a moment some time later.

Also noted at this time was the moderate success of the defined hinging points of the slab. The slab maintained its rigidity during the experiment with some cracking throughout its area. The shear failure pictured in Figures 3.60 and 3.61 only occurred after the vertical reinforcing bars had ruptured causing a significant redistribution of loading through the slab to the remaining walls. Since this failure happened during post-peak loading, the main analysis presented in Chapter 4 will focus on the data collected up to the peak lateral loading.

4 Analysis of Test Results

4.1 Introduction

The collected data is analyzed in this chapter and the actual response of the structure is compared to predicted response as it relates to the structure's seismic performance. The global values of the seismic ductility related reduction factor R_d , presented in CSA S304.1 (2004) and the National Building Code of Canada (NBCC, 2010) are examined to determine if they are underestimated for reinforced masonry as a system. Additionally, the behaviour of the individual walls will be examined relative to their observed behaviour as tested in isolation by Wierzbicki (2010).

4.2 General Building Response

The load-displacement data for the test structure was presented in Chapter 3. In this chapter, the building response will be examined in more detail. First, the initial predicted response, based on cracked section properties and no coupling between walls, will be presented. Following this, an analysis considering coupling between the shear wall elements will be presented. These predicted behaviours will then be compared against the observed structural response.

4.2.1 Initial Prediction of Structural Response

Prior to testing, a simplified analysis of the building was carried out to establish a reasonable experimental procedure. Prediction of the response of the structure consisted of predicting the individual wall responses which were assumed to have

perfect elastic-plastic responses. Since the initial intent of the test program was to limit inter wall coupling via section reduction, the initial assessment of the strength and stiffness of the structure was found as an algebraic sum of the strengths of the in-plane walls. The out-of-plane walls were intended to resist torsion as the in-plane walls reached plastic conditions. A related idealization that was made was that the building was assumed to deflect in the plane of loading without twisting. Therefore, for analytical purposes, the walls were all assumed to undergo the same in-plane displacement. Figure 4.1 shows the total load displacement curve for this simplified analysis.

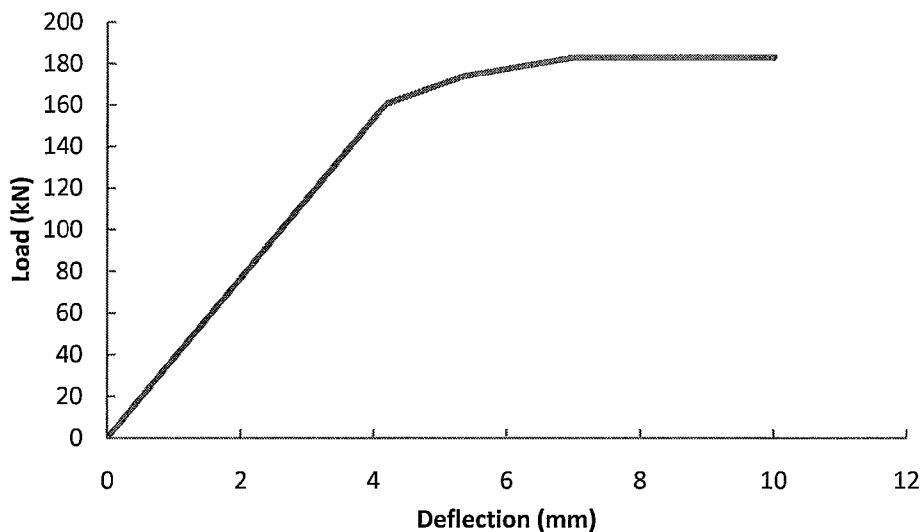


Figure 4.1: Preliminary Idealized Elastic-Plastic Building Behaviour

This analysis predicted first yield and ultimate strengths of 161 and 183 kN, respectively. Initially, all in-plane walls contributed via their in-plane elastic stiffness. The C-Wall (Wall 8) reached yield first at approximately 4.3 mm of in-plane deflection

and was assumed to then behave perfectly plastically while the Centre Wall (Wall 5) and both portions of the Double Wall (Walls 1 and 2) reached their plastic states at 5.4 and 7 mm, respectively. At the point of C-Wall (Wall 8) yielding, the stiffness of the building decreased significantly. This analysis is obviously very conservative in that ultimate wall capacities are much larger than the yield loads. However, it was deemed sufficient for organizing the load increments.

During the initial design phase, the predicted centre of rigidity was calculated using elastic cracked section properties. This analysis was performed initially to determine torsion and to check the response of the out-of-plane walls. For the final wall layout, the centre of rigidity was calculated as 27% of the width of the building or 540 mm towards the C-Wall (Wall 8) from the geometric centre of the building where the lateral load was applied. At peak load during plastic deformation, the eccentricity of the resultant of the wall resistances can be found by determining the position of the resultant of the ultimate strengths of all of the in-plane walls which can be expressed as:

$$e = \frac{P_{ult-c}(e_c) + P_{ult-center}(e_{center}) + P_{ult-Double}(e_{Double})}{\sum P_{ult}} \quad \text{Eq. 4.1}$$

where:

P_{ult-i} = Ultimate Lateral Loading of Respective Wall (kN)

e = Eccentricity of Resultant of in – plane Lateral Force Resistances

e_i = Eccentricity of Wall

At plastic conditions, this gives the position of the resultant of the in-plane internal forces acting on the building at an eccentricity of 345 mm from the location of

the externally applied force. The objective of the out-of-plane walls (Walls 3, 4, 6, and 7) was to resist the resulting torsion based on these calculated eccentricities.

4.2.2 Coupling Behaviour

As mentioned previously, it was discovered during construction that decoupling of the walls was not feasible given the relatively small size of the specimen and associated restrictions for distances between adjacent walls. Subsequently, hinge locations were chosen to control coupling rather than eliminate it so that a more detailed analysis could be performed. This analysis was performed based on observed behaviour and cracking patterns as well as basic structural mechanics. The system coupling could be defined by the weak beam/strong column mechanism as outlined by Drysdale, and Hamid (2005). Figure 4.2 illustrates this structural mechanism.

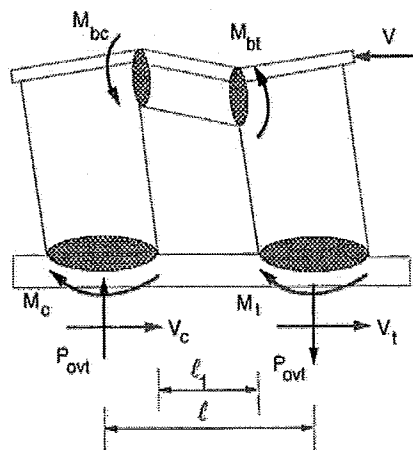


Figure 4.2: Weak Beam-Strong Pier Mechanism (Drysdale and Hamid, 2005)

where:

M_c, M_t
= Flexural strength of the compression and tension piers, respectively

P_{ovt} = Overturning force developed in the piers
defined by shear force in the coupling beam

M_{bc}, M_{bt} = Flexural strengths of the compression and tension
end of the coupling beam, respectively

l_1 = clear length of coupling beam

l = distance between centre lines of piers

h = height of applied lateral load

with:

$$V = \frac{M_c + M_t + P_{ovt}l}{h} \quad \text{Eq. 4.2}$$

$$P_{ovt} = \frac{M_{bc} + M_{bt}}{l_1} \quad \text{Eq. 4.3}$$

In this case, the out-of-plane walls were connected via the floor slab to the other shear walls. Due to the close proximity of the out-of-plane walls to the C-Wall (Wall 8) and Double Walls (Walls 1 and 2), the analysis was performed based on coupling occurring only between the Double Wall (Walls 1 and 2) and the two closest out-of-plane walls and between the C-Wall (Wall 8) and the remaining two out-of-plane walls. The width of slab considered to be effective in coupling the in-plane walls to the respective out-of-plane walls is illustrated in Figure 3.11. For the Double Wall (Walls 1 and 2), the effective width of the slab for coupling is denoted by the dimension A. For the C-Wall (Wall 8), the effective widths are B and C for the North and South end of the wall, respectively. As originally intended, the slab cross section was notched in the region of high slab moment near the Centre Wall (Wall 5); this was an attempt to create hinges which were assumed to reduce its coupling with the other walls. Therefore,

although some moment would be developed in the slab due to the short distance between 'hinge' and the Centre Wall (Wall 5), for the purposes of this analysis, it was assumed that the Centre Wall (Wall 5) did not participate in the overall system coupling.

As shown in Figure 4.3, the slab was considered to be hinged at the mid-length distance between the coupled walls where the slab was notched. However, because the slab reinforcement was located at 65 mm from the top of the 90 mm thick slab, for constant shear along the length of this coupling element, the maximum moment that would be developed was controlled by the minimum capacity. In the illustration this is at the left end where negative moment capacity is:

$$M_{1Plastic} = T_1(d_1 - a) \quad \text{Eq. 4.4}$$

with:

$$T_1 = A_s f_y$$

$$A_s = \text{Area of Steel (mm}^2\text{)}$$

$$f_y = \text{Yield Strength of Reinforcing Steel (MPa)}$$

$$a = \text{Depth of Equivalent Rectangular Stress Block (mm)}$$

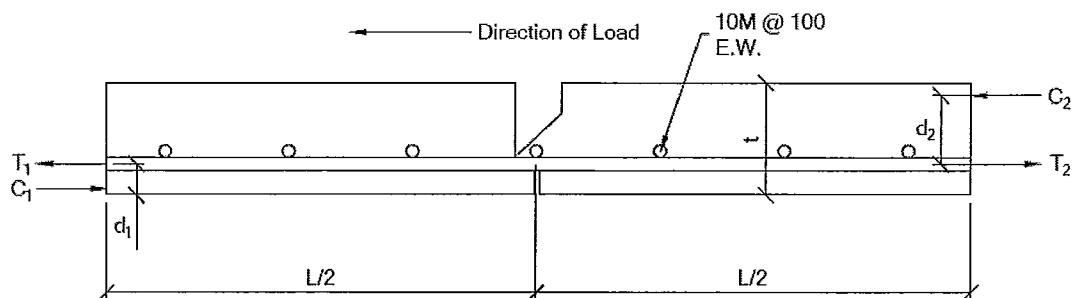


Figure 4.3: Development of Plastic Moment through Idealized Hinges

In order to identify the amount of actual coupling in the structure, three scenarios were examined. First, the building was considered to be uncoupled; second, the building was coupled via idealized hinges as described above; and third, the building was considered to be fully coupled by the floor slabs. In this final case, the out-of-plane walls (Walls 3, 4, 6, and 7) were coupled by the slab. This was considered to be a general coupling case governed by diaphragm behaviour. The North out-of-plane walls (Walls 3 and 6) were considered to be tensile piers governed by the tensile yielding of their vertical reinforcing while the South out-of-plane walls (Walls 4 and 7) were considered to be compression piers with roughly the same force (but compression) as the tensile piers. This coupling moment was then added to the flexural strengths of the Coupled Double Wall (Walls 1 and 2), the Centre Wall (Wall 5) and the C-Wall (Wall 8). Table 4.1 contains the results of the analysis for these different coupling scenarios.

Table 4.1: Summary of Building Analysis for Effect of Coupling

Scenario	Ultimate Predicted Lateral Loading (kN)
No Coupling	183
Idealized Diaphragm Hinging	382
Complete Coupling	500

In considering the reliability of this analysis, the close agreement between the theoretically calculated wall strengths and experimental results including the coupling behaviour of the Double Walls (Walls 1 and 2) is noted (Wierzbicki, 2010). From Table 4.1, it is clear that the building, which achieved a maximum lateral load of 392 kN, is most accurately classified in the middle category as one with idealized diaphragm

hinging. For the hinged diaphragm, the calculated building strength was 2.4% less than the actual experimental peak load. The difference between these values could easily be accounted for by the fact that the Centre Wall (Wall 5) would have provided some additional coupling and therefore additional strength that is not accounted for here. Also, it is noted that some small moment could be developed at the ‘hinges’ which could allow slightly more moment to be developed at the non-controlling end of the coupling element. Admittedly, this analysis is simplified and, in reality, the actual distribution of coupling could be different than that which was assumed. However, for this preliminary step in system testing and analysis, this method seems sufficient to explain the observed building capacity.

4.3 General Experimental Observations

The structure performed well despite the relatively brittle nature of the vertical reinforcing bars. As previously mentioned, the predicted lateral yield and ultimate capacity of the structure was 161 kN and 183 kN, respectively. The point of predicted first yield was defined by yielding of the extreme flexural reinforcement in the C-Wall (Wall 8). As discussed in Chapter 2, unreliable strain gauge data prevented this point from being identified and, therefore, the theoretical yield displacement was chosen as the step size for the displacement controlled loading. It is known that, because of coupling, shear deformation, and use of actuator displacement instead of absolute building displacement, this will not represent actual first yield but simply serve as a convenient displacement increment size. As such, the following analysis relies on

previously collected deflections and curvature data to identify yield displacements and subsequent load distributions (Wierzbicki, 2010).

4.3.1 Displacement Response

The load increments used for the push loading to failure were based on the actuator displacement. Since the extension of the actuator included both the deflection of the structure and the deflection of the supporting frame, the absolute building deflection is less. Also, since the building was unsymmetrical, the in-plane walls did not deflect the same amount at each load increment. The Double Wall (Walls 1 and 2), located at the East side of the structure, represented the weak side of the structure and subsequently experienced the greatest deflections. This is the expected result of torsion because, even though the out-of-plane walls were designed to resist torsion, it would be shared by the in-plane walls until they became fully plastic. The C-Wall (Wall 8), located at the West end of the structure, was on the stiff side of the structure and therefore experienced the smallest deflections of the three in-plane walls for a given lateral load. This was consistent with the prediction of the unsymmetrical response as outlined in subsequent sections.

4.3.2 Torsional Response

As stated earlier, the building was unsymmetrical in the plane of loading. Therefore, as lateral load was applied to the structure, both in-plane and lateral deflections at the South end of the building were observed.

During the experiment, due to safety concerns, efforts were made to laterally stabilize the hydraulic actuator. This reduced the ability of the structure to twist freely. Initially, the supports consisted of chains tied back to the main trusses of the test rig as well as a basement jack under the midpoint of the actuator which would have allowed some lateral movement of the actuator. During the test, it became apparent that additional stabilization of the jack was required for safety purposes. Therefore, cargo straps were connected to the jack and used for additional lateral support. The result of this effort was that these supports prevented the actuator from freely moving laterally thereby restricting the lateral movement of the North end of the building. Although, this prevents a reasonable analysis of the torsional response of the structure, at the stage of plastic behaviour of the in-plane walls, all that is required of the out-of-plane walls is that they provide adequate torsional stability.

Figure 4.4 shows the in-plane and out-of-plane movements of the South East and South West corners individually which clearly show the lateral movement of the structure.

Each data point on the line of each corner of the slab is associated with the corresponding point on the other line. For example, both final points on each line denoted by A and A' represent the corner displacement at the peak loading. Following each data point down one by one yields subsequent associated points as shown by B and B'. From this, it can be seen that at the onset of loading, the corners of the slab moved in a nearly identical fashion. However, as the loading progressed and the

building twisted, the South West corner, which was nearest to the stiff C-Wall (Wall 8) deflected less in its plane relative to the South East Corner but moved more in the lateral direction. As can be seen, the North Corners nearest to the lateral restraint provided by the actuator had similar in-plane deflections but lower out-of-plane movement.

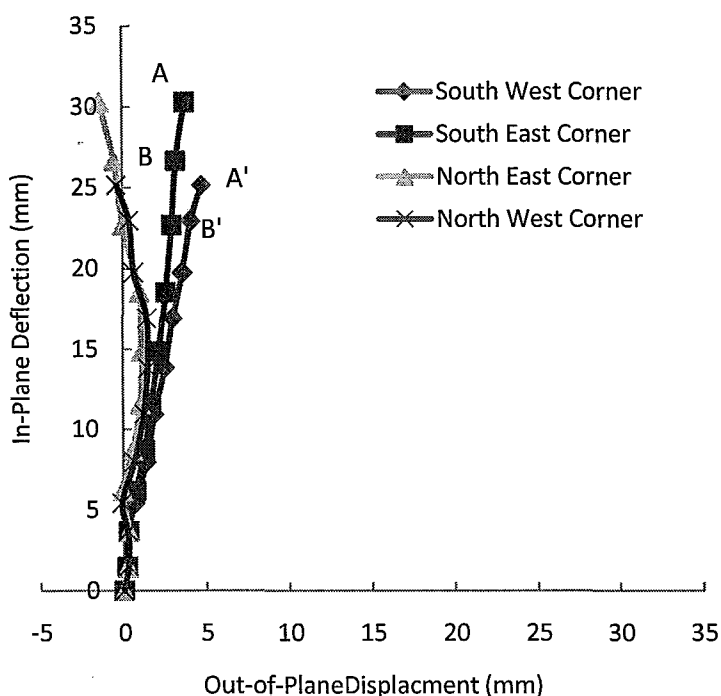


Figure 4.4: Movement of Slab Corners

The East end of the building achieved an in-plane deflection of 29.9 mm (1.36% Drift) at peak loading of 392 kN at which time the vertical reinforcing bars in both portions of the Double Wall (Walls 1 and 2) ruptured. The West end of the building reached a corresponding maximum deflection of 25.6 mm (1.16% Drift) without

significant damage. The lateral movements of both corners of the South face were similar with the West corner showing the greater lateral movement. It moved 4.8 mm (0.22% Drift) to the West whereas the East corner moved 3.8 mm (0.17% Drift) in the same direction. This represents a lateral movement of 19% and 12.5% of the in-plane displacement for the C (Wall 8) and Double Wall (Walls 1 and 2) respectively. Due to the restrictions noted above, as shown in Figure 4.4 the lateral movements of the North corners of the slab were negligible. The lateral movement that was observed at the South end of the structure can be attributed to the centre of rigidity occurring at a large eccentricity. The larger lateral movement observed at the South end of the building was able to occur because the pin at the head of the actuator allowed an angle of twist to develop in the structure. Figure 4.5 illustrates the movement of the south face of the building for different load levels along with an exaggerated illustration of the building movement.

The plot is the two dimensional movement of the face of the entire width of the roof slab face as seen in plan. The left of the graph, or where $x = 0$, is the corner of the slab nearest to the location of the Double Wall (Walls 1 and 2) while the right ($x = 2350$ mm) corresponds to the corner of the slab nearest to the C-Wall (Wall 8). Each plotted line relates to the loading as shown in the legend. This plot shows the increased twisting of the structure as the load increased.

At low load levels, the amount of twist was not discernable. However, as the loading increased, a definite discrepancy appeared between the in-plane deflections of

each end of the building. The East side of the structure deflected noticeably more than the West side. This was consistent with the prediction that the C-Wall (Wall 8) was much stiffer than the coupled Double Wall (Walls 1 and 2) and, therefore, due to the location of the centre of rigidity, would deflect less. At the peak load, the deflection of the East side of the building had reached 30.3 mm while the West side reached 25.2mm. This corresponds to an angle of twist of approximately 0.125 degrees. The corresponding in-plane deflections of the Double Wall (Walls 1 and 2) and the C-Wall (wall 8), were 29.9 and 25.6 mm, respectively.

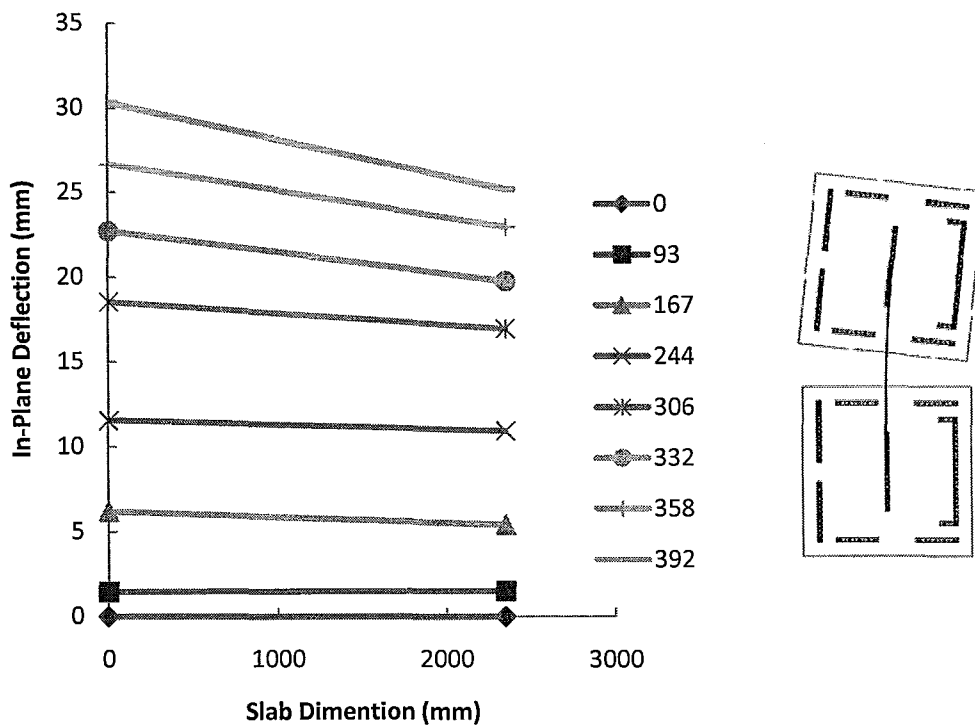


Figure 4.5: Movement of the Top Floor Slab South Face and Representation of Overall Building Movement

4.3.3 In-Plane Wall Displacements

Although the torsional response of the structure was restricted near the North end, relative in-plane movement of each in-plane wall did occur due to twisting about a point near the end of the actuator. From the above presented data, the in-plane deflection of each in-plane wall can be calculated given the movement of the slab corners and assuming that the floor slab acts as a rigid diaphragm. Figure 4.6 shows the in-plane deflection of each wall.

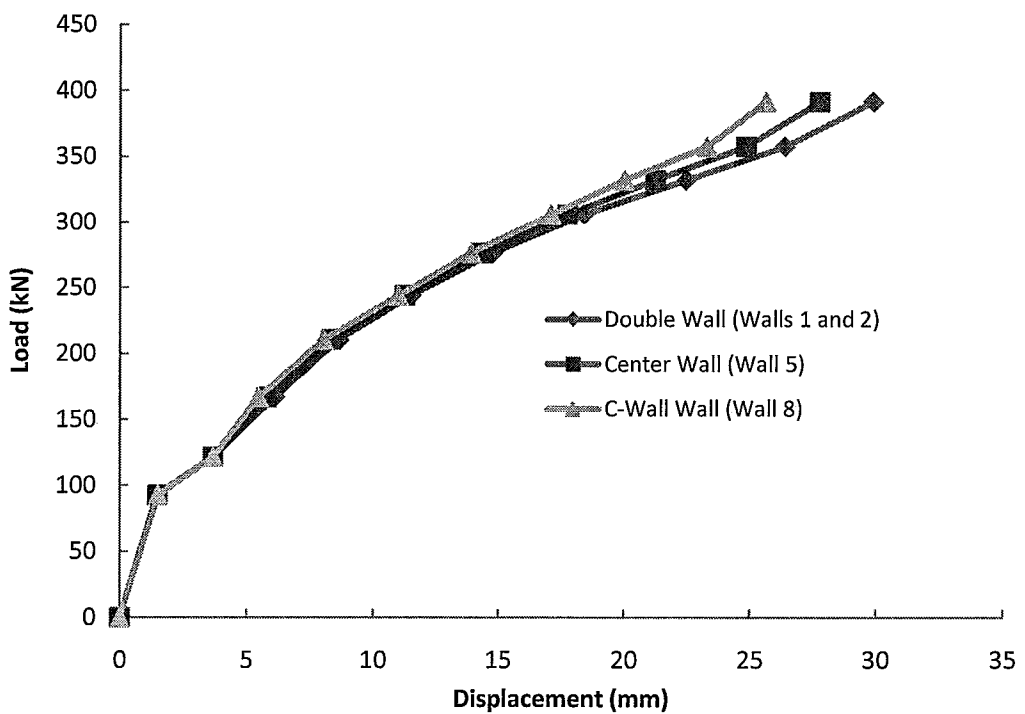


Figure 4.6: In-Plane Deflection of In-Plane Walls

Given these in-plane deflections, a distribution of loading between each wall can be presented using experimental load-displacement data collected by Wierzbicki

(2010). His testing documented the behaviour of all the in-plane walls found in this building. Naturally, no coupling with out-of-plane walls is included in these load resistance values. This documentation is presented in Figure 4.7.

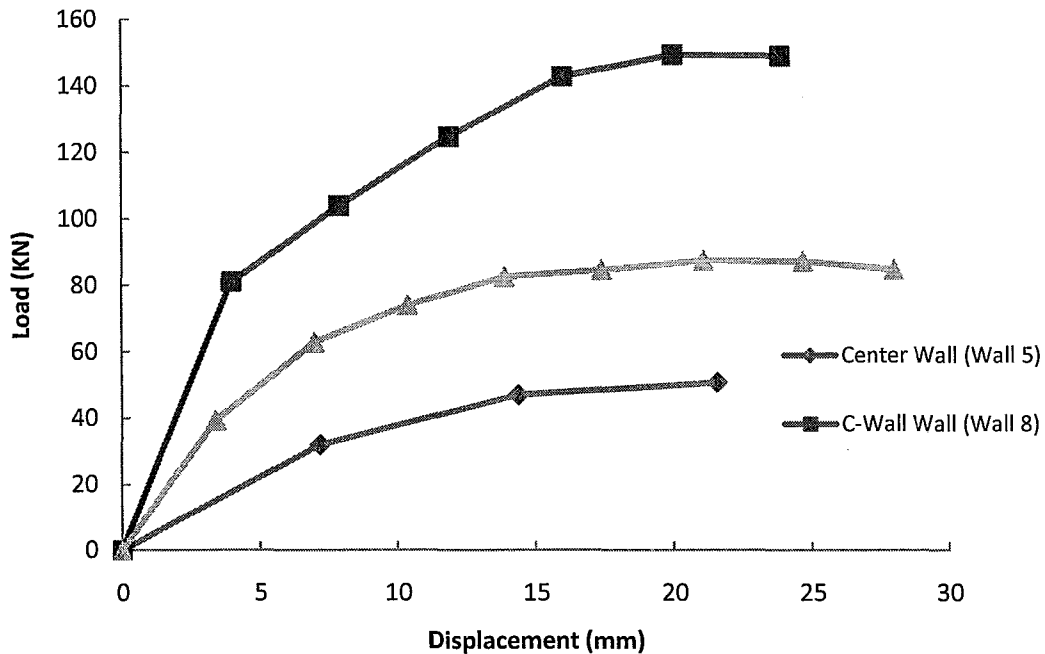


Figure 4.7: Load-displacement Curves for In-Plane Walls (Wierzbicki, 2010)

These are the actual uncoupled response curves for the in-plane walls found in the test structure. Through linear interpolation (and extrapolation in some cases) combined with the displacement data from this experiment, the loading values can be related to the walls found in the structure based on their observed displacement. Then, the load on each wall simply can be added to get an estimate of total building load at each displacement and the uncoupled building strength at maximum displacement. Figure 4.8 contains a comparison of the actual building response versus the predicted

loading based on the observed data taken from Wierzbicki (2010) as well as the preliminary simplified theoretical estimation as presented in Section 4.1.

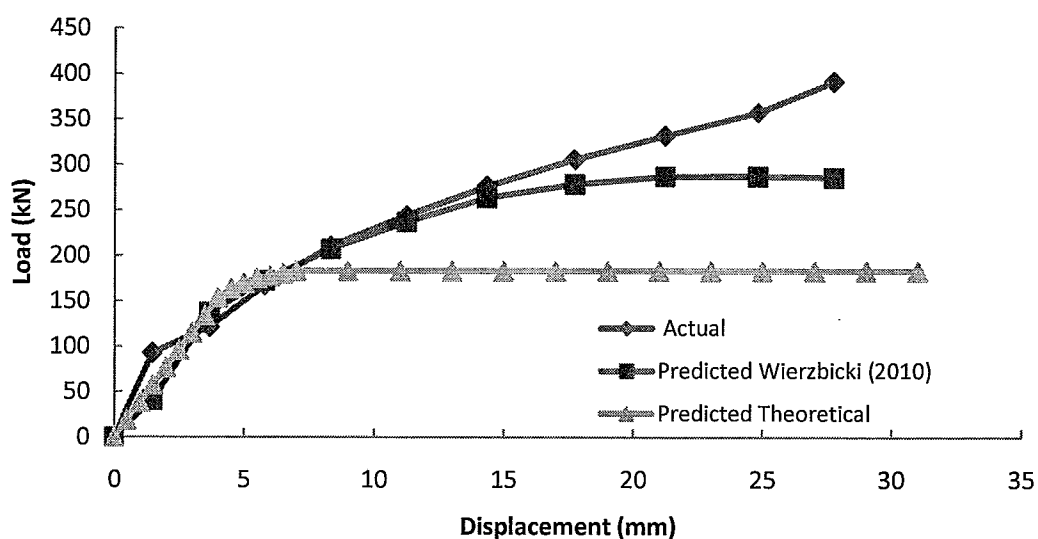


Figure 4.8: Actual Building Response as Plotted versus Predictions

The slope of the load-displacement graph can be interpreted as the building stiffness. The simplified theoretical model and the cumulative response established using Wierzbicki (2010) data show very similar initial stiffnesses and yield points. Beyond yield, these two curves deviate since the walls did not follow the perfect elastic-plastic behaviour at initial yield as assumed in the simplified analysis. The actual building response however, showed a greater initial stiffness with an apparent softening prior to the theoretically predicted yield point that resulted in a lower stiffness than both predicted responses. The predicted elastic stiffness was 37.4 kN/mm while the calculated initial stiffness of the building was found to be 66 kN/mm (Presented in Section 4.4.1.1). The predicted elastic stiffness was only 57% of the actual stiffness of

the building. As the building progressed further into plastic drift levels, the building maintained a larger stiffness than the sum of the individual in-plane walls. This discrepancy can be explained by the interaction between the slab and the walls and the related coupling behaviour as described in the analysis presented in Section 4.1.

4.3.4 Establishment of Experimental First Yield

First yield can be identified as the point where the measured curvature in each wall matched the predicted yield curvature. These predicted yield curvatures were calculated based on the strain profile as determined at the first yield of the extreme tensile reinforcing bar. Table 4.2 shows a summary of the observed load at which this took place.

Table 4.2: Gross Load at Predicted Yield Curvature

Wall	Predicted Yield Curvature	Gross Load at Yield Curvature (kN)
Out-of Plane Walls (Walls 3, 4, 6, 7)	0.0062	N/A
Double Wall (Wall 1)	0.0043	178
Double Wall (Wall 2)	0.0043	197
Centre Wall (Wall 5)	0.0033	185
C-Wall (Wall 8)	0.0022	164

The values in Table 4.2 were calculated using linear interpolation of the gross building load where the observed curvature matches the predicted yield curvature. The measured curvatures profiles and their plots against gross building load are presented and explained in more detail in Section 4.6. From Table 4.2, it is noted that the first yield of the structure does occur in the C-Wall (Wall 8) first as predicted. Furthermore,

the observed first yield loading of 164 kN falls within 2% of the predicted first yield load. It also follows from coupling behaviour that the tensile pier, the pier closer to the applied load, would yield prior to its associated compression pier. The two portions of the Double Wall (Walls 1 and 2) experienced a similar tension/compression couple where the North portion of the Double Wall (Wall 1), which in this case would be predicted to be the tensile pier, did yield prior to yielding of its associated compression pier (Wall 2).

The first yield curvature was observed at 164 kN and the building deflection measured approximately 12.5 mm. This was 2.9 times the predicted yield deflection. Since the predicted deflection was based solely on flexure curvature without coupling, it is expected that this estimation of yield displacement would be conservative. Next, the building response will be examined from the perspective of seismic performance.

4.4 Seismic Reduction Factor

The intent of this study is to establish a base for future studies examining reinforced masonry system behaviour. Since no previous models have been established with regard to the ductility and energy dissipation characteristics of a reinforced masonry system, an equal energy approach will be established as a baseline. In order to perform such an analysis, the elastic stiffness of the structure may be a required value.

4.4.1 Structural Stiffness

Under seismic excitation, a structure must possess adequate ductility to dissipate the energy supplied by the ground motion while also maintaining adequate strength to resist the lateral loading. It is important for a structure to be capable of enduring displacements several times larger than the yield displacement. Other important considerations are stability in terms of supporting the gravity loads while undergoing seismic excitation as well as limiting drift levels to prevent excessive damage. In the past, research has focused on providing models to describe the ability of individual shear wall elements in these regards (Shing 1989, Paulay and Priestley 1992, Paulay and Priestley 1993, Shedid 2006, Shedid 2009, Wierzbicki 2010). These, along with other studies, have supplied many models to quantify the ductility characteristics of shear wall elements using many different combinations of elastic stiffness and assumed yield points. Due to the complex nature of the response of an entire building, this problem is re-examined below.

4.4.1.1 Observed Elastic Stiffness

The elastic stiffness was established during the two pre-yield displacement cycles. Good correlation was shown in the data between both the 20% and 40% of first yield load cycles. Figure 4.9 contains both load displacement graphs for these cycles.

As noted in Chapter 3, the stiffness of each of the cycles in both push and pull directions appear to be very similar indicating good consistency. Figure 4.10 shows the trend lines established for each cycle.

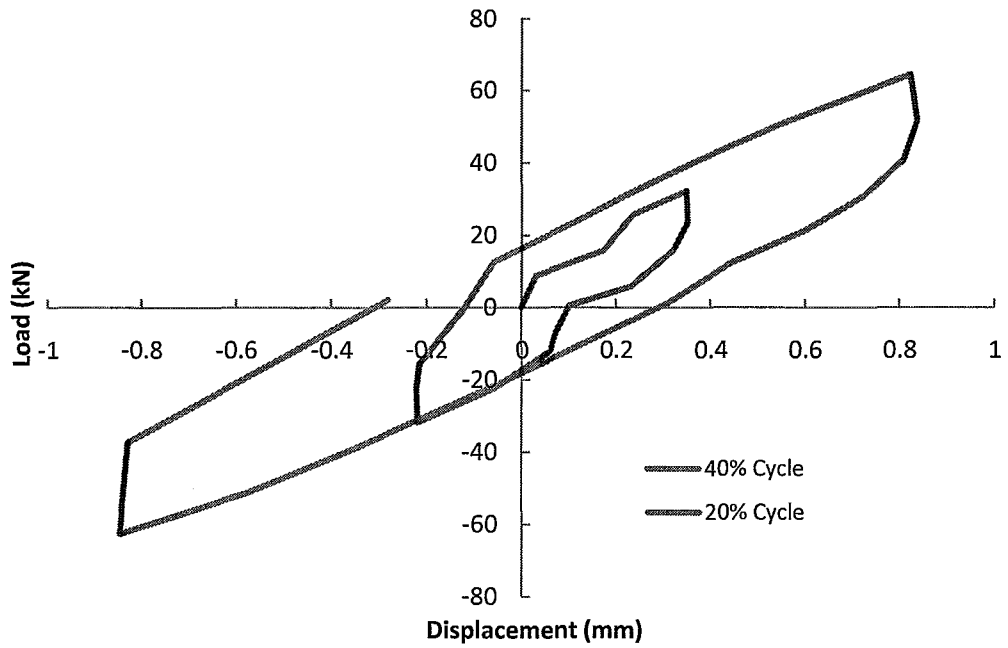


Figure 4.9: Load Displacement Cycles of $0.2\Delta y$ and $0.4\Delta y$

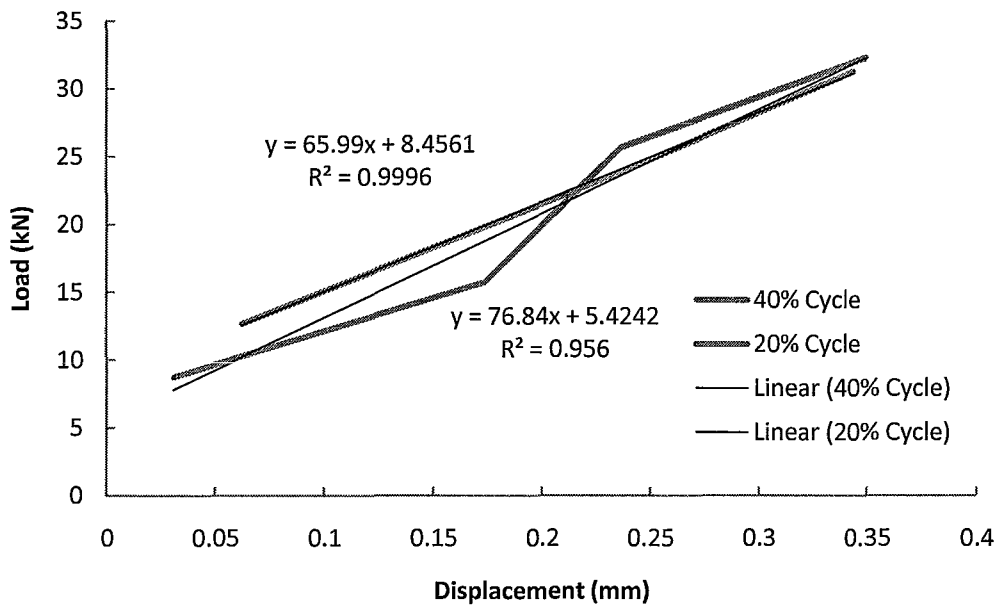


Figure 4.10: Pre-Yield Building Stiffness

To establish a cracked elastic stiffness, the initial data points, which were assumed to be pre-cracking, were left out to prevent skewing of the trend lines. Here the calculated stiffness was 14% higher for the 20% of yield load cycle than for the 40% of yield load cycle. This difference can be accounted for by the fact that some initial cracking that occurred during the 20% of yield load cycle may have led to slight softening for the 40% of first yield cycle. Furthermore, the slope of the load-displacement graph was much more stable for the 40% of first yield cycle. Therefore, the stiffness of the 40% of first yield cycle will be used as the elastic stiffness of the structure.

As mentioned earlier, the building softened as it entered into the plastic state. Figure 4.11 shows the secant stiffness degradation as the building progressed into the plastic state during the final push to failure test. The building stiffness reduced from 63 kN/mm at the loading onset to 14.1 kN/mm at peak load.

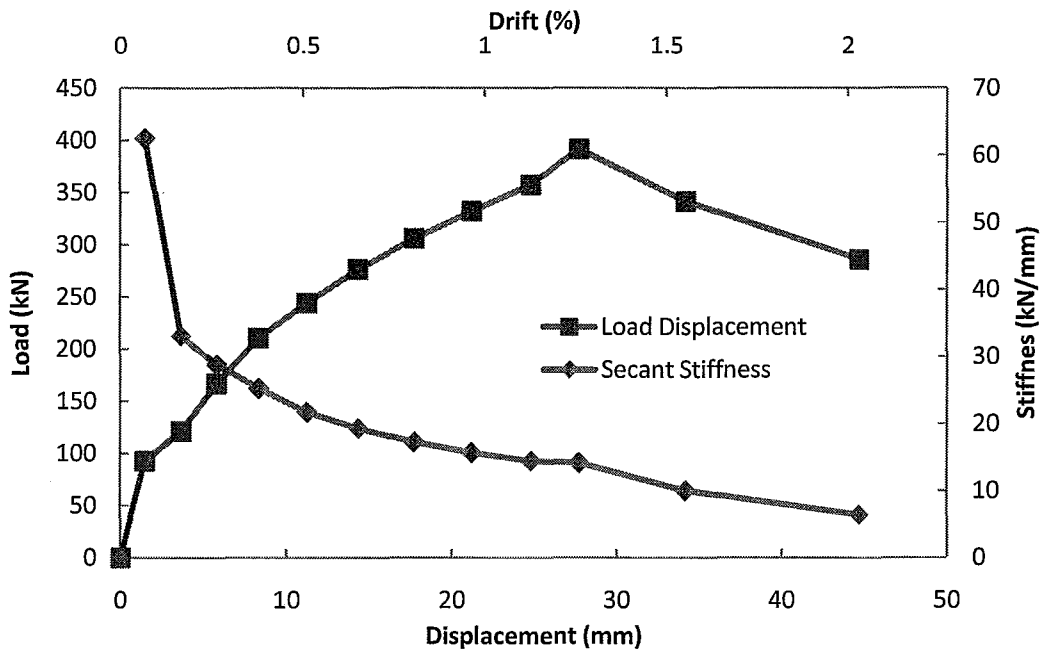


Figure 4.11: Building Secant Stiffness Degradation

4.4.2 Equal Area Method to Quantify Ductility

After defining the elastic stiffness and assuming an elastic-plastic response the equal area rule can be applied. The area under the experimental load-displacement curve can be set equal to the area beneath the idealized elastic plastic response graph. After choosing a reasonable ultimate drift limit of 1%, the areas under each graph are set equal to each other. To draw the idealized curve, it is necessary to define the slope of the elastic part. This may be done using the initial stiffness as shown in Figure 4.12 by Curve 1, which results in a high estimation of ductility. Alternatively, it is generally thought to be more acceptable to define the elastic slope by a line from zero load to a point on the load-displacement envelope. If known, this may be the point of first yield of a bar. In this case, the point of first yield curvature will be used. For the elastic-

plastic curves, new idealized yield displacements and associated yield loads are defined. As an example, the first idealization results in a yield displacement of Δ'_1 and a corresponding plastic load of P'_1 . The second idealization is noted similarly by Δ'_2 and P'_2 for yield displacement and plastic load, respectively. Figure 4.12 shows these idealizations with respect to a general load-displacement curve.

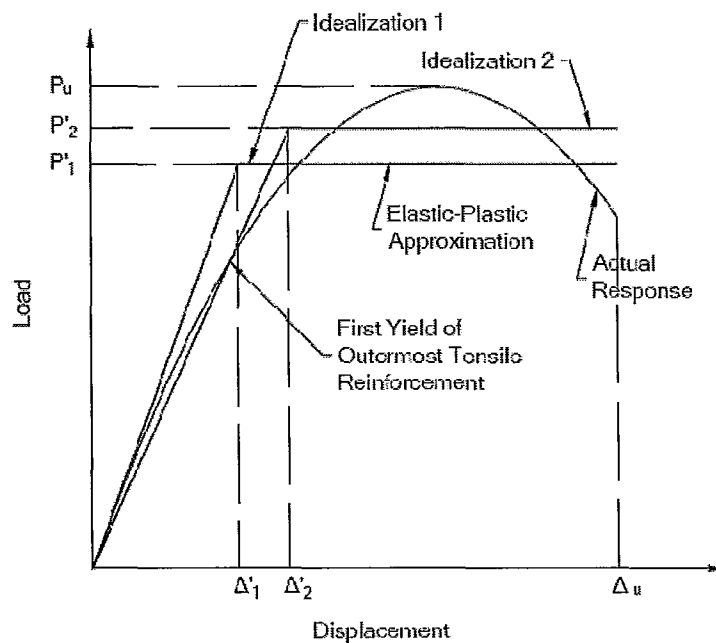


Figure 4.12: Elastic-Plastic Idealization for Reinforced Masonry Shear Walls

As mentioned previously, for the first idealization, the slope of the first section of the elasto-plastic response curve will be taken as the slope of the 40% load displacement diagram. Figure 4.13 contains the result of this idealization plotted against the actual load-displacement diagram up to 22 mm (1%) Drift. The second

idealization is also shown where the slope of the elastic part is established by the point of initial yield at a load of 164 kN.

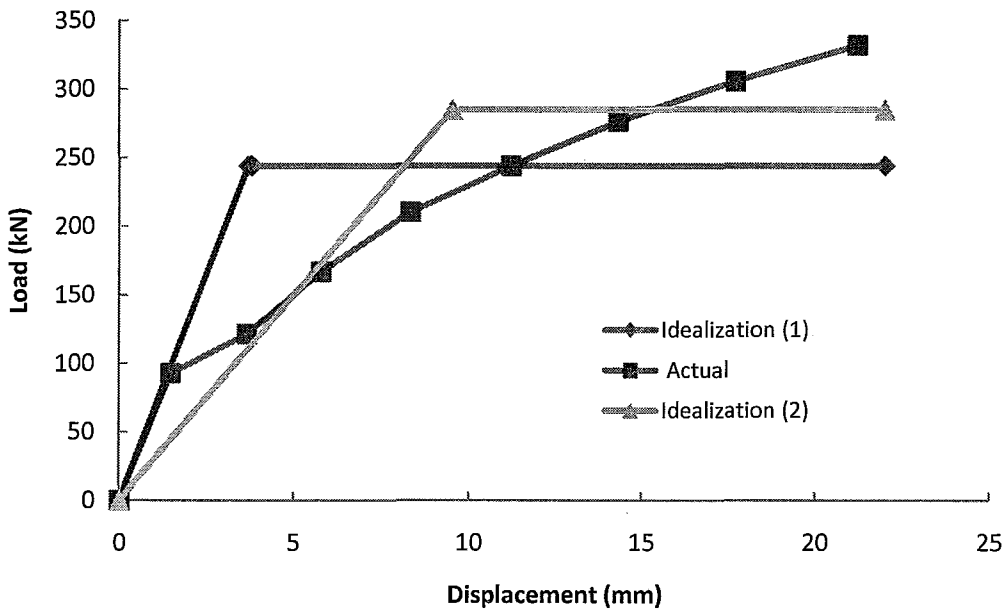


Figure 4.13: Idealized Elasto-Plastic Building Response

For the first idealization, it is noted that the stiffness used for the elasto-plastic response matches very closely to the stiffness of the final pushover test. The idealized response curve remains nearly identical to the actual response curve up until approximately 100 kN. According to the first idealization the yield displacement is approximately 3.7 mm and the ultimate displacement is limited to 22 mm (Drift = 1%). If we consider the seismic reduction factor to be based on equal area then:

$$R = \frac{\Delta_u}{\Delta_y} \quad \text{Eq. 4.5}$$

With:

R = Seismic Reduction Factor

Δ_u = Ultimate Displacement

Δ_y = Yield Displacement

According to Eq. 4.5 the seismic reduction factor for the structure based the first idealization was equal to 5.9. This is nearly triple the reduction factor of 2.0 allowed for by the NBCC (2010). Based on this idealization it is realistic to say that the NBCC underestimated the ductility of this structure.

The second idealization uses the observed point of first yield, identified by the occurrence of predicted yield curvature in the C-Wall (Wall 8). A line drawn from the origin through the corresponding point on the load-displacement diagram provided the estimate of secant stiffness. Using the equal area approach again, the resulting idealized yield displacement and lateral load were 9.5 mm and 285 kN respectively. The resulting seismic reduction factor based on equation 4.5 for the second idealization is 2.3. This exceeds the allowable code limit by a marginal 16%. Nevertheless, the conservative selection of the 9.5 mm yield displacement (almost 30 mm in full-scale), as well as scaled-steel rupture before any masonry compression failure have both contributed to this significant underestimation of building ductility. With both of the ductility results and the limitations in mind, this test gives a positive indication to the capabilities of reinforced masonry systems to provide ductile response to seismic loading beyond what is currently allowed in Canada.

4.5 Theoretical Analysis of Individual Walls

4.5.1 General

As mentioned previously, each wall specimen was analyzed to establish a baseline strength and stiffness for the structure. In order to use these values, some additional information had to be gathered from the material testing data. The Young's modulus of 13, 217 MPa for the masonry prisms was calculated as the slope of the stress strain curve using the secant between 10 and 50% of the maximum stress. The elastic modulus of the steel of 200, 000 MPa along with its yield stress and strain was found via the tensile test results. The yield stress of 540 MPa at 0.0047 strain was found using the 0.2% offset method. The nominal yield strain was $f_y/E_s = 0.0027$ where f_y and E_s are the yield stress and the elastic modulus of the steel, respectively.

Using the above material characteristics, the yield and ultimate strength and corresponding curvatures of each wall were found. For initial analysis, the perfectly elastic-plastic behaviour of the steel reinforcing was assumed. The tensile strength of masonry was ignored for all calculations as is common in reinforced masonry analysis. The self-weight of both the walls themselves plus the tributary weight of the supported slabs were accounted for in the analysis of each wall.

A perfectly elastic response was assumed for the yield prediction of each wall including both the compression masonry and all reinforcing bars. The compression bars were included in this analysis since the wall was in its elastic range. The yield point of

the wall was defined as the moment when the extreme flexural bar reached the nominal yield of 0.0027 rather than the actual 0.0047 strain representing nonlinear behaviour. The yield curvature was calculated from this predicted strain profile. This yield curvature could not be confirmed due to malfunction of the strain gauges during the test.

4.5.2 Predicted Lateral Capacity, Curvature and Deflection

For the ultimate loading capacity calculation, the provisions of CSA S304.1 (2004) methodology employing the equivalent rectangular stress block were utilized but also included the flexural compression bars in the analysis. Including the bars in the theoretical calculations was done to more accurately predict the wall strengths considering that, even at very large drift levels, these bars will be effective (Shedid, 2006). Furthermore, the material reduction factors were not used in these calculations.

As per the CSA S304.1 (2004) provisions for moderately ductile walls, the maximum masonry compressive strain was limited to 0.0025 for prediction of the ultimate strength and ultimate curvature for each wall. Table 4.3 contains the predicted lateral loading capacity for each wall along with its associated ultimate curvatures and deflections.

The predicted ultimate curvatures were calculated based on the strain profile at ultimate conditions. The resulting deflections were based on the equivalent plastic hinge length as presented in CSA S304.1 (2004) and the previously computed ultimate curvatures. The equations used in these deflection calculations are presented in

Appendix D. It is noted, especially for the C-Wall (Wall 8), that these predictions may be skewed by the over simplification of the predicted equivalent plastic hinge length as provided for in CSA S304.1 (2004). According to this standard, the plastic hinge length for the C-Wall (Wall 8) was calculated to be 1533 mm long which is 70% of the height of the wall. The calculated ultimate displacement corresponds to a drift level of 3.5%. For most structures, drift levels are usually limited to between 1 and 2%. This level of drift may not be usable but this suggests that walls with end elements, if properly detailed, can exhibit substantial ductility and therefore could be useful for improved seismic behaviour of reinforced masonry buildings.

Table 4.3: Predicted Conditions at Ultimate Capacity of Individual Walls.

Wall	Predicted Ultimate Lateral Loading (kN)	Predicted Ultimate Curvature (rad/m)	Predicted Ultimate Deflection (mm)
Out-of Plane Walls (Walls 3, 4, 6, 7)	15.0	0.0338	38.5
Double Wall (Wall 1)	30.2	0.0242	37.1
Centre Wall (Wall 5)	52.0	0.0204	37.7
C-Wall (Wall 8)	150.9	0.0354	77.9

4.5.3 Equivalent Plastic Hinge Length

The length of plasticity up the height of wall is an important criterion in evaluating structural elements under high ductility demand. Plasticity can be associated with the occurrence of inelastic behaviour of the flexural reinforcing steel along with damage to the masonry. The extent of plasticity is the height of wall over which this behaviour occurs. The collective effect of plasticity over this height of the wall

determines the magnitude of the plastic displacement and consequently the ultimate displacement. The ability of specific elements to undergo plastic deformations directly affects the ductility force modification R_d used in seismic design. In design and research, numerous approximations have been presented to suggest equivalent plastic hinge lengths wherein use of constant plastic curvature over the equivalent hinge length leads to simplified calculation of Δ_p .

4.5.3.1 CSA S304.1

As mentioned previously, the plastic length is defined in CSA S304.1 (2004) as the greater of $l_w/2$ or $h_w/6$ for limited ductility shear walls where length and height of the wall are l_w and h_w , respectively. For moderately ductile shear walls, this distance is increased to the greater of l_w or $h_w/6$. The classification of ductility is defined by the ability of the wall to reach a level of ductility without exceeding a masonry strain of 0.0025. This ductility level is achieved by applying specific reinforcing details and minimum wall dimensions and may be deemed to comply through satisfying limits on the length of the compression zone. The walls in this study meet the requirements for moderately ductile walls.

4.5.3.2 Literature and Comparisons

As noted in the literature, Paulay and Priestley (1992) have provided multiple methods of defining equivalent plastic hinge lengths. The first is the previously mentioned equal energy principle. This approach assumes that the wall behaviour is characterized by an elastic perfectly plastic response and the area under that curve

denotes the energy dissipated by that particular wall. Comparing these two responses and rearranging equation 4.6 yields Δ'_y and P'_y which are denoted by the following equations.

$$\mu'_{\Delta} = 1 + 3 \left(\mu'_{\varphi} - 1 \right) \left(\frac{l_p}{h_w} \right) \left(1 - \frac{0.5l_p}{h_w} \right) \quad \text{Eq. 4.6}$$

$$\mu'_{\Delta} = \frac{\Delta_{max}}{\Delta'_y}$$

$$\mu'_{\varphi} = \frac{\varphi_y}{\varphi'_u}$$

$$\Delta'_y = \Delta_y \frac{P'_y}{P_y}$$

$$\varphi'_y = \varphi_y \frac{P'_y}{P_y}$$

This model will not be used since no accurate load-displacement diagram could be produced for each wall independently. Additional models presented by Paulay and Priestley (1992, 1993) depend on the diameter and yield strength of the reinforcing bars while ignoring the percentage of flexural reinforcement or wall aspect ratio (Paulay and Priestley, 1992) while the others depend solely on wall geometry (Paulay and Priestley, 1993). These are characterized by Equations 4.7 and 4.8, respectively.

$$l_p = 0.08h_w + 0.022d_b f_y \quad \text{Eq. 4.7}$$

where:

$$l_p = \text{Equivalent Plastic Hinge Length (mm)}$$

$$h_w = \text{Wall Height (mm)}$$

$$d_b = \text{Reinforcement Bar Diameter (mm)}$$

$$f_y = \text{Yield Strength of Reinforcement (MPa)}$$

$$l_p = (0.2 + 0.044A_r)l_w \quad \text{Eq. 4.8}$$

where:

$$A_r = \text{Aspect Ratio of wall} = \frac{h}{l_w}$$

$$l_w = \text{Wall Length}$$

Many other idealizations in addition to these are presented as summarized by Shedid (2009). A short investigation into this matter is summarized in Table 4.4.

Table 4.4: Predicted Equivalent Plastic Hinge Lengths Based on Various Equations versus Measured Extent of Plasticity.

Wall	CSA S304.1 (2004)	Eq. 4.7	Eq. 4.8	Measured Extent of Plasticity (mm)
Out-of Plane Walls (Walls 3, 4, 6, 7)	600	270	217	N/A
Double Wall (Wall 1)	867	270	270	563
Double Wall (Wall 2)	867	270	173	631
Centre Wall (Wall 8)	1133	270	323	496
C-Wall	1533	270	403	170

These measured curvatures, as previously mentioned, are assumed to be located at the mid-height between points of measurement over a segment of wall. The measured extent of plasticity values listed in Table 4.4 are based on linear interpolation between two vertical segments of wall having measured average curvature values that traverse the predicted yield curvature. It can be noted that the extent of plasticity was greatest in the Double Wall (Walls 1 and 2) reaching over 25% of the wall height. The

Centre Wall (Wall 5) had a similar extent of plasticity while the C-Wall (Wall 8) exhibited the least extent of plasticity. The lower extent of plasticity for the C-Wall (Wall 8) can be attributed to the fact that it did not reach ultimate conditions.

The idealizations for equivalent plastic hinge length presented in Table 4.4 apply to individual shear wall elements. Keeping in mind that the equivalent plastic hinge length and the measured extent of plasticity are different items, one would still expect some correlation between the two since they are intrinsically related. However, as can be seen from Table 4.4, no correlation can be recognized. This can be rationalized when considering the many additional parameters introduced when studying a complete structure, such as diaphragm influence, coupling, torsion and the like. The position of each of these walls within the structure and their proximity to other in-plane as well as out-of-plane elements cause many of the proposed idealizations for individual shear wall elements to become ambiguous. It would seem that the comparison of zones of plasticity of individual walls with those in buildings provides another way of assessing coupling effects. It would be useful then, to directly compare elements present in this structure with data collected from the same elements tested in isolation.

4.6 Individual Wall Responses

Here the load-displacement behaviour of each wall will be examined as deciphered from the vertical displacement data collected at the ends of each wall at several locations over the height of the wall as illustrated in Chapter 2. Instrumentation for each wall contained within the building structure focused specifically on gathering

the curvature profile of the wall. Since the strain gauge data was unreliable, data collected using the LVDT's will be used to examine the curvature behaviour observed in the walls and used in comparison to observations made by Wierzbicki (2010).

Average curvatures over segments of the wall height were determined based on the average strains measured for each vertical segment over the height of the wall using the displacement transducer described in Section 2.8.1. The strains were calculated based on the net change in height over the vertical segment of the wall divided by its original height. This yielded the average strain at the ends of each wall at intervals up the wall height. The average curvatures are then easily calculated as the slopes of the strain profiles otherwise known as the strain gradient. Figure 4.14 serves as a refresher and a reference to the building wall layout.

4.6.1 North Portion of the Double Wall (Wall 1)

The North portion of the Double Wall (Wall 1) measured approximately 865mm long and was reinforced vertically with 7.6 mm diameter bars in every other cell ($p_v=0.58\%$). The predicted lateral loading required for yield of the extreme tensile flexural bar was calculated as 19.4 kN with a corresponding curvature of 0.0043 rad/m. Ultimate predicted lateral loading for each wall acting independently was calculated to be 30.2 kN with a corresponding curvature of 0.020 rad/m.

The extent of plasticity in the wall was determined using the calculated curvatures based on the collected data. Figure 4.15 contains the curvature profile along

the wall height, plotted for different loading levels, as average curvature over the vertical wall segment located at the segment mid-height.

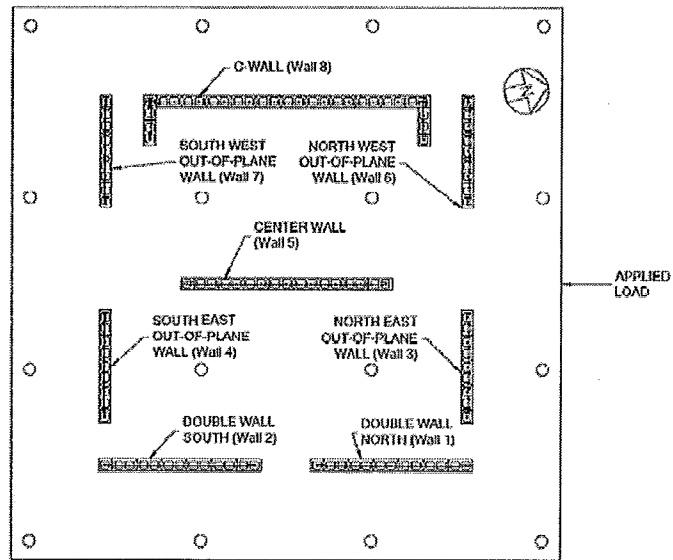


Figure 4.14: Wall Layout

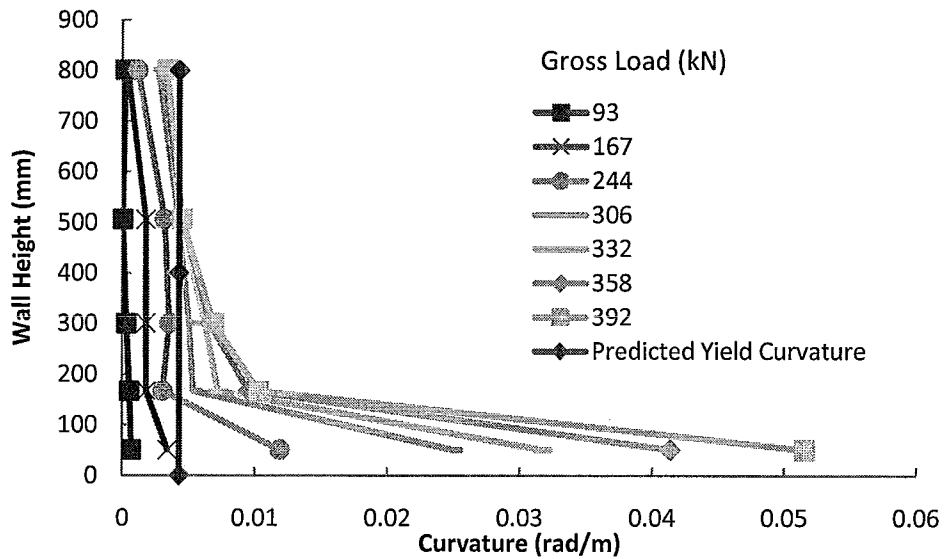


Figure 4.15: Average Curvature Profile: North Portion of the Double Wall (Wall 1)

Rupture of the vertical reinforcing in this wall occurred very shortly after the bars were noted to rupture in the Southern portion of the Double Wall (Wall 2) but at curvatures well beyond the predicted ultimate. Therefore, it can be said that the measured curvature at peak loading corresponded to the ultimate curvature. The curvature measured at the peak loading was 0.052 rad/m. This is 2.6 times the predicted ultimate curvature but less than the ultimate curvature as presented by Wierzbicki (2010) where the curvature neared 0.1 rad/m. When coupled with an additional similar wall in its plane, Wierzbicki (2010) documented the curvature as reaching only 0.045 rad/m which is similar to the curvature observed here. The extent of plasticity noted in his study for the individual wall fell in the range of 315-520 mm for the Double Wall while in this case the plasticity extended to 563 mm. The discrepancy here can be attributed to the random cracking pattern that occurs in every shear wall element that can change the shape of the curvature profile since only a small number of average curvatures can be determined from the data. Furthermore, the proximity of this wall to an out-of-plane wall may have affected the observed curvatures.

Figure 4.16 illustrates how the large curvatures are concentrated in the lower portion of the wall. While the plasticity ranged quite high in the wall, the major curvature was limited to the lower 100 mm of wall height.

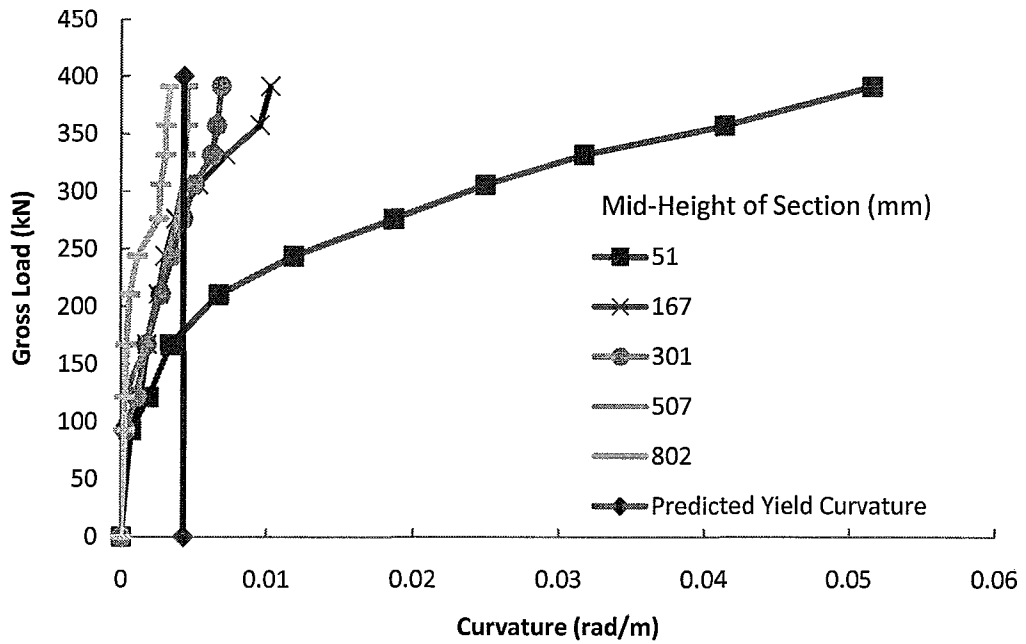


Figure 4.16: Average Curvature vs. Gross Load: North Portion of the Double Wall (Wall 1)

The curvature profile of the wall can also be used to predict the top deflection of the wall using the approach presented in Appendix D. Considering the multiple average curvature measurements collected, a prediction of top deflection can be made based on these values taken as rotations at the mid-height of measurement multiplied by the distance from this measurement location to the top of the building. Figure 4.17 contains the predicted deflection based on the collected curvature data versus the actual in-plane deflection of the North portion of the Double Wall (Walls 1 and 2).

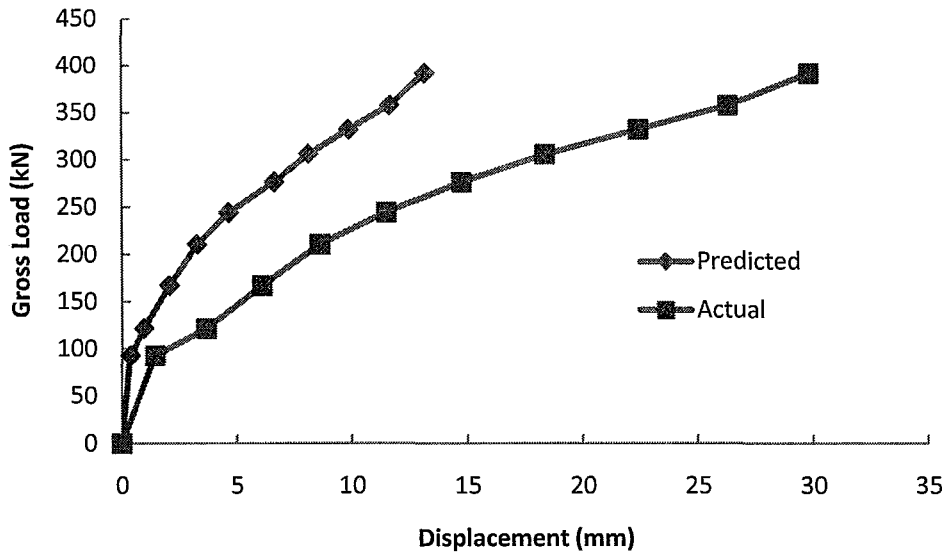


Figure 4.17: Predicted Displacement Based on Measured Average Curvature for Wall 1

The predicted deflection based on collected curvature data was only 44% of the actual in-plane deflection over the full height of the wall. Curvature values can be used to predict the top deflection of a wall based on the associated rotation at the location of the measured curvature and the distance of the location from the top of the wall. Underestimation of the deflection is to be expected since the curvature data only accounts for flexural deflections and does not include deflections from base slip, shear deformations or flexural curvatures for the second story. Additionally, at the bottom segment of the wall height, the elongation (and therefore curvature) is concentrated at the bottom due to bar debonding in the concrete base. That being said, base slip was negligible for all in-plane walls and curvatures at the top of the first story were all below yield. All factors considered, it seems that this wall experienced a similar amount of deflection due to shear deformation as due to flexural deformation.

4.6.2 South Portion of the Coupled Wall (Wall 2)

The South portion of the Double Wall (Wall 2) also measured approximately 865mm long and was similarly reinforced ($p_v=0.58\%$). The predicted lateral loading and curvature values were the same as was noted previously. Figure 4.18 contains the curvature profile along the wall height, plotted for different loading levels, as average curvature over the vertical wall segment located at the segment mid-height.

Again, the ultimate predicted lateral loading for a single in-plane wall was calculated to be 30.2 kN with a corresponding curvature of 0.020 rad/m. Since this was the only wall that reached a failure loading (rupture of vertical reinforcing bars), it can be said that the measured curvature corresponds to the ultimate curvature. The curvature of 0.044 rad/m measured for this portion of the Double Wall (Walls 1 and 2) at the peak loading was very similar to the curvature observed in the North portion of the wall. This observed curvature is 2.2 times the predicted ultimate curvature. This is again similar to the push cycle of this wall tested alone but much less than the same test result for the corresponding pull where the curvature neared 0.1 rad/m. Wierzbicki (2010) noted that when coupled with an additional similar wall in its plane, the curvature reached nearly 0.08 rad/m. This is again almost double the curvature observed in this experiment. The extent of plasticity noted in that study, (Wierzbicki, 2010), fell in the range of 245-515 mm while in this case the plasticity extended in a similar manner to the North portion of this coupled wall to 631 mm. The discrepancy can be attributed to similar reasons mentioned for the North portion of this wall.

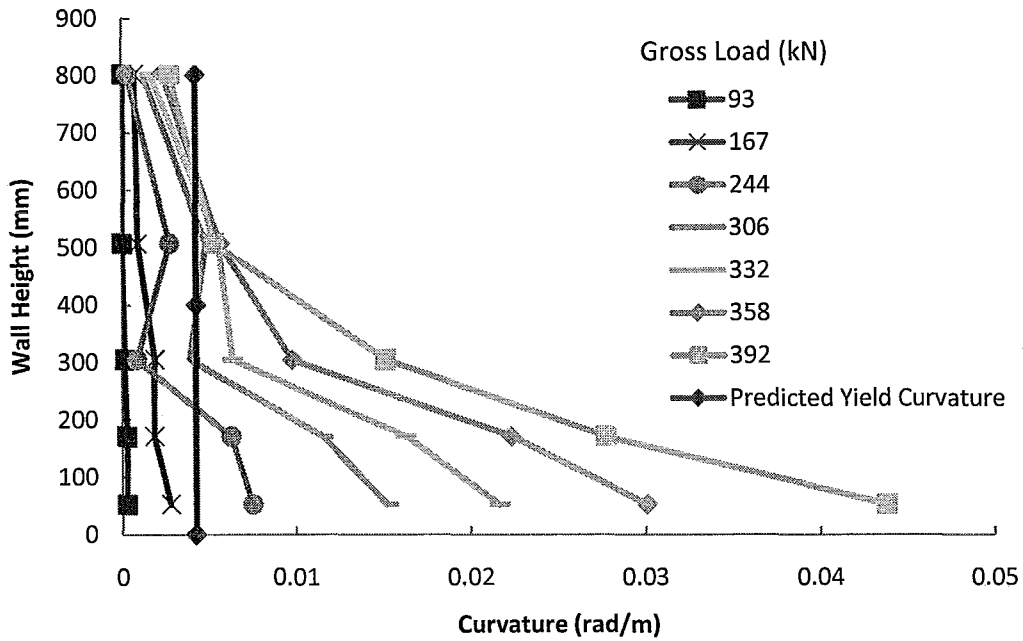


Figure 4.18: Average Curvature Profile: South Portion of the Double Wall (Wall 2)

Figure 4.19 illustrates how the average curvatures varied for the different wall segments as the load increased. Compared to Figure 4.16, Figure 4.19 shows that the larger curvatures are seen higher up this wall. The most significant curvature remains in the lower 171 mm of wall height.

Figure 4.20 contains the predicted deflection based on the collected curvature data versus the actual in-plane deflection of the South portion of the Double Wall (Wall 2). The predicted deflection based on collected curvature data was greater than observed for the Northern portion of the wall at 64% of the actual in-plane deflection. The discrepancy between the predicted and the actual displacement can be accounted

for by the same reasons as presented previously. Flexural deformation dominated the behaviour of this wall.

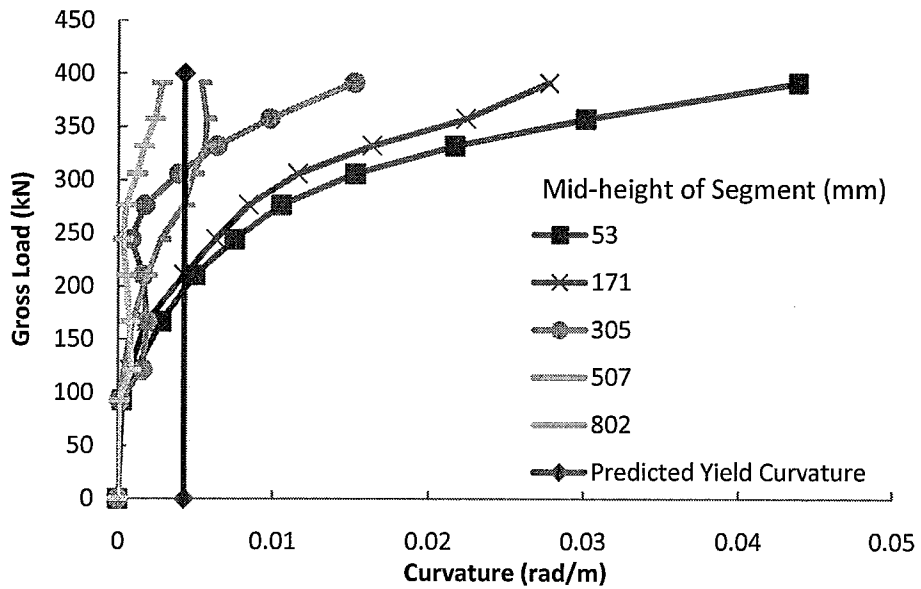


Figure 4.19: Average Curvature vs. Gross Load: South Portion of the Double Wall (Wall 2)

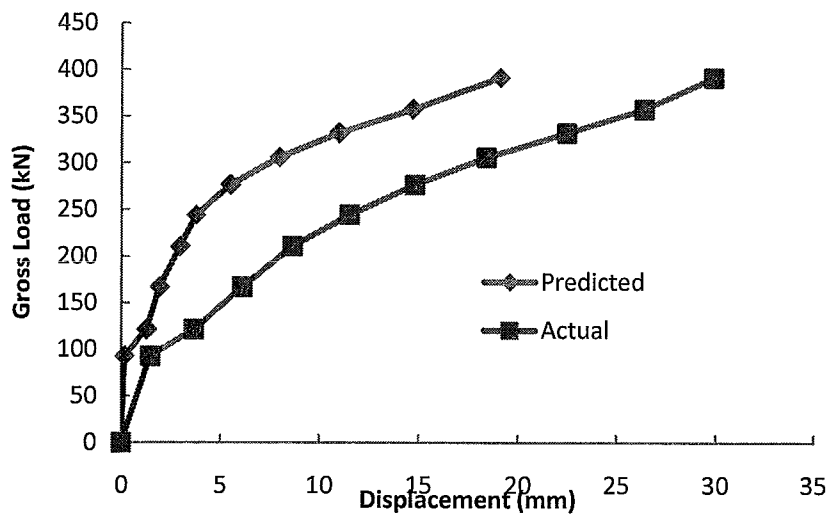


Figure 4.20: Predicted Displacement Based on Measured Average Curvature for Wall 2

4.6.3 North Out-of-Plane Walls (Walls 3 and 6)

Both of the Northern out-of-plane walls behaved in a similar manner. Each wall measured approximately 600 mm long and was reinforced vertically with 7.6 mm diameter bars in every other cell ($p_v=0.59\%$). Figures 4.21 and 4.22 contain the average curvature profiles for these out-of-plane walls.

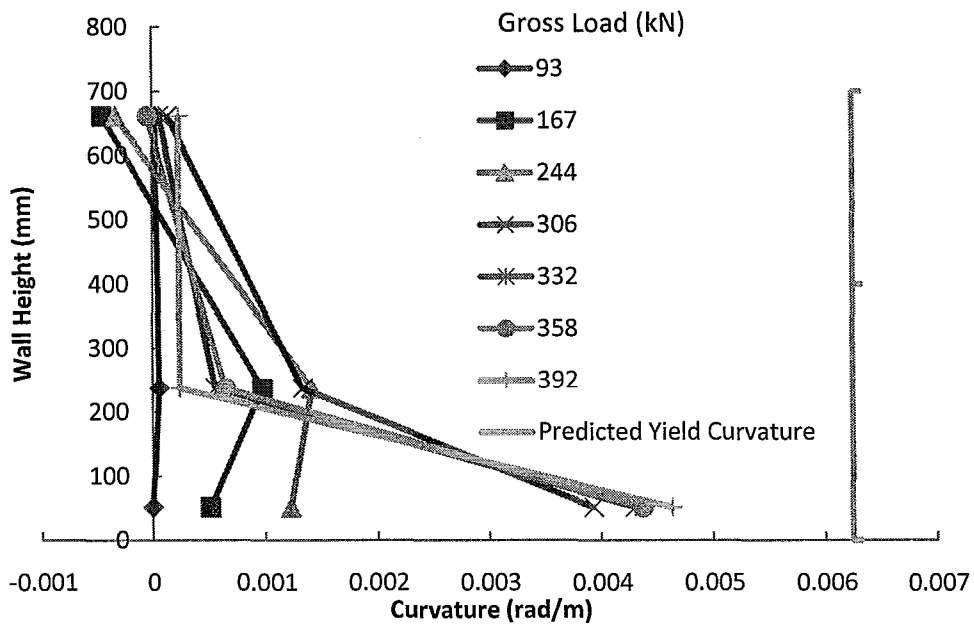


Figure 4.21: Average Curvature Profile: North East Out-of-Plane Wall (Wall 3)

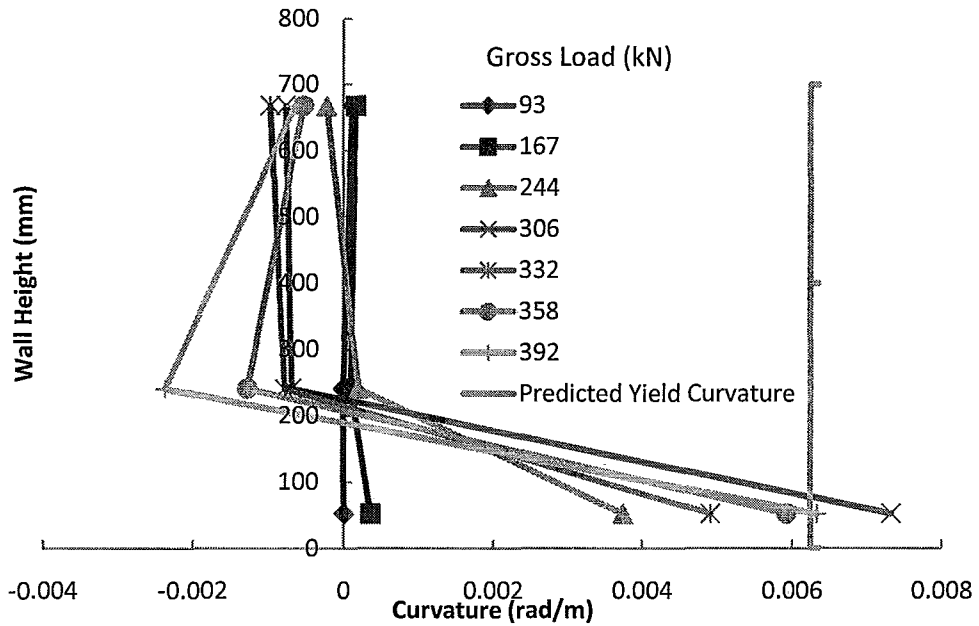


Figure 4.22: Average Curvature Profile: North West Out-of-Plane Wall (Wall 6)

The maximum curvatures were measured as 0.0046 and 0.0063 rad/m for the North East and North West Out-of-Plane Walls (Walls 3 and 6, respectively). These curvature values were attained at the peak loading experienced by the building. The curvature was calculated to be 0.0062 rad/m at predicted yield. At first glance it appears that both walls were under or on the verge of reaching yield. However, upon further examination, it is seen that all vertical LVDT's on both ends of the walls are measuring positive displacements suggesting that these walls are primarily subject to axial tensile loading. This observation is supported by the noted cracking pattern which was seen along the entire length of many of the bed joints of each wall. Considering the direction of loading and associated coupling, it seems obvious that these walls were subjected to significant axial tension resisted primarily by the vertical reinforcing. It is

not possible to separate the flexural and tensile loading experienced by the wall from the collected data. Additionally, due to inadvertent restraint of the hydraulic actuator attached to the building near these walls (explained in more detail in Section 4.3.2), these walls were subject to limited lateral in-plane loading due to building torsion. Since the loading was primarily tensile in nature rather than flexural, the observed curvatures are not indicative of the actual wall loading and very little information can be deduced from these charts.

4.6.4 The Centre Wall (Wall 5)

The Centre Wall (Wall 5) measured approximately 1133 mm long and was similarly reinforced to all other rectangular walls ($p_v=0.57\%$). The predicted lateral loading for first yield of the flexural reinforcing steel was 32 kN with an associated curvature of 0.00099 rad/m.. Figure 4.23 contains the curvature profile along the wall height, plotted for different loading levels, as average curvature over the vertical wall segment located at the segment mid-height.

The ultimate predicted lateral loading for this wall was calculated to be 52 kN with a corresponding curvature of 0.017 rad/m. This wall did experience rupture of vertical reinforcing bars but this did not occur until after peak loading and rupture of vertical bars in both portions of the Double Wall (Walls 1 and 2) had occurred. Therefore, the measured maximum curvature corresponds to a curvature value near but not at its ultimate state. Furthermore, upon rupture of bars in the Double Wall (Walls 1 and 2), the characteristics of the system, including the stiffness and load distribution

would have changed significantly beyond this peak load. As such, it would be imprudent to compare the curvatures noted before peak load and after peak load. The measured curvature of 0.027 rad/m measured for this wall at the peak loading was 1.6 times the predicted ultimate curvature but less than 30% of the observed ultimate curvature witnessed by Wierzbicki (2010) which approached 0.1 rad/m at failure.

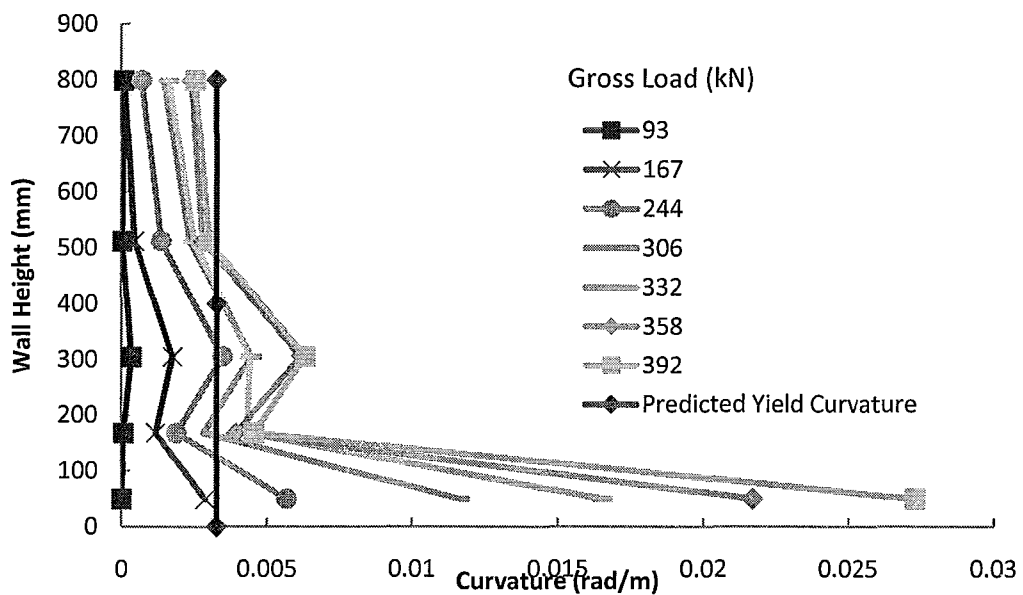


Figure 4.23: Average Curvature Profile: Centre Wall (Wall 5)

The extent of plasticity noted in that study, (Wierzbicki, 2010), fell in the range of 270-540 mm for the push direction and 540-820 in the pull direction. Similarly, in this experiment, the extent of plasticity was observed to be 496 mm.

Figure 4.24 illustrates how the average curvatures varied for the different wall segments as the load increased. This wall again shows that the most significant curvature remained near the bottom of the wall.

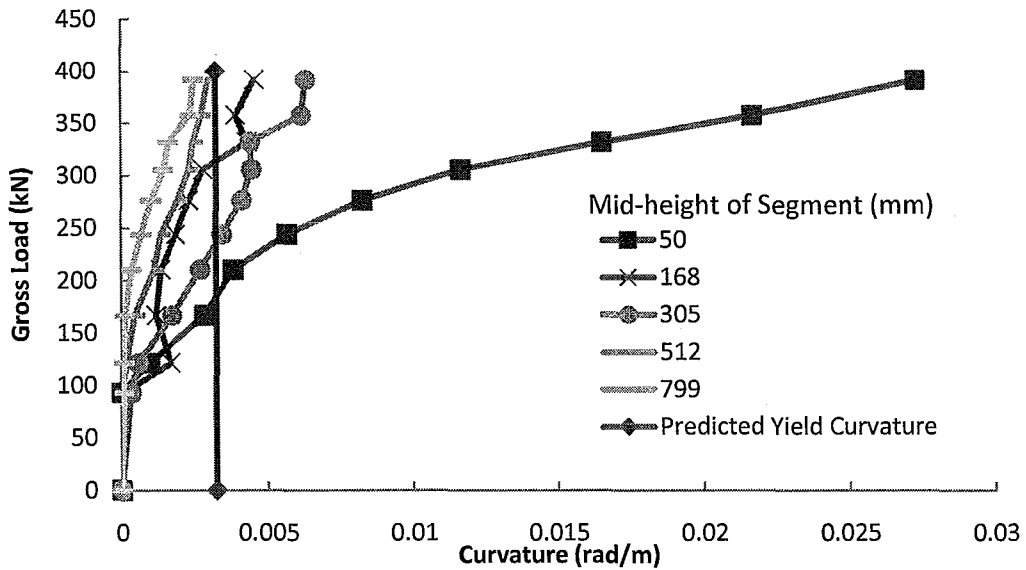


Figure 4.24: Average Curvature vs. Gross Load: Centre Wall (Wall 5)

Figure 4.25 contains the predicted deflection based on the collected curvature data versus the actual in-plane deflection of the Centre Wall (Wall 5).

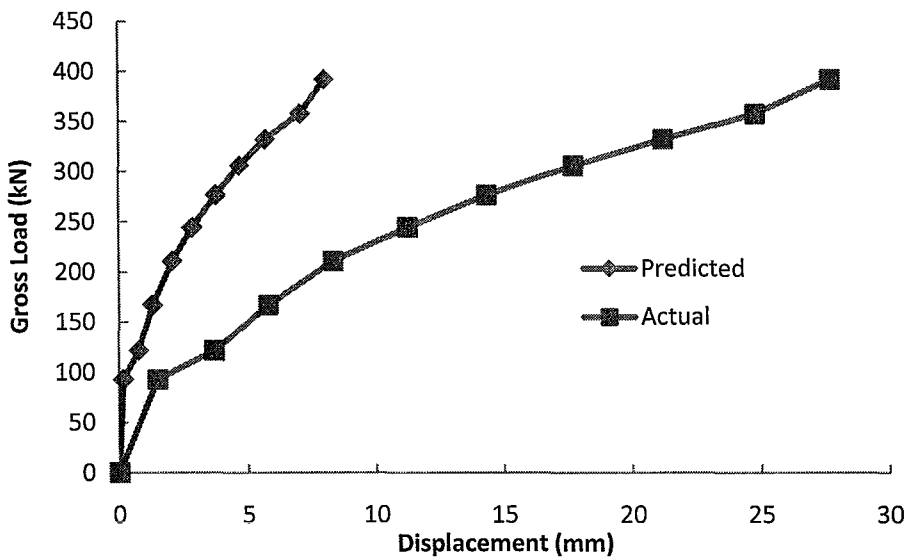


Figure 4.25: Predicted Displacement Based on Measured Average Curvature for Wall 5

The predicted deflection based on collected curvature data was only 29% of the actual in-plane deflection. Shear deformations dominated the behaviour of this wall. Shedid (2006), found that shear deformation accounted for 20-30% of lateral deflection. For this building, much higher shear loads occur due to the coupling of the in-plane walls with the out-of-plane walls. However, the out-of-plane walls will not share in resisting much shear. Therefore, at much higher loads and, particularly as plastic deformations occur, it is conceivable that shear deformations, particularly in the plastic zone, could be quite high.

4.6.5 South Out-of-Plane Walls (Walls 4 and 7)

Similar to what occurred at the North side of the building, the two Southern out-of-plane walls (Walls 4 and 7) behaved in a similar manner. Again, each wall measured approximately 600 mm long and was reinforced vertically with 7.6 mm diameter bars in every other cell ($p_v=0.59\%$). Figures 4.26 and 4.27 contain the average curvature profiles for these out-of-plane walls.

The maximum curvatures were measured as 0.0015 and 0.002 rad/m, respectively, for the South East (Wall 4) and South West (Wall 7) Out-of-Plane Walls. These curvature values were attained near the base of the wall at the peak loading experienced by the building. As mentioned previously, the predicted yield curvature for these walls was calculated as 0.0062 rad/m. Neither of the walls reaches even 1/3 of that yield value. Upon further examination, it is seen that all vertical LVDT's on both ends of the walls recorded negative displacements or relatively small positive

displacements suggesting that these walls are primarily subject to compressive loading. This conclusion is supported by the lack of any visible cracks in either of these walls. Considering the direction of loading and associated coupling, it seems obvious that these walls were indeed subjected to axial compression due to coupling with the neighbouring in-plane walls.

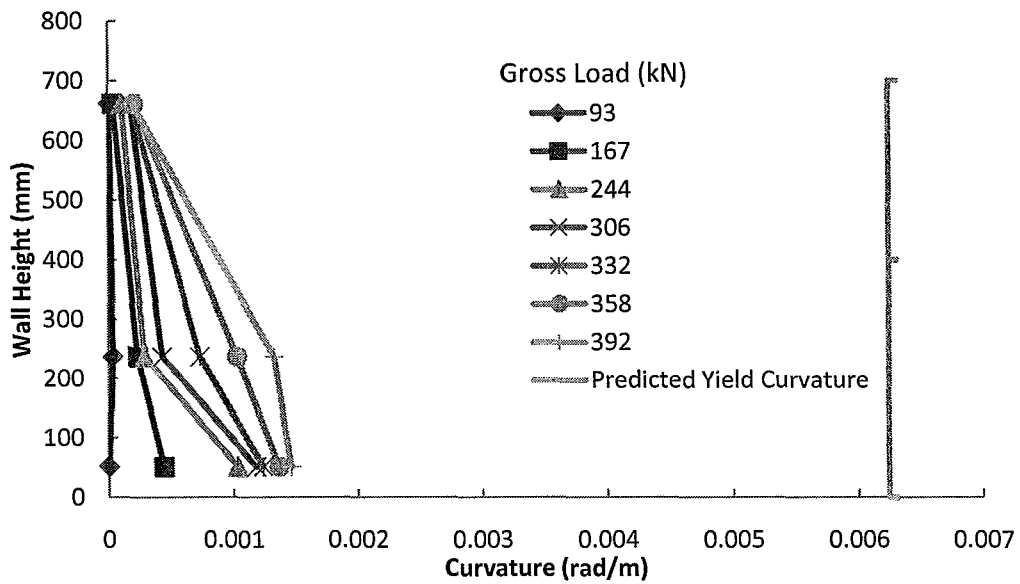


Figure 4.26: Average Curvature Profile: South East Out-of-Plane Wall (Wall 4)

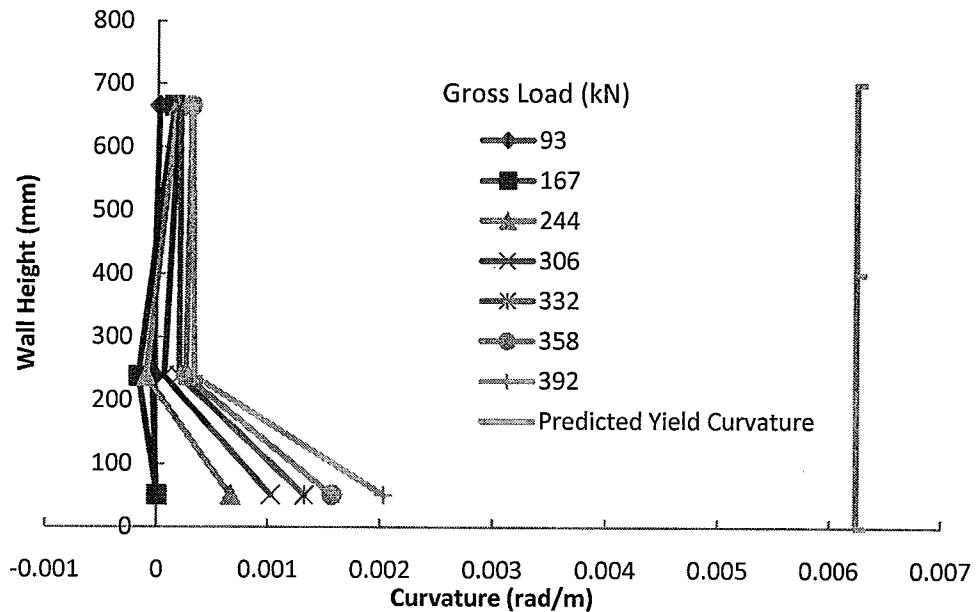


Figure 4.27: Average Curvature Profile: South West Out-of-Plane Wall (Wall 7)

There is however, a definite trend to the collected curvature data. The South end of the building was not restrained like the North end of the building and therefore the building twisted in a manner reflecting its unsymmetrical nature. Both walls show larger compression strains on the West end of the walls, indicating a lateral load in that direction. This is consistent with the observed direction of deflection obtained through the diaphragm displacement measurements. The additional compressive loading experienced by these out-of-plane walls offset most of the tension due to bending and allowed these walls to respond elastically to the resultant torsional loading thereby providing the building with torsional stability.

4.6.6 The C-Wall (Wall 8)

The C-Wall (Wall 8) measured approximately 1533 mm long and was similarly reinforced to all other rectangular walls along its linear portion but was reinforced with a bar in every cell in its flanges ($p_v=0.66\%$). The predicted lateral loading for first yield of the flexural reinforcing steel was 112.3 kN with an associated curvature of 0.0022 rad/m. Figure 4.28 contains the curvature profile along the wall height, plotted for different loading levels, as average curvature over the vertical wall segment located at the segment mid-height.

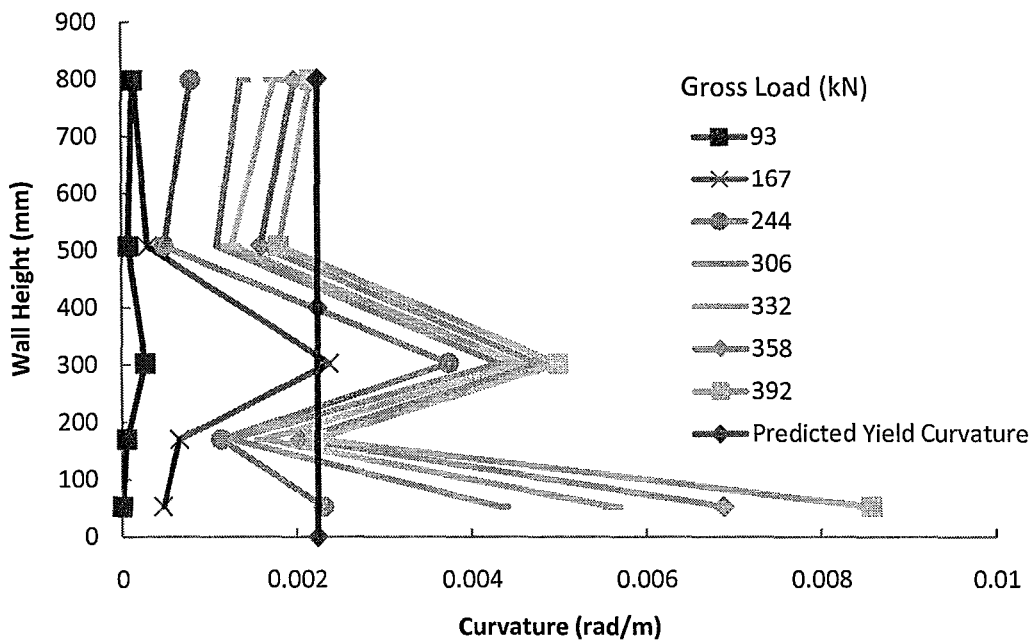


Figure 4.28: Average Curvature Profile: C-Wall (Wall 8)

The ultimate predicted lateral loading for this wall was calculated to be 150.9 kN with a corresponding curvature of 0.033 rad/m. This wall did not experience rupture of

the vertical reinforcing bars and actually showed very little distress even beyond peak loading. Therefore, the measured curvature corresponds to a curvature value that is not near the walls ultimate limit state. The maximum measured curvature of 0.0086 rad/m occurred at the base of the wall at peak loading. This is only 26% of the predicted ultimate curvature and approximately 34% of the maximum curvature observed by Wierzbicki (2010). As discussed, the close proximity of the North West and South West Out-of-Plane Walls (Walls 6 and 7) significantly affected the behaviour of this wall. Due to the observed strong coupling between these elements, it would be expected that the curvature of this shear wall element would be reduced through their interaction.

The extent of plasticity was calculated to be 170 mm but could have increased if additional ductility had been provided by the vertical reinforcing bars. Since it is unknown how close the wall was to its ultimate capacity, there is no useful comparisons to the experimental results for the ultimate condition as found by Wierzbicki (2010).

Figure 4.29 illustrates how the average curvatures varied for the different wall segments as the load increased. For this wall, the large curvatures were more spread out over the height of the wall but, again, the largest curvature was noted at the base of the wall.

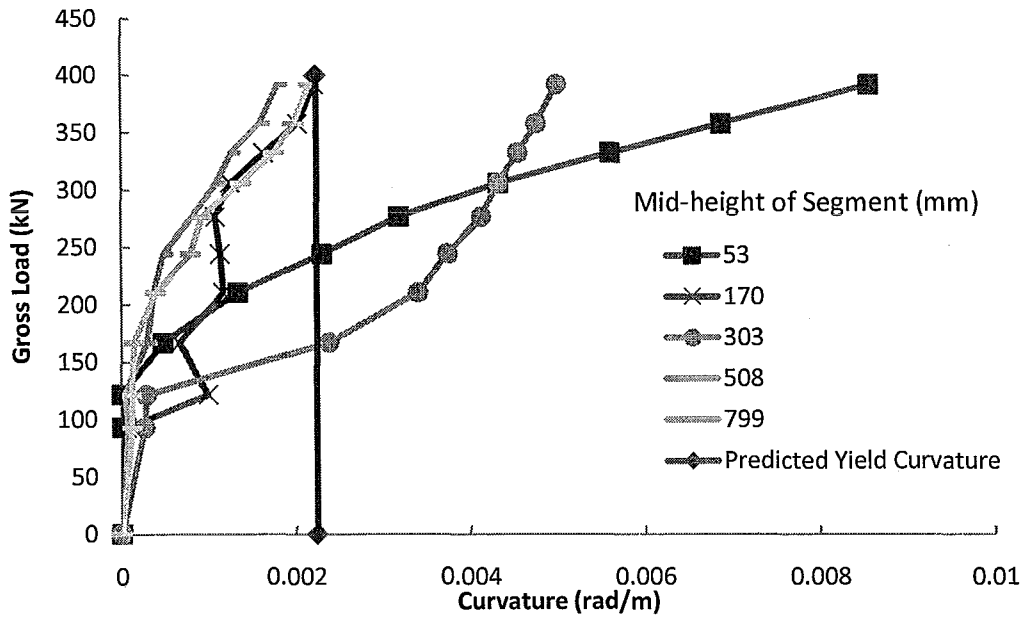


Figure 4.29: Average Curvature vs. Gross Load: C-Wall (Wall 8)

It can also be noted that the curvatures at 303 mm above the base of the wall exceeded those lower on the wall at 170 mm. This may be due to the nature of the cracking pattern of a shear wall with lower aspect ratio. An inclined shear crack can cause additional curvatures up the height of a wall by transferring tensile force to a location higher up the wall via their incline. If more shear cracks pass through the area located higher up the wall say between 235-370 mm of the wall height, they could cause larger curvatures to be observed for that vertical segment.

Figure 4.30 contains the predicted deflection based on the collected curvature data versus the actual in-plane deflection of the C-Wall (Wall 8). The predicted deflection based on collected curvature data was only 17% of the actual in-plane

deflection. Again it is suggested that shear deformations dominated the behaviour of this wall.

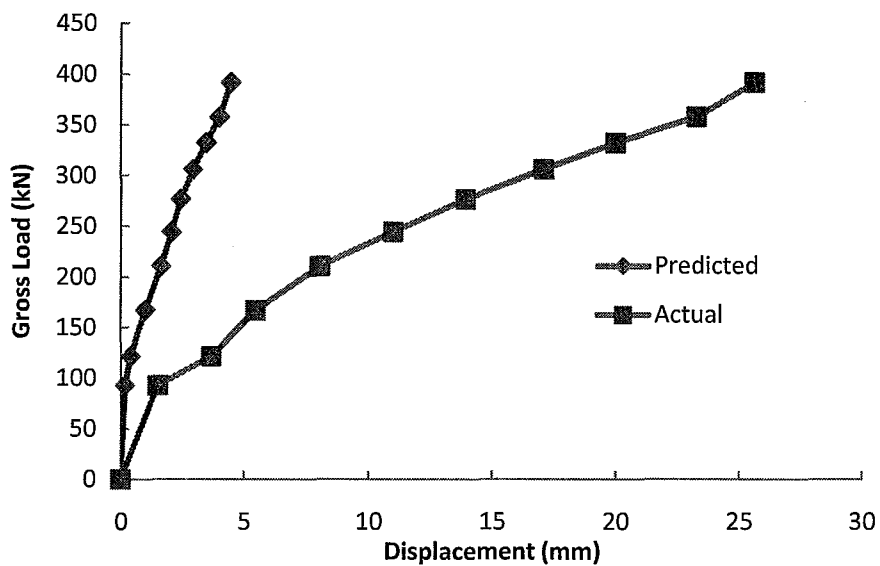


Figure 4.30: Predicted Displacement Based on Measured Average Curvature for Wall 8

4.7 Conclusions

4.7.1 Predicted and Experimental Building Capacity and Deflections

When analyzing a complete structure, many factors should be considered. However, without the aid of advanced computer software, simplifications must be made. Here, the most important consideration for predicting the building capacity and in-plane displacement was the inclusion of inter-wall coupling while minor contributors to behaviour which were not accounted for included base slip and the assumption of a nominal yield value for the vertical reinforcing bars. It was found that predictions based on theoretical analysis of coupling combined with experimentally determined capacities

for individual walls provided a reasonable estimation of building capacity in the post yield state. The idealization of inter-wall coupling appeared to be satisfactory.

4.7.2 Building Response

4.7.2.1 Torsion

The original design of the building was to have the out-of-plane walls resist the torsion as all of the in-plane walls reached their peak and post-peak lateral load resistances. However the restraint of the actuator restricted rotation of the structure at the North end. As the building deflected in the plane of loading, it was forced to rotate at the point of applied load. However, the in-plane deflections of the walls were nearly the same with the softer side of the building experiencing slightly greater deflections in its plane than the stiffer side of the building at all load levels. Examination of the lateral movement of the structure at the South end, showed that the out-of-plane walls were effective in preventing excessive building twist, even at the ultimate condition. Therefore, the objective of minimizing the effect of torsion on the in-plane walls was achieved.

4.7.2.2 In-Plane Behaviour

The in-plane deflection of each wall was calculated from displacement measurements taken at the South end of the building at the roof slab level. Three of the four in-plane walls reached their ultimate condition. These deflections were comparable with those found experimentally by Wierzbicki (2010). However,

predictions of building strength based on those same results did not give accurate predictions of the post-yield building in-plane response but significantly underestimated the strength of the structure. As mentioned in Section 4.2.2, coupling of in-plane walls (Walls 1, 2, 5, and 8) with the out-of-plane walls (Walls 3, 4, 6, and 7) accounted for this discrepancy.

4.7.2.3 Ductility

System ductility estimations were performed based on two idealizations. Both idealizations used the equal area principle. The first idealization used the observed initial stiffness in tandem with the equal energy principle to establish idealized yield displacement and load. The resulting seismic reduction factor based on this idealization was 5.9. This is nearly triple the allowable reduction factor as presented by the NBCC (2010).

The second idealization used the calculated secant stiffness defined by the slope of a line passing from the origin to the point on the load-displacement diagram defined as the point of first yield (where the first in-plane wall matched predicted yield curvature). The calculated seismic reduction factor for this case was 2.3. Considering the limitations imposed on the structure by the relatively brittle nature of the vertical reinforcing steel, this experiment can be considered a lower bound test. With this in mind, the buildings performance shows promise for the ductile characteristics of reinforced masonry.

4.7.3 Individual Wall Behaviour

The main intent of this study was to identify, in addition to the seismic performance of reinforced masonry, whether the cumulative behaviour of individual walls as designed and analyzed in isolation, is truly comparable to use of those same elements within a structural system. Examination of the curvatures of the in-plane walls suggest that the observed curvatures are much smaller for the walls in the structure as compared to the same walls tested individually by Wierzbicki (2010). Coupling behaviour, structural redundancy, the diaphragm effect and load redistribution are all factors that change the response of shear wall elements placed in a structural system. Further analysis showed that use of measured curvatures to predict overall building displacement was inaccurate. For most walls in the building, flexural deformations as predicted by measured curvatures made up less than half of the top displacement of the wall suggesting that shear deformations are critical when considering walls in a system setting.

5 Conclusions and Recommendations

5.1 Conclusions

5.1.1 Use of Third Scale for Testing Structures

Previous and concurrent research shows the applicability and practicality of utilizing 1/3rd scale masonry units. The associated placement tolerances (head joint and bed joint thicknesses, plumbness of walls etc.) had to be tightly controlled and required the skill of an experienced mason. These tolerances also affected the bar position within the cells of the block. Given the small cell size, very little flexibility was available in the way of bar spacing or lack of plumbness. Effort was required during construction to realign bars within the cells in an endeavor to maintain the alignment of the bars to prevent forming any voids in the grout.

Although scaling has to be accounted for in relation to stiffness and period calculations, this is a comparatively simple process that does not detract from the benefits of testing at the smaller scale.

5.1.2 Ductility of Reinforcing Bars

Unfortunately, it was not known before building the structure that the bars had very limited ductility under monotonic loading and became increasingly brittle under cyclic loading into the inelastic range. This lack of ductility in the vertical reinforcement had a detrimental effect on the observed structure ductility. Premature rupture of the flexural tensile bars in three in-plane walls prevented sufficient yielding from occurring

to eventually reach failure by compressive damage in the masonry. The plastic behaviour of the walls was limited as the masonry was unable to undergo large compressive strains and subsequent toe damage. In addition, the lack of a well-defined yield point and subsequent plastic zone made interpretation of the results more difficult. Significantly more energy dissipation and displacement ductility would have been realized if the reinforcement had provided the usual level of ductility found in standard reinforcing bars.

5.1.3 Building Ductility

Even with the brittle nature of the flexural reinforcing bars, the building exhibited good ductility and high drift levels. The building achieved drift levels in excess of 1.2% while maintaining strength and stability as well as drift levels in excess of 2.0% while maintaining over 70% of the peak loading. Equal area idealizations performed on the building load envelope yielded calculated seismic reduction factors of 5.9 and 2.3. The first value is nearly three times the current ductility related force modification factor while the second is 16% higher. However, considering the aforementioned brittle reinforcing, and the overestimation of the building yield displacement in the second idealization approach, this study can be considered a lower bound study and therefore suggests that the current seismic reduction factor is underestimated.

5.1.4 Ductility of Individual Walls

Recent research into the ability of reinforced masonry shear wall elements has shown their ability to provide energy dissipation while retaining adequate strength.

However, most of this research has examined the behaviour of the characteristics of shear wall elements without consideration of the surrounding system. The plastic behaviour and ductile response of individual shear wall elements must be maintained when placed in a structure and surrounded with other structural and non-structural elements.

Present application of code parameters applies seismic reduction factors to individual shear wall elements. This is based on the aforementioned research in this area. Considering that literature in the area of system behaviour is very limited, practical testing must be performed to ensure that previous research applies and affirm or modify current code practice. From this study, it is obvious that the behaviour of the walls in this structure was very different from those noted by Wierzbicki (2010). Although the analysis of the individual walls presented a reasonable estimation of low-load system behaviour, the response of the wall elements and related apparent stiffnesses changed a great deal as the building entered into the plastic state. The difference noted in the curvature distributions over the height of the wall as well as the extent of plasticity in each wall suggest that the load experienced by walls in a system setting can be significantly different from the same walls top loaded as cantilevers.

5.1.5 Deformations in Walls

Observed curvature profiles for all walls reaching their ultimate state in the building were smaller than those noted for the same walls tested in isolation. This suggests that curvature ductility of a cantilevered wall may not be the best predictor of

actual wall ductility in a system. As shown in this study, walls that experience large in-plane deflections do not necessarily achieve this deflection via primarily flexural deflections characterized by curvature. In fact, flexural deflections found from curvature in three out of four cases found in this structure made up less than half of the total observed deflection. This suggests that shear deformations make up a larger portion of the in-plane deflection than is observed for individual shear wall elements in a structure. The difference in shear deformation compared to that in individual walls is likely the result of much higher shear forces created by the increased lateral load resisting capacity introduced by coupling. For the individual walls, studies have shown that the ductile response is governed mostly by flexure with reasonably small and relatively constant ratios of shear deformation (Shedid, 2008). Yet, for an entire building, the displacements may be comprised of both flexural and significantly irregular shear deformations depending on the location of the wall within the structure. This suggests that it may not be useful to only focus on, and improve, the response of an individual wall, if that response is not what is observed when the element is placed in a system. Even if the building ductility can be reasonably predicted by utilizing the average ductility of the main individual elements, the form of ductile response may be different. The true form of system ductility must be studied in more detail so that research in this area will be more relevant to improving system behaviour, not just elemental behaviour.

5.1.6 Torsion

The test setup had a significant effect on the response of the building. The decision to restrict lateral movement of the actuator prevented the building from exhibiting its true torsional behaviour. However, significant lateral movement of the North end of the building did occur and resulted in lateral drift levels of 0.2%. These significant drift levels were adequately restrained by the out-of-plane walls at this location. It was also noted that these walls were subject to significant compressive stresses due to inter-wall coupling. This compressive force delayed the onset of yield curvatures in these walls and increased their ability to resist the lateral forces developing as a consequence of the lack of symmetry of the structure.

5.2 The Effects of the Reduction in Stiffness

The load displacement response of the structure was interesting from the standpoint of structural stiffness. It is well known that stiffer structures tend to have lower fundamental periods of vibration and therefore attract comparatively greater seismic loading. Currently, dynamic analysis of reinforced masonry considers the initial stiffness of the structure to determine seismic forces yet research shows that structures entering the plastic state show a reduced stiffness. The following is presented as a rudimentary analysis pointing to further necessary testing.

The secant stiffness of the building at its ultimate condition reduces to just 21.4% of the original stiffness. This reduction of stiffness inherently causes an increase in fundamental period and a corresponding reduction of attracted seismic loading. This

must be a consideration for any structural system but is especially important for reinforced masonry given the substantial disadvantage it acquires when utilizing the elastic stiffness for seismic response.

5.2.1 Structural Period

The period of any structure is inversely proportional to its stiffness; that is, the stiffer the structure the lower its corresponding period of vibration and vice versa. In reinforced masonry, the initial stiffness of a structure is much greater than the stiffness found after plastic deformations start to occur. Following cracking of the masonry in the early drift stages which significantly reduces stiffness, stiffness further decreases as the walls enter the plastic stages and the flexural steel yields along with the masonry crushing.

Typical masonry structures are characterized by very large initial stiffnesses and correspondingly low periods. Typical low rise masonry buildings are very stiff with fundamental periods of vibration of less than 0.2 seconds (Paulay and Priestley, 1992). However, the stiffnesses of masonry structures are significantly reduced by plastic deformations and, therefore, will have much larger associated periods of vibration. It is well known that in seismic response, structures with longer periods of vibration attract less seismic loading thereby reducing seismic demand. Drysdale and Hamid (2005), note that a decrease in stiffness of 50% for a masonry structure with an initial fundamental period of 0.4 to 0.8 seconds will correspond to a new period ranging from 0.6 to 1.1 seconds which would result in a major reduction of seismic demand. It is therefore

useful to examine the response of a structure with respect to its corresponding stiffness degradation.

5.2.2 Normalized Period

As establishing the actual building period was not within the original scope of this study, ratios of period (assuming a constant mass) will be used instead to create a comparison of the pre-yield building stiffness to that at its ultimate state. The fundamental period of vibration is related to the structure's stiffness and mass. If the mass of the structure remains constant, the period of vibration will change in relation to its change in stiffness. Therefore, a ratio between the two periods based on the initial stiffness and the secant stiffness at ultimate conditions can be determined by the following equation:

$$\frac{T_i}{T_{initial}} = \sqrt{\frac{K_{initial}}{K_i}} \quad \text{Eq. 5.1}$$

where:

$K_{initial}$ = Initial Stiffness of Structure

K_i = Secant Stiffness of Structure at drift level i

$T_{initial}$ = Initial Period of Structure

T_i = Period of Structure at drift level i

5.2.3 Post-Yield Stiffness

The pre-yield stiffness of the building was established from the 40% pre-yield loading cycle, as shown in Section 4.4.1.1, as 66 kN/mm. This was 76% greater than the predicted stiffness of 37.4 kN/mm based on the summation of the cracked stiffnesses of

the in-plane walls. The secant stiffness at ultimate displacement is defined by the slope of a line passing through the load envelope at the point of ultimate displacement from the origin. In this case, the slope of the secant line passing through the point of 1% drift, was found to be 14.1 kN/mm.

Using these calculated stiffness values in equation 5.1 results in a period ratio of 2.16. This means that the period of the structure more than doubles as it approaches its ultimate state. Therefore, this structure would attract significantly less seismic load at large drift levels.

5.2.4 Structural Stiffness and Period

While a reasonable prediction, the stiffness observed for the building exceeded the predictions of initial stiffness based on the algebraic sum of the in-plane shear wall elements by 76%. Beyond yield, the stiffness of the structure far exceeds the stiffness of the cumulative sum of the load displacement curves of the individual wall elements (Wierzbicki, 2010). However, the building did show considerable softening in its plastic range. The secant stiffness at 1% drift was approximately 21.4% of the initial observed stiffness. This suggests that under seismic excitation causing plastic behaviour, this structure would have shown a substantial increase in structural period and a corresponding reduction in attracted seismic forces.

5.3 Recommendations

Testing of an unsymmetrical structure creates some difficulties with details of the test setup as well as with interpretation of the test data for a highly redundant system.

5.3.1 Test Setup Modifications

In general, as a first trial, the test setup performed quite well. The only major difficulty was the restriction of lateral movement of the specimen at the point of applied load. This problem can be addressed by installing a new support for the actuator as a beam spanning between the two main frames. In this way, the actuator can be hung which will allow it to move safely in the lateral direction and will permit any specimen mounted in the test rig to move laterally as the structure dictates rather than having the test rig dictating how the specimen will rotate. Further examination of this suggestion must be performed to confirm the effects of a moving load. If the actuator is permitted to move laterally while the building twists, the analysis must account for the fact that lateral out-of-plane load, in addition to the in-plane load, is being applied to the structure.

Although complicating the construction of the model building, use of sufficient out-of-plane walls to provide similar lateral load capacity to the in-plane walls is logical for seismic design and at least at the high loads when in-plane walls are behaving plastically. These walls would remain elastic and limit twisting to very small levels.

5.3.2 Building Layout

As mentioned earlier, construction with 1/3rd scale blocks required exceptional precision. These tight tolerances, along with the fact that a representatively thin slab is difficult to construct, leads the author to suggest increasing the space between the walls that would be coupled. This will simplify the construction process and also eliminate potential diaphragm difficulties. Walls too closely spaced together create shear capacity problems within the slab. In fact, combining out-of-plane walls with the in-plane walls will create flanged sections which have enormous advantages for ductility and can also simplify the analysis.

5.3.3 Reinforcing Steel

It is well known that the ductile characteristics of the reinforcing steel are of critical importance in the hysteretic response of reinforced masonry. As mentioned many times, the vertical reinforcing used in this structure had limited ductility. Ultimate steel strain required for reasonable plastic shear wall response is more than what can be supplied by the deformed wire. In order to achieve steel properties more representative of regular reinforcing steel, heat treatment should be applied to this reinforcing to improve its ductility.

5.4 Overall Conclusions

This experiment gave a positive indication of ductility in reinforced masonry systems. Testing of reinforced masonry shear wall buildings will more accurately identify the true behaviour of shear wall elements in a system setting resulting in more

relevant results for ductile design. Additional testing with improved materials is expected to demonstrate that the current seismic provisions as outlined in CSA S304.1 (2004) are conservative and should be modified to more closely reflect the true performance of reinforced masonry.

References

- Abboud, B. E., Hamid, A. A., Harris, H. G. "Small-Scale Modeling of Concrete Block Masonry Structures." *ACI Structural Journal*, Vol. 87(2), March-April 1990. pp. 145-155.
- Abrams, D. "Measured Hysteresis in a Masonry Building System." *Proceedings of the Third U.S. National Conference on Earthquake Engineering*. Vol. 2, 1986. pp. 1371-1382.
- Abrams, D. "Effects of Scale and Loading Rate of Tests of Concrete and Masonry Structures." *Earthquake Spectra*, Vol. 12(1), February, 1996. pp. 13-28.
- ASCE 7 (2008), "Minimum Design Loads for Buildings and Other Structures." American Society of Civil Engineers, Reston, Virginia.
- ATC, 1995. "Structural Response Modification Factors, ATC-19 report, Applied Technology Council, Redwood City, California.
- Bertero, R. D., "Inelastic Torsion for Preliminary Seismic Design." *Journal of Structural Engineering*, Vol. 121(8), August, 1995. pp. 1183-1189.
- Canadian Standards Association, "Design of Masonry Structures." CAN/CSA S304.1 (2004), Mississauga, Ontario.
- Canadian Standards Association, "Limit States Design of Steel Structures." CAN/CSA S16-01 (2005), Mississauga, Ontario.
- Chopra, A. "Dynamics of Structures." Prentice Hall, 1995.
- Cohen, G. L., Klinger, R. L., Hayes Jr., J. R., Sweeny, S. C. "Seismic Evaluation of Low-Rise Reinforced Masonry Buildings with Flexible Diaphragms I. Seismic and Quasi-Static Testing." *Earthquake Spectra*, Vol. 20(3), August, 2004. pp. 779-801.

- Cohen, G. L., Klinger, R. L., Hayes Jr., J. R., Sweeny, S. C. "Seismic Evaluation of Low-Rise Reinforced Masonry Buildings with Flexible Diaphragms II. Analytical Modeling." *Earthquake Spectra*, Vol. 20(3), August, 2004. pp. 803-824.
- Cohen, G. L., Klinger, R. L., Hayes Jr., J. R., Sweeny, S. C. "Seismic Evaluation of Low-Rise Reinforced Masonry Buildings with Flexible Diaphragms III. Synthesis and Application." *Earthquake Spectra*, Vol. 22(3), May, 2006. pp. 329-347.
- Cohen, G. L., Klinger, R. L., Hayes Jr., J. R., Sweeny, S. C. "Seismic Evaluation of Low-Rise Reinforced Masonry Buildings with Flexible Diaphragms I. Seismic and Quasi-Static Testing." *Earthquake Spectra*, Vol. 20(3), August, 2008. pp. 779-801.
- Drysdale, R. G., Hamid, A. A. "Masonry Structures: Behaviour and Design." The Masonry Society, Boulder Colorado, 2005.
- Drysdale, R. G., Khattab, M. M. "In-Plane Behaviour of Grouted Concrete Masonry Under Biaxial Tension-Compression." *ACI Structural Journal*, Vol. 92(6), November-December 1995. pp.1-13.
- Hughes, K., "Behaviour of Reduced-Scale Reinforced Concrete Masonry Shear Walls and Componentenets." M.a.Sc Thesis, The Department of Civil Engineering, McMaster University, Ontario, Canada (2010).
- Humar, J. L., Kumar, P. "Effect of Orthogonal In Plane Structural Elements on Inelastic Torsion Response." *Earthquake Engineering and Structural Dynamics*, Vol. 28, 1999. pp. 1071-1097.
- Kelly, T. "A Blind Prediction Test of Nonlinear Analysis Procedure for Reinforced Concrete Shear Walls." *Bulletin of the New Zealand Society for Earthquake Engineering*, Vol. 40(3), September, 2007. pp. 142-159.

- Kikuchi, K., Yoshimura, K. Tanaka, A. "Effect of the Presence of Masonry Units on the Seismic Behaviour of Reinforced Fully Grouted Concrete Masonry Walls." 8th North American Masonry Conference, June 1999, Austin, Texas.
- Miranda, E., Bertero, V. V. "Evaluation of Strength Reduction Factors for Earthquake-Resistant Design." *Earthquake Spectra*, Vol. 10(2), 1994. pp. 357-379.
- MSJC (2008), Masonry Standards Joint Committee, "Building Code Requirements for Masonry Structures." ACI 530-05/ASCE 5-05/TMS 402-05, American Concrete Institute, American Society of Civil Engineers and The Masonry Society, Detroit, New York, Boulder.
- NBCC, National Building Code of Canada (2010), Institute for Research in Construction, National Research Council of Canada, Ottawa, ON, 2010.
- Paulay, T. "Seismic Design for Torsional Response of Ductile Buildings." *Bulleting of the New Zealand National Society for Earthquake engineering*, Vol. 29(3), 1996, pp. 178-198.
- Paulay, T. "Torsional Mechanisms in Ductile Building Systems." *Earthquake Engineering and Structural Dynamics*, Vol. 27, 1998. pp. 1101-1121.
- Paulay, T., Priestley, M. J. N. "Seismic Design of Reinforced Concrete and Masonry Buildings." John Wiley and Sons, New York, New York, 1992.
- Paulay, T., Priestley, M. J. N., Syngge, A. J. "Ductility in Earthquake Resisting Squat Shearwalls." *ACI Journal*, July-August 1982. pp. 257-269.
- Paulay, T., Priestley, M. J. N. "Stability of Ductile Structural Walls." *ACI Structural Journal*, Vol. 90(4), July-August 1993. pp. 385-392.

- Seible, F., Priestley, M. J. N., Kingsley, G. R., Kurkchubasche, A. G. "Seismic Response of Full-Scale Five-Story Reinforced Masonry Building." *Journal of Structural Engineering*, Vol. 120(3), March, 1994. pp. 925-946.
- Seible, F., Hegemier, G., Priestley, N., Kingsley, G., Igarashi, A., Kurkchubasche, A. "Preliminary Results from the TCCMAR 5-Story Full-Scale Reinforced Masonry Research Building Test." *TMS Journal*, August 1993. pp. 53-60.
- Shedid, M, "Ductility of Reinforced Concrete Masonry Shear Walls." M.a.Sc, Thesis, The Department of Civil Engineering, Mcmaster University, Ontario, Canada (2006).
- Shedid, M. T., Drysdale, R. G., El-Dakhakhni, W. W. "Behaviour of Fully Grouted Reinforced Concrete Masonry Shear Walls Failing in Flexure: Experimental Results." *Journal of Structural Engineering*, Vol. 134(11), November 2008. pp. 1754-1767.
- Shing, P. B., Noland, J. L., Spaeh, H., Klamerus, E. "Inelastic Behaviour of Masonry Wall Panels Under In-Plane Cyclic Loads." 4th North American Masonry Conference, Los Angeles, California, 1989.
- Shing, P. B., Noland, J. L., Klamerus, E., Spaeh, H. "Inelastic Behaviour of Concrete Masonry Shear Walls." *Journal of Structural Div., ASCE*, Vol. 115(9), September 1989.
- Shing, P. B., Shuller, M., Hoskere, V. S. "In-Plane Resistance of Reinforced Masonry Shear Walls." *Journal of Structural Engineering*, Vol. 116(3), March 1990. pp. 619-640.
- Shing, P. B., Shuller, M., Hoskere, V. S., Carter, E. "Flexural and Shear Response of Reinforced Masonry Walls." *ACI Structural Journal*, Vol. 87(6), November-December 1990. pp. 646-656.

- Stathopoulos, K. G., Anagnostopoulos, S. A. "Inelastic Torsion of Multistory Buildings Under Earthquake Excitations." *Earthquake Engineering and Structural Dynamics*, Vol. 34, June, 2005. pp. 1149-1465.
- Tena-Colunga, A., Abrams, D. P. "Seismic Behaviour of Structures with Flexible Diaphragms." *Journal of Structural Engineering*, Vol. 122(4), April, 1996. pp. 439-445.
- Tobriner, S., "A History of Reinforced Masonry Construction Designed to Resist Earthquakes: 1755-1907." *Earthquake Spectra*, Vol. 1(1), 1984, pp. 125-149.
- Tomazevic, M., Klemenc, I. "Verification of Seismic Resistance of Confined Masonry Buildings." *Earthquake Engineering and Structural Dynamics*, Vol. 26, 1997. pp. 1073-1088.
- Tomazevic, M., Weiss, P. "Seismic Behaviour of Plain and Reinforced Masonry Buildings." *Journal of Structural Engineering*, Vol. 120(2), February, 1994. pp. 323-338.
- Tomazevic, M., Velechovsky, T. "Some Aspects of Testing Small-Scale Masonry Building Models on Simple Earthquake Simulators." *Earthquake Engineering and Structural Dynamics*, Vol. 21, February, 1992. pp. 945-963.
- Uang, C. "Establishing R (or R_w) and C_d Factors for Building Seismic Provisions." *Journal of Structural Engineering*, Vol. 117(1), January, 1991.
- Wierzbicki, J., "Behaviour of Reduced-Scale, Fully-Grouted Concrete Block Shear Walls." M.a.Sc Thesis, The Department of Civil Engineering, McMaster University, Ontario, Canada (2010).

Zonta, D., Zanardo, G., Modena, C. "Experimental Evaluation of the Ductility of a Reduced-Scale Reinforced Masonry Building." *Materials and Structures*, Vol. 34, December 2001.

Appendix A: Flexural Design

The following equations were taken from CSA S304.1 along with regular structural analysis principles and used to predict the ultimate flexural strength of the test walls. Units used for all of the following equations are N and mm.

$$P = C_m + C_s - T_s$$

$$C_m = 0.85f'_m t(0.8c)$$

$$C_s = \sum A_s f'_s \text{ Where } 0 \leq f'_s \leq f'_y, \quad f'_s = \frac{c - d_i}{c} 0.0025E_s < f_y$$

$$T_s = \sum A_s f_y \text{ Where } 0 \leq f_s \leq f'_y, \quad f_s = \frac{d_i - c}{c} 0.0025E_s < f_y$$

$$M_u = C_m \left(\frac{l_w}{2} - 0.4c \right) + \sum A_s f_s \left(d_i - \frac{l_w}{2} \right)$$

Where:

A_s = Area of vertical reinforcement in the wall.

c = Distance from extreme compression fiber to the neutral axis;

C_m = Compression force in cross section of a masonry wall;

C_s = Compression force in reinforcement;

d_i = Distance from the compression fiber to the location of reinforcement;

E_s = Modulus of elasticity for steel reinforcement;

f'_m = Average compressive strengths of masonry;

f_s = Tensile stress in vertical reinforcement;

f'_s = Compressive stress in vertical reinforcement;

f_y = Yield strength of vertical reinforcement;

l_w = Wall length;

M_u = Moment resistance at maximum strain in masonry; and

P = Applied axial load;

t = Thickness of wall;

T_s = Tensile force in reinforcement in cross section of a masonry wall;

Appendix B: Mortar Cube Data

I.D.	Date Created	Date Tested	Age at Testing (days)	Load (KN)	Strength (MPa)	Average (MPa)
1.1	25-May-09	12-Nov-09	159	60.1	23.3	25.0
1.2	25-May-09	12-Nov-09	159	67.3	26.1	
1.3	25-May-09	12-Nov-09	159	66.5	25.8	
2.1	25-May-09	12-Nov-09	159	63.0	24.4	24.7
2.2	25-May-09	12-Nov-09	159	61.0	23.6	
2.3	25-May-09	12-Nov-09	159	67.6	26.2	
3.1	26-May-09	12-Nov-09	158	56.4	21.9	22.6
3.2	26-May-09	12-Nov-09	158	60.7	23.5	
3.3	26-May-09	12-Nov-09	158	57.6	22.3	
4.1	27-May-09	12-Nov-09	157	75.3	29.2	28.4
4.2	27-May-09	12-Nov-09	157	76.8	29.8	
4.3	27-May-09	12-Nov-09	157	67.7	26.2	
5.1	27-May-09	12-Nov-09	157	79.5	30.8	29.7
5.2	27-May-09	12-Nov-09	157	75.3	29.2	
5.3	27-May-09	12-Nov-09	157	75.2	29.1	
6.1	10-Jun-09	12-Nov-09	143	64.0	24.8	24.0
6.2	10-Jun-09	12-Nov-09	143	60.0	23.3	
6.3	10-Jun-09	12-Nov-09	143	61.8	23.9	
7.1	10-Jun-09	12-Nov-09	143	57.7	22.4	23.2
7.2	10-Jun-09	12-Nov-09	143	61.2	23.7	
7.3	10-Jun-09	12-Nov-09	143	61.0	23.6	
8.1	17-Jun-09	12-Nov-09	136	77.5	30.0	29.5
8.2	17-Jun-09	12-Nov-09	136	78.7	30.5	
8.3	17-Jun-09	12-Nov-09	136	72.4	28.1	
9.1	17-Jun-09	12-Nov-09	136	81.3	31.5	30.9
9.2	17-Jun-09	12-Nov-09	136	79.2	30.7	
9.3	17-Jun-09	12-Nov-09	136	78.6	30.5	
Average					26.5	26.5
				SD	3.2	
				COV (%)	12.1	

Appendix C: Test Frame Shop Drawings

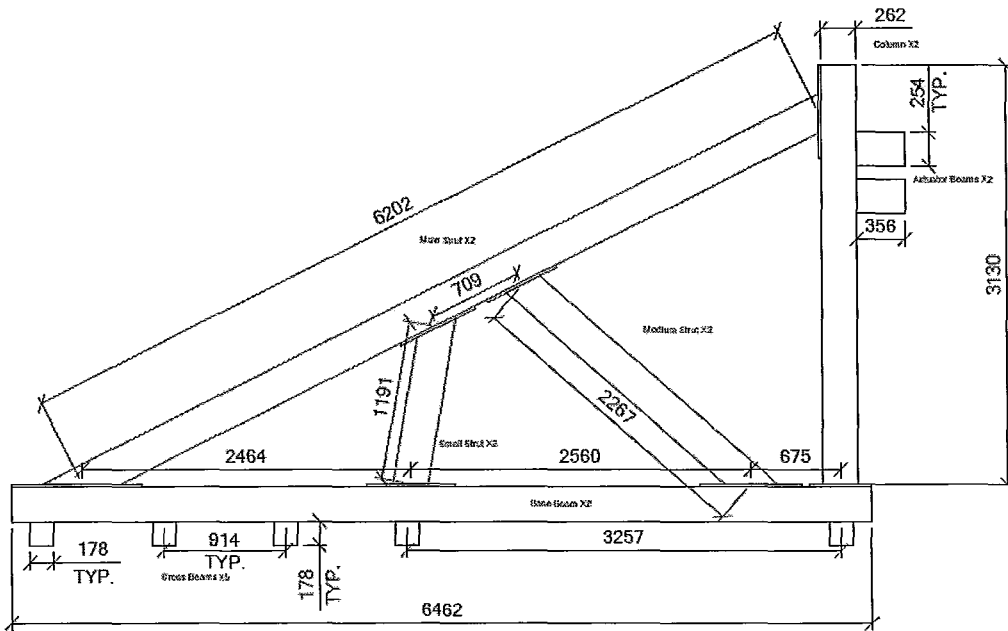


Figure C.1 Elevation

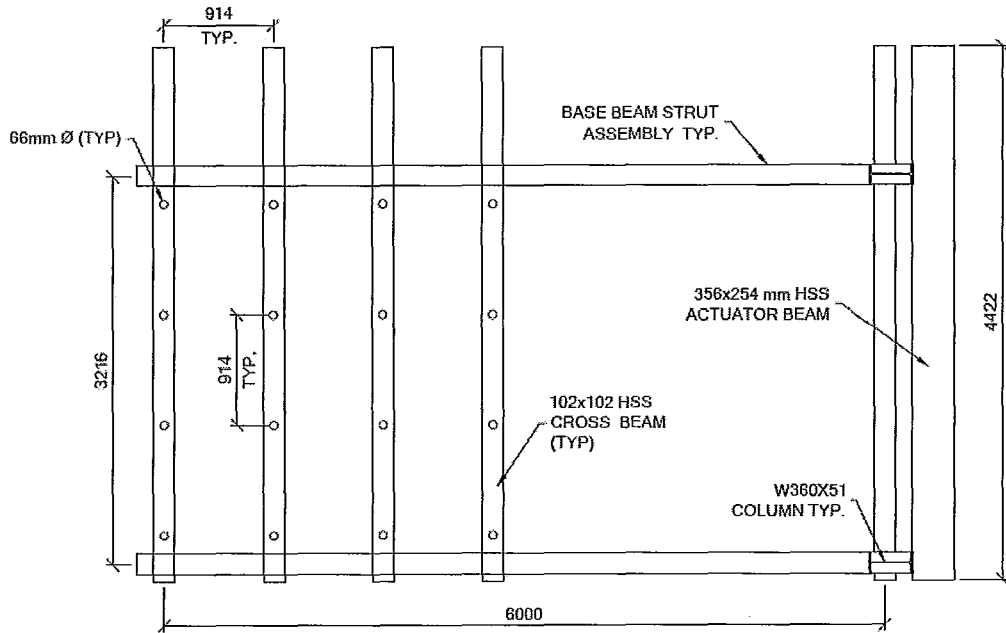


Figure C.2 Plan

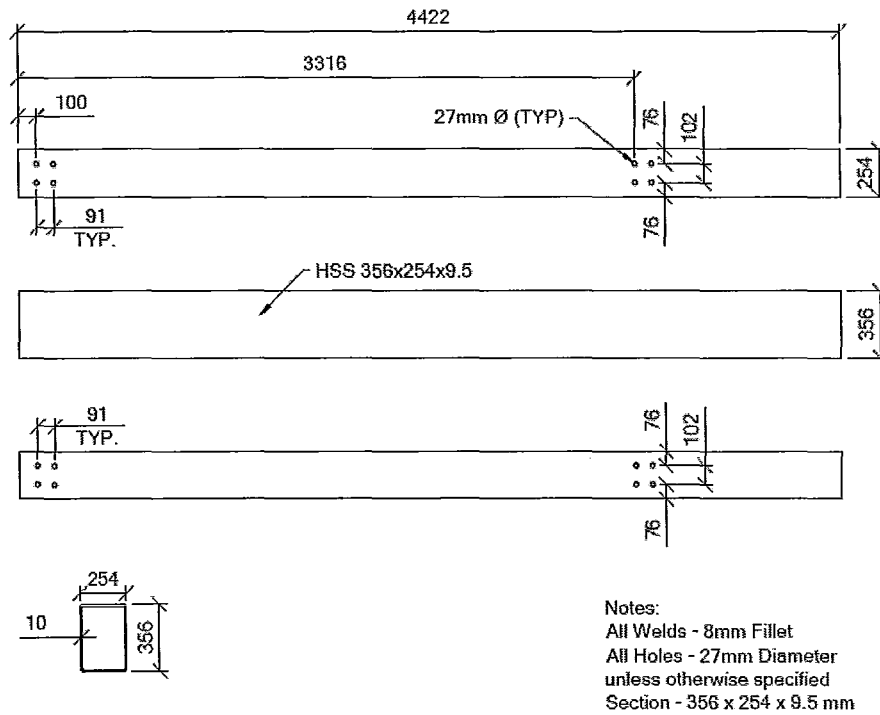


Figure C.3 Actuator Beam

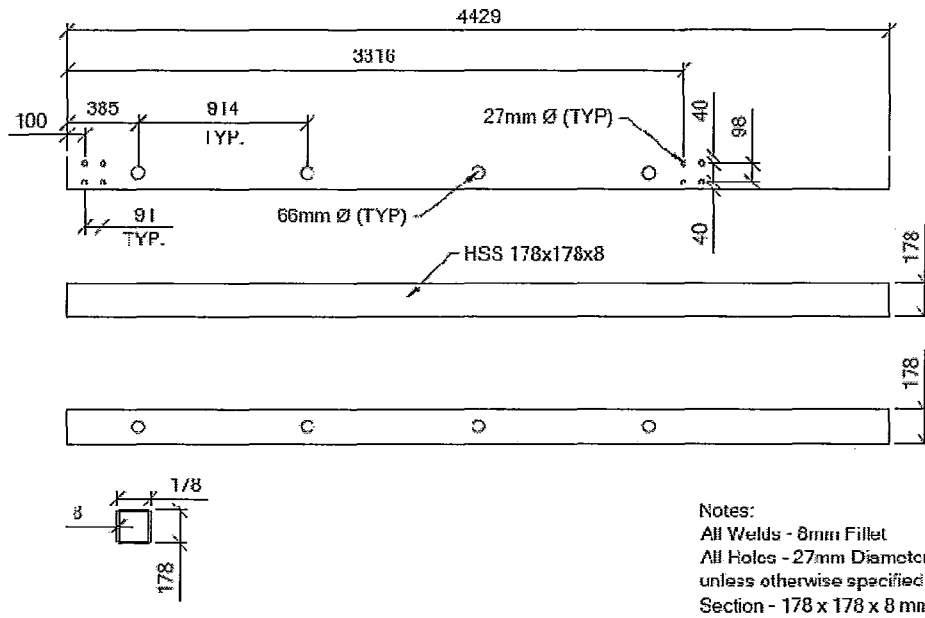


Figure C.4 Cross Beam

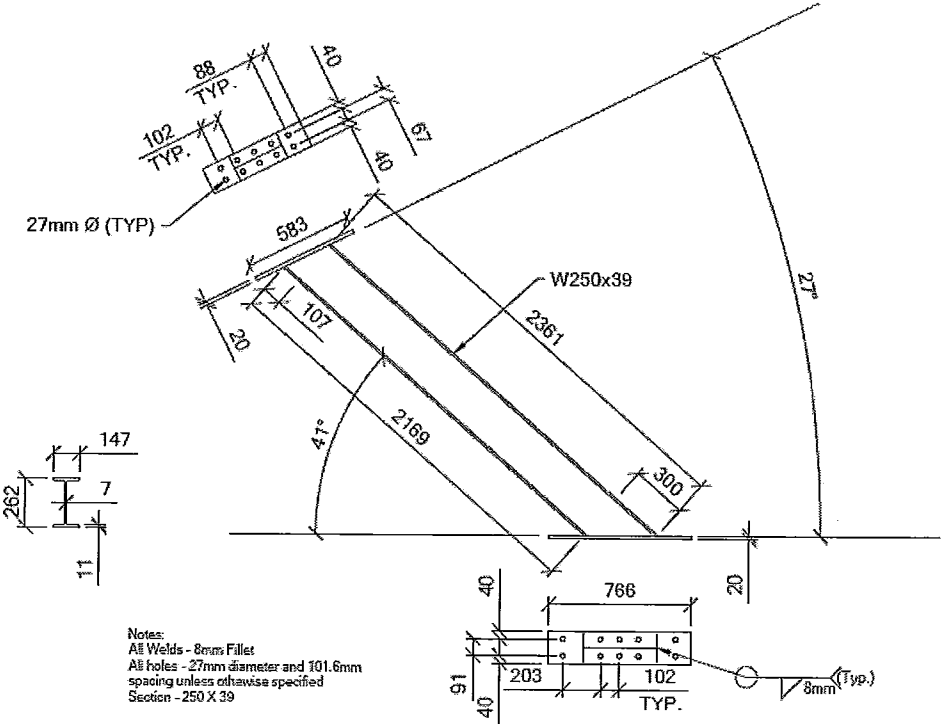


Figure C.8 Medium Strut

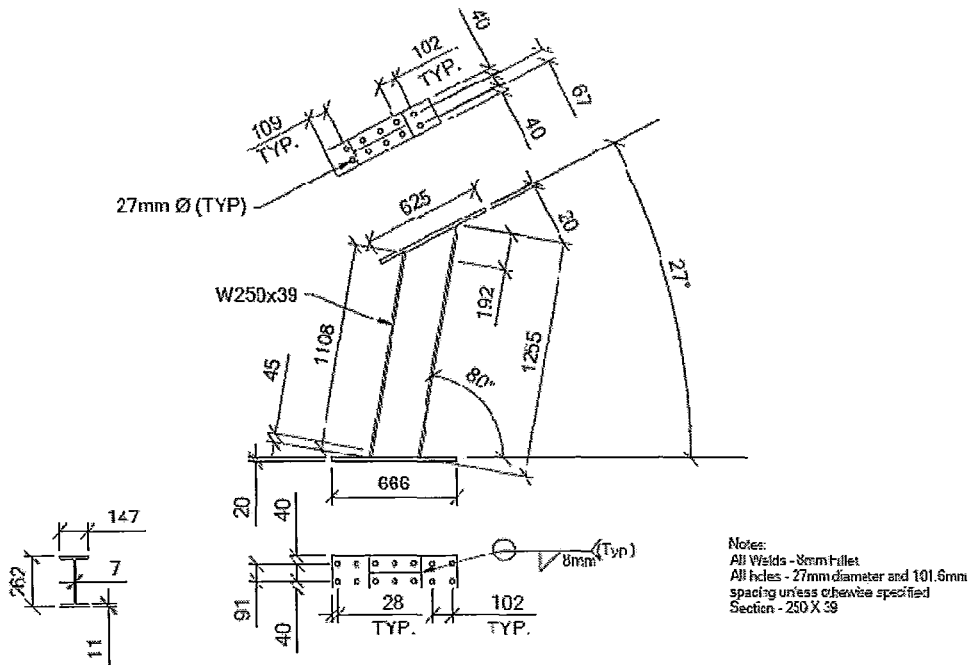


Figure C.9 Small Strut

Appendix D: Displacement Prediction

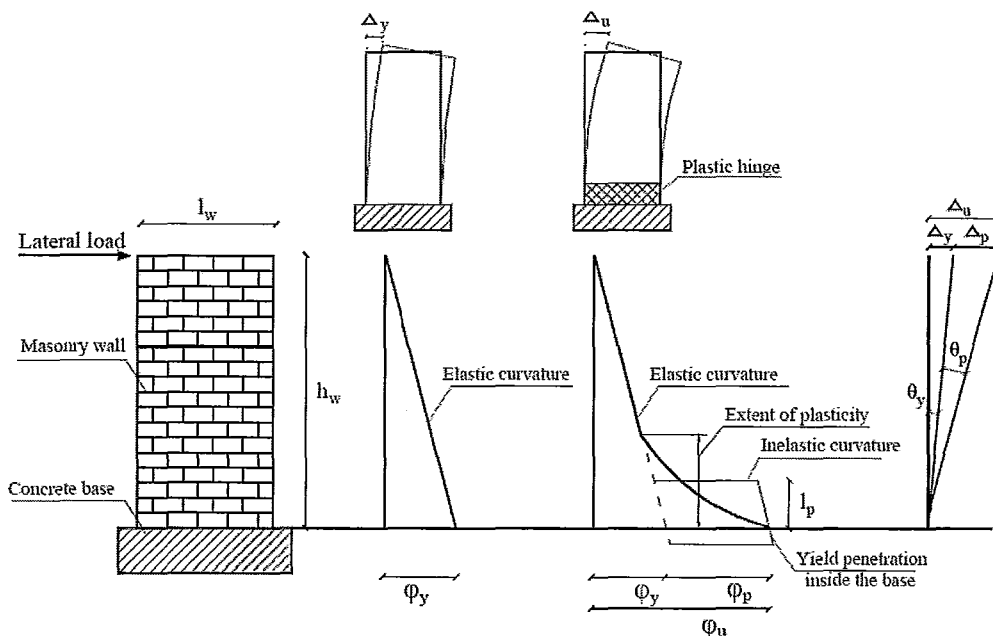


Figure D.1: Curvature and Deflection Relationship of a Reinforced Cantilever Masonry Shear Wall (Shedid, 2006)

The top displacement of the wall is predicted based on the curvatures over the height of the wall. The equations used for these displacement predictions are found below:

$$V_y = \frac{M_y}{h_w}$$

$$\phi_y = \frac{d_1 - c_y}{\epsilon_y}$$

$$\theta_y = \phi_y \frac{h_w}{2}$$

$$\Delta_y = \phi_y \frac{h_w^2}{3} = \theta_y \frac{2h_w}{3}$$

$$V_u = \frac{M_u}{h_w}$$

$$\varphi_u = \frac{c_u}{\varepsilon_m}$$

$$\theta_p = \varphi_y l_p, \text{ where: } \varphi_p = \varphi_u - \varphi_y$$

$$\Delta_p = \theta_p (h_w - 0.5l_p)$$

$$\Delta_u = \Delta_y + \Delta_p$$

Where:

c_u = Depth of compression zone at maximum load

c_y = Depth of compression zone at first yield

d_1 = Depth to extreme tensile bar

l_p = Length of plastic hinge

l_w = Length of Wall

M_u = Moment resistance at maximum strain in masonry

M_y = Moment resistance at first yield of tensile reinforcement

V_y = Lateral load resistance at first yield of tensile reinforcement

V_u = Lateral load resistance at maximum strain in masonry

φ_y = Curvature at base of wall at first yield

φ_u = Curvature at base of wall at maximum strain in masonry

θ_y = Rotation at the base of wall at first yield

θ_p = Plastic rotation of wall

Δ_y = Lateral displacement of wall at first yield

Δ_p = Plastic displacement of wall

Δ_u = Maximum lateral displacement of wall

ε_y = Yield strain of the outermost reinforcing bar in tension

ε_m = Compressive strain at the extreme masonry fibre

